CAPITAL UNIVERSITY OF SCIENCE AND TECHNOLOGY, ISLAMABAD

Scattering Analysis of the Wave-bearing Cavity Bridged by Vertical Elastic Boundaries

by

Hazrat Bilal

A thesis submitted in partial fulfillment for the
degree of Doctor of Philosophy

in the
Faculty of Computing
Department of Mathematics

2022

Scattering Analysis of the Wave-bearing Cavity Bridged by Vertical Elastic Boundaries.

By

Hazrat Bilal

(DMT 151007)

Dr. Hongyu Liu, **Professor**

City University of Hong Kong, **Hong Kong**

(Foreign Evaluator 1)

Dr. Danila, **Prikazchikov**, **Reader**

Keele University, Staffordshire, **UK**

(Foreign Evaluator 2)

Dr. Muhammad Afzal

(Thesis Supervisor)

Dr. Muhammad Sagheer

(Head, Department of Mathematics)

Dr. Muhammad Abdul Qadir

(Dean, Faculty of Computing)

DEPARTMENT OF MATHEMATICS

CAPITAL UNIVERSITY OF SCIENCE AND TECHNOLOGY

ISLAMABAD

2022

Copyright © 2022 by Hazrat Bilal

DEDICATED

To

My Parents

&

Kids

CERTIFICATE OF APPROVAL

This is to certify that the research work presented in the thesis, entitled "**Scattering Analysis of the Wave-bearing Cavity Bridged by Vertical Elastic Boundaries**" was conducted under the supervision of **Dr. Muhammad Afzal**. No part of this thesis has been submitted anywhere else for any other degree. This thesis is submitted to the **Department of Mathematics, Capital University of Science and Technology** in partial fulfillment of the requirements for the degree of Doctor in Philosophy in the field of **Mathematics.** The open defence of the thesis was conducted on **September 16, 2022**.

Student Name :   Hazrat Bilal (DMT151007)

The Examination Committee unanimously agrees to award PhD degree in the mentioned field.

Examination Committee :

(a)   External Examiner 1:   Dr. Aftab Khan
                             Professor
                             COMSATS University, Islamabad

(b)   External Examiner 2:   Dr. Tufail Ahmad Khan
                             Assistant Professor
                             UET, Peshawar

(c)   Internal Examiner :   Dr. Abdul Rehman Kashif
                             Associate Professor
                             CUST, Islamabad

Supervisor Name :   Dr. Muhammad Afzal
                             Associate Professor
                             CUST, Islamabad

Name of HoD :   Dr. Muhammad Sagheer
                             Professor
                             CUST, Islamabad

Name of Dean :   Dr. Muhammad Abdul Qadir
                             Professor
                             CUST, Islamabad

AUTHOR'S DECLARATION

I, **Hazrat Bilal (Registration No. DMT-151007)**, hereby state that my PhD thesis titled, '**Scattering Analysis of the Wave-bearing Cavity Bridged by Vertical Elastic Boundaries**' is my own work and has not been submitted previously by me for taking any degree from Capital University of Science and Technology, Islamabad or anywhere else in the country/ world.

At any time, if my statement is found to be incorrect even after my graduation, the University has the right to withdraw my PhD Degree.

(Hazrat Bilal)

Dated: 16ᵗʰ September, 2022

Registration No: DMT151007

PLAGIARISM UNDERTAKING

I solemnly declare that research work presented in the thesis titled "**Scattering Analysis of the Wave-bearing Cavity Bridged by Vertical Elastic Boundaries**" is solely my research work with no significant contribution from any other person. Small contribution/ help wherever taken has been duly acknowledged and that complete thesis has been written by me.

I understand the zero tolerance policy of the HEC and Capital University of Science and Technology towards plagiarism. Therefore, I as an author of the above titled thesis declare that no portion of my thesis has been plagiarized and any material used as reference is properly referred/ cited.

I undertake that if I am found guilty of any formal plagiarism in the above titled thesis even after award of PhD Degree, the University reserves the right to withdraw/ revoke my PhD degree and that HEC and the University have the right to publish my name on the HEC/ University Website on which names of students are placed who submitted plagiarized thesis.

(Hazrat Bilal)

Dated: 16ᵗʰ September, 2022

Registration No: DMT151007

List of Publications

It is certified that following publication(s) have been made out of the research work that has been carried out for this thesis:-

1. **H. Bilal** and M. Afzal "On the extension of mode-matching procedure for modeling wave bearing cavity", *Mathematics and Mechanics of Solids*, vol. 27, Issue no. 2, pp. 348-367, 2021.

2. **H. Bilal** and M. Afzal "Reflection and transmission of acoustic waves through bridging membrane junction", *Waves in Random and Complex Media*, DOI: 10.1080/17455030.2022.2051771, 2022.

3. M. Afzal and **H. Bilal**, "Silencing performance analysis of a membrane cavity with different edge conditions", *Journal of Vibration and Control*, DOI:10.1177/10775463221118707, 2022.

(Hazrat Bilal)

Registration No: DMT 151007

Acknowledgement

"Glory be to you, we have no knowledge except what you have taught us. Verily, it is You, the All-Knower, the All-Wise O'All-Knowing, grant me knowledge" (AL-QURAN).

First and foremost, I would like to thank Allah almighty for giving me the puissance, knowledge, competence and opportunity to undertake this research study and to get it out and complete it satisfactorily. Without his benison, this achievement would not have been attainable. I had not enough wisdom and strength to conquer this milepost. It is one of his infinite benedictions that He bestowed upon me with the potential and ability to complete the present research.

I wish to show my gratitude to all the people whose support was a milestone in the completion of this project, specially my righteous supervisor Dr. Muhammad Afzal, for his priceless suggestions, constant support, great patience and encouragement. I wish to express my sincere thank to the head of department Dr. Muhammad Sagheer, for valuable guidance and encouragement extended to me. I would like to thanks Capital University of Science and Technology, Islamabad, Pakistan, for providing suitable environment for research purpose. I would also appreciate the positive concern of my all research fellows, who supported me at the time of stress when I was about to lose my heart.

Last but not the least, I cannot forget my whole family especially my beloved parents, my sister, brothers for their prayers, continuous support, love. Their prayers have lightened up my spirit to finish this thesis. Special thanks to my wife who encouraged me throughout to complete my degree. I would like to express gratitude to my beloved kids Muhammad khan, Aroosh Manal khan and Hansa khan for being such a good kids who always cheering me up.

(Hazrat Bilal)

Abstract

The present thesis discusses the modeling, propagation and scattering of fluid-structure coupled waves through ducts or channels containing flexible components that support structure-borne as well as fluid-borne vibrations. The boundary value problems are governed by Helmholtz's equation and have Dirichlet, Neumann, Robin types and/or higher order boundary conditions. The mode-matching (MM) scheme in connection with Galerkin formulation is applied to solve the governing boundary value problems. In MM technique, the solution is projected on the eigenfunctions obtained from the eigenvalue problem associated with modeled boundary value problems. The eigenvalue problems having rigid, soft or impedance types of boundary conditions reveal orthogonal eigenfunctions, and the resulted eigen-sub-systems undergo Sturm-Liouville (SL) category. However, the eigenvalue problems achieved against the problems containing the elastic membrane or elastic plate type boundaries reveal eigenfunctions that are non-orthogonal and satisfy generalized orthogonality conditions, and the corresponding eigen-sub-systems undergo non-SL category.

The main aim of current study is to model and analyze the effects of vertically bridging elastic membranes and plates walls along with different edge conditions on acoustic scattering in a flexible waveguide. The traditional MM approach that is useful in modeling acoustically rigid, soft or impedance step-discontinuities fails for the cases having flexible bridging height discontinuities. For such problems, MM technique is applied in connection with three different approaches including Galerkin approach, Model approach and tailored-Galerkin approach. In first approach, the orthogonal basis priori solutions are assumed to express the response of bridging flexible components whose description varies by changing the edge conditions. Further, for some sets of edge conditions the eigenvalues of associated eigen-system cannot be expressed explicitly, and must be found numerically through some root finding algorithm. On the other hand, the Model approach expresses the displacements of bridging flexible components in terms of a set of non-orthogonal basis functions, which are already known and have non-zero derivatives at edges. However, the key to the success of this approach is the satisfaction

of generalized orthogonal properties of eigenfunctions. This technique avoids the need of additional root finding algorithm, but has higher computational cost due to the slow convergence of generalized Fourier series. Besides, the tailored-Galerkin approach incorporates the vibrational response of the bridging flexible components having different sets of edge conditions in a simpler and computationally more effective way. The displacements of vertical flexible components are defined in such a way that their homogeneous parts involve the material properties of elastic components, whereas, their integral parts link the cavity vibrations. Moreover, a unique general description of the displacement of vertical elastic component can deal a variety of edge conditions.

Different physical problems involving bridging flexible components and that can have applications having applications in structural acoustics, elasticity, water wave theory, aeroacoustics etc. are addressed in this thesis.

Contents

List of Figures

List of Tables

Abbreviations

HVAC	Heating Ventilation and Air-Conditioning
LFA	Low-Frequency Approximation
MM	Mode-Matching
MMG	Mode-Matching Galerkin
MMTG	Mode-Matching tailored Galerkin
OR	Orthogonality Relation
SL	Sturm-Liouville
STP	Standard Temperature Pressure
TL	Transmission-Loss
WH	Wiener-Hopf

Symbols

p	Acoustic pressure
ω	Angular frequency
ρ_0	Density in equilibrium state
ρ_p	Density of the plate
f	Frequency
L	Half length of expansion chamber or cavity
F_ℓ	Incident forcing due to structure or fluid
ψ_{inc}	Incident scalar field potential
δ_{mn}	Kronecker delta
ρ_m	Mass density
$\bar{W}\left(\bar{x}, \bar{y}, \bar{t}\right)$	Membrane displacement
μ	Membrane wavenumber in *vacuo*
α	Membrane fluid loading parameter
$\bar{W}_1\left(\bar{x}, \bar{y}, \bar{t}\right)$	Plate displacement
μ_1	Plate wavenumber in *vacuo*
α_1	Plate fluid loading parameter
B	Plate bending stiffness
υ	Poisson's ratio
P_i	Power incident
P_r	Power reflected
P_t	Power transmitted
P_{abs}	Power absorb
$P\rfloor_{\text{fluid}}$	Power through fluid

$P\rfloor_{\text{memb}}$	Power through membrane
$P\rfloor_{\text{plate}}$	Power through plate
ψ_{ref}	Reflected scalar field potential
ψ	Scalar field potential
Z	Specific impedance in dimension form
ς	Specific impedance in dimensionless form
c	Speed of sound
c_m	Speed of sound on membrane
T	Tension
t	Time
ψ_{tran}	Transmitted scalar field potential
N	Truncation number
$\mathbf{v}$	Velocity vector
k	Wave number
E	Young's modulus

Chapter 1

General Introduction

1.1   Introduction

This thesis is dedicated to the study of the Acoustic waves scattering in a rectangular cavity containing flexible boundaries. In the present era acoustic, the science of sound has become an interdisciplinary field. It embodies many disciplines such as physics, mathematics, mechanical engineering, speech and hearing sciences. Acoustic is an interesting and challenging research area to engineers and scientists [1–7].

The research interest in this field is motivated by the necessity to design objects or channels useful in the reduction of structural vibrations and the associated noises. Such noises are usually generated by the variety of mechanisms occurring in systems of automobiles, turbofan engines, aero-engines, heating ventilation and air-conditioning (HVAC) systems and other engineering designs [8–12].

The duct-like structure is a common component in all of these systems. Their key objective is to distribute air flow from the buildings or exhausts to environment. But, many times the waveguide acts as a conduit for a plethora of annoying sounds to living and working environment. To reduce the noise level, the study of noise reduction problems has received considerable attention of scientific community. In engineering applications, noise is reduced by controlling through unsteady flow

phenomena and vibrations of boundaries. The noise reduction techniques are classified into active noise control and passive noise control. In the first technique, mitigation is achieved by noise cancellation (see, for instance, [13–16]). In passive noise control, sound absorbing materials are used into the original system designs to mitigate sound.

These physical problems are usually governed by Helmholtz or Laplace's type equation having rigid, soft or impedance type of boundaries. The mathematical form of impedance boundary condition as given in [25] is

$$\rho\phi_t + Z\mathbf{n} \cdot \nabla\phi = 0, \tag{1.1}$$

where $\mathbf{n}$ is unit normal vector directed into the surface, ϕ represents the field potential, ϕ_t denotes the derivative of field potential with respect to time and, ρ is the density of fluid. Here Z denotes the specific impedance of the bounding surface, when $Z \to \infty$ the surface is acoustically rigid but if $Z \to 0$ the surface is soft. The acoustics scattering through different physical configuration containing boundaries of the type (1.1) have been addressed by many authors, for instance, see [26–29, 31, 33]. Note that the boundaries defined in (1.1) do not support vibration along the surfaces. However, if the bounding surfaces are dynamical in nature that support vibration such as elastic membranes or plates, the boundary conditions involve second or higher order derivatives and are referred to as higher order boundary conditions. The general form of higher order boundary condition as given in [34] is

$$\mathcal{L}_p\left(\frac{\partial}{\partial x}\right)\frac{\partial\phi}{\partial y} + \mathcal{M}_p\left(\frac{\partial}{\partial x}\right)\phi = 0, p \in \{0, a\}, \qquad y \in \mathbb{R}. \tag{1.2}$$

Here $\mathcal{L}_p\left(\dfrac{\partial}{\partial x}\right)$ and $\mathcal{M}_p\left(\dfrac{\partial}{\partial x}\right)$ are differential operators of the form

$$\mathcal{L}_p\left(\frac{\partial}{\partial x}\right) = \sum_{h=0}^{H_p} c_h^p \frac{\partial^{2h}}{\partial x^{2h}} \quad \text{and} \quad \mathcal{M}_p\left(\frac{\partial}{\partial x}\right) = \sum_{j=0}^{J_p} d_j^p \frac{\partial^{2j}}{\partial x^{2j}}, \tag{1.3}$$

where c_h^p and d_j^p are constants and H_p and J_p are non-negative integers.

The aforementioned form of higher order boundary conditions (1.2) is more general and comprises particular forms as elastic membranes and plates type boundaries, that have been used in literature by several authors in different physical situations for instance see, [35–37].

1.2   Literature Overview

A fluid-structure coupled system composed of flexible walls and fluid space is extensively found in structural acoustics, elasticity, water wave theory and aero-acoustics, for instance see [38–45]. The physical insight of the interaction between the surface vibrations and sound field of cavity, and the scattering phenomenon are important to control the noise of aero-engines, heating, ventilation and air conditioning (HVAC) system of buildings, and other engineering structures [104–109, 111]. Recently. the rectangular panel cavity coupled systems have been discussed in the context of active noise control measures. For instance, Pan and Bies [110] studied acoustics of cavity-panel coupled system to investigate theoretically the panel characteristics of the enclosure. Likewise, Kim and Brennan [55] focused on the rectangular cavity comprising five rigid surfaces and a flexible plate, and analyzed the acoustic attenuation of the enclosure in the presence of piston source and/or point-force acoustic attenuator experimentally as well as theoretically. Ming and Pan [56] considered the acoustical enclosure, and discussed about the interaction of inside sound and structural vibration to analyze the insertion loss of enclosed cavity. More recently, Du et al. [57] investigated vibro-acoustic coupled system of flexible panels and developed a generalized approach for the analysis of three-dimensional model containing elastically restrained boundary conditions. The aforementioned studies are mainly established on the basis of so-called modal coupling theory [58], wherein the structure and fluid-borne modes are determined from a priori solution, and then the system response is found through the evaluation of the spatial coupling coefficients. However, this approach is inappropriate for the cases involving strong coupling conditions, such as the system of thin flexible surfaces including various edge conditions or heavy material medium (water or

oil). Moreover, the continuity conditions on coupling interface cannot be satisfied with modal coupling theory, for more detail see [59, 60, 110]. On the other hand, the analysis of fluid-structure coupled waves in non-planar ducts or channels is challenging as well as important subject with a diverse range of applications in structural acoustics, water wave theory, seismological waves through lyres of rocks, and noise reduction problems etc. The motivation behind is the necessity to model and understand the scattering behavior, in channels or guiding structures, with the help of which the structural vibrations and related issues could be addressed. In general, the analytical approaches are found useful in obtaining the solution of the boundary value problems involving flexible components (higher order derivative involving boundary conditions) such as elastic membranes, plates or vibrating elastic shells. A range of such physical situations can be modeled to the boundary value problems (BVPs) that are solvable with the analytical methods like Wiener-Hopf (WH) technique or variety of Fourier integral and/or Greens theorem-based approaches, for instance see [83–90].

The physical problems of this category may comprise of variation in the material properties of its boundaries (multi-part boundary conditions) but have geometrically continuous structures. However, if the modeled configurations involve discontinuities in their geometry, the use of classical WH technique is not appropriate. Furthermore, such analytical techniques are not always easily generalized, see for instance [115]. Huang [111] considered thin elastic membranes backed by slender cavities to achieve the better performance of reactive device at low to medium frequencies. He applied a Fourier transform based approach to analyze the fluid-membrane coupled system. Warren at al [112] considered a rigid bridging height discontinuity in an elastic membrane bounded waveguide, and analyzed the physical insight of the structure by using the mode-matching (MM) technique. Also, for the continuous waveguide (without bridging height), they compared their MM results with Wiener-Hopf (WH) approach. The MM approach followed in [112] was different from classical approach, and involves the non-Strum-Louisville (SL) systems. They applied generalized orthogonality conditions to match the pressure and velocity fields at the interface. The characteristics of eigen-sub-systems of

fluid-membrane or fluid-plate coupled systems are different from the traditional eigen-sub-systems, and are classified in [113]. The eigenfunctions are linearly dependent, and the development and implication of generalized orthogonality conditions is indispensable to ensure the point wise convergence eigen-sub-systems. Subsequently, the physical problems comprising fluid-membrane/plate coupling have been addressed by many authors via MM technique together with the generalized orthogonality conditions as suggested by Lawrie [113], see for instance [114–119].

The mode-matching methods that are based on the matching of pressure and velocity modes at some interface, have proved a viable tool to resolve the planar and non-planar configurations [115–120]. This technique is conceptually simpler that often yields a linear algebraic system to solve rather than the Fourier integrals as obtained with the application of WH technique or Green' function methods. Nevertheless, the mode-matching technique (MMT) is only effective if the eigenfunctions form a set of orthogonal bases or the matrix of a linear algebraic system is diagonally dominant. The eigen-sub-systems corresponding to the orthogonal basis functions are classified as Strum-Liouville type. Lawrie in [113] showed that if the BVPs are governed with Helmholtz or Laplace type of equation and comprise flexible boundaries (second or higher order derivative involving boundaries), the eigenfunctions do not satisfy the usual orthogonal properties. In these cases, the separation of variable method corresponds the eigenfunctions that satisfy the generalized orthogonality relation and are linearly dependent. The orthogonality relations are utilized in the process of implementation of matching conditions. The application of the generalized orthogonality relations governs additional constants. These constants are evaluated through the edge conditions which make the linear combinations of the eigenvectors to be zero.

The advanced mode-matching method works well for the BVP containing horizontal membranes or elastic plates and having rigid, soft or impedance typed conditions at interface. But if the physical problem involves vertical higher order boundaries such as bridging elastic membrane or plate, this procedure fails. Recently, Lawrie and Afzal [120] have applied mode-matching technique (MMT) in

connection with the Galerkin and tailored-Galerkin methods to discuss the scattering effects of fluid-structure coupled waves of bridging membrane. Their adopted Galerkin scheme is based upon the assumptions of appropriate basis functions, which may vary with the variation of conditions on the physical problem. Further, for some conditions the eigenvalues cannot achieved explicitly and must be obtained numerically through some root finding algorithm. This approach is very well established and has been extensively applied in literature, see for instance [98–100]. The main disadvantage of first technique is the assumption of appropriate orthogonal basis that changes with the variation of edge conditions on the bridging height. On the other hand, the second approach contains a unique description for all set of edge conditions but has high computational cost. The reason behind the computational cost is the slow convergence rate of sums which appear with the imposition of edge conditions and that depend upon the non-orthogonal modes of semi-infinite region.

Moreover, the aforementioned problems can be analyzed physically by using the Low Frequency Approximation (LFA). This approach is well known, see for example [114] and [101, 102], especially in low frequency regime, wherein the contributions from the fundamental and/or next mode are significant. This approximation relies on the limited number of modes whose selection is subjected to the number of physical conditions. The scheme is not useful on higher frequencies and/or in the cases whereby the information about the higher modes is required.

1.3 Objective and Physical Problems

The present dissertation addresses problems including the modeling of fluid-structure coupled waves through the elastic structures bounding fluid space and their scattering from geometric and material discontinuities.

The subject is challenging as well as interesting, and have gained much attention of engineers and scholars. The envisaged problems are mathematically complex that contain non-Strum-Louisville systems, flexible bridging heights along with different edge conditions and multiple interface conditions. Further, these problems

include different bridging flexible height discontinuities instead of a bridging membrane or rigid height as assumed by Lawrie and Afzal [119]. In the present thesis, a class of such problems with ongoing and some new forms of mode-matching techniques including Galerkin, tailored-Galerkin and modal approaches to encounter the vibrational response of bridging flexible height, are addressed. Further, the low frequency approximation for certain cases to compare the results in low frequency regime is developed. Following physical problems are addressed in this dissertation:

1. 1. Acoustic scattering through a membrane bounded cavity comprising acoustically rigid extended inlet and outlet. The problem is solved through the extended form of mode-matching technique.

2. 2. Analysis of fluid-structure coupled wave scattering from a bridging-membrane junction by using a tailored-Galerkin approach, and its comparison in low frequency regime with low frequency approximation.

3. 3. Silencing performance of a membrane cavity connected with elastic plates bounded inlet and outlets with different edge conditions.

4. 4. The modeling of fluid-structure coupled response of the elastic structures bounding fluid space and their scattering from geometric and material discontinuities.

1.4   Outline of the Thesis

The dissertation outlines are as follows.

Chapter 2:   This chapter introduces some preliminaries concepts and definitions that are useful in understanding the work presented in rest of the chapters.

Chapter 3: In this chapter scattering of fluid-structure coupled waves in a wave-bearing cavity is discussed. The cavity consists of horizontal as well as vertical elastic boundaries and filled with a compressible fluid. To incorporate the vibrational response of the vertical elastic boundaries with different edge conditions, the mode-matching technique is extended by tailored-Galerkin and Galerkin procedures. It is found that in mode-matching tailored-Galerkin (MMTG) method, a unique general description of the displacement of vertical elastic component can deal a variety of edge conditions. Whereas, the mode-matching Galerkin (MMG) technique relies upon the orthogonal basis a priori whose description varies by changing the edge conditions of vertical elastic components. Accordingly, for spring-like conditions the eigenvalues cannot be expressed explicitly and must be found numerically. The eigen modes of the cavity region satisfy the generalized orthogonal conditions which ensure the point-wise convergence of MMTG and MMG approaches.

Moreover, the truncated MMTG and MMG solutions reconstruct the matching conditions as well as satisfy the conserved power identity. It confirms the accuracy of performed algebra and retained solutions. From the numerical results it is found that by varying the conditions on the edges of bridging elastic components, the stop-bands can be enhanced and shifted as well as broadened over the certain frequency regimes. The contents of this chapter are published in Mathematics and Mechanics of Solids journal.

Chapter 4: This chapter discusses the reflection and transmission of fluid-structure coupled waves through a membrane bounded cavity. The vertical walls of the cavity at the junctions are assumed to be the rigid plates or the elastic membranes. The problem with rigid vertical plates is amenable by following the traditional Mode-Matching technique (MMT). However, if the rigid vertical plates at junctions are replaced with elastic membranes, the standard mode-matching procedure fails. Alternatively, the mode-matching tailored-Galerkin (MMTG) approach is developed. In this approach, the Galerkin technique to express the displacements of the bridging membranes is adopted. The method chosen herein

provides a unique description of displacements to cater a verity of edge conditions on the joints of vertical membranes. The Low frequency approximation (LFA) which valid only in low frequency regime, for the rigid plates and membrane heights is formulated and compared. To analyze the scattering behavior, two types of incidents forcing; structure-born mode and fluid-born mode are assumed. It is found that the material properties of vertical surfaces of the cavity at junctions as well as the selection of edge conditions in case of vertical membranes significantly affect the scattering powers and the transmission loss. The contents of this chapter are published in Wave in Random and Complex Media.

Chapter 5: This chapter discusses the application of Galerkin and tailored-Galerkin procedures to model the vibrational response of a membrane bounded cavity connected to the elastic plates with different types of edge conditions. The plates contain clamped or pin-jointed type of edge conditions on finite edges, whilst the membranes are assumed to contain fixed, free or spring-like edge conditions. Both Galerkin and tailored-Galerkin techniques require the priori solutions to determine the displacements of bridging membranes. In the first approach, the priori solution is expressed in terms of Fourier series which changes by varying the conditions on the edges of membranes. However, in late approach, a unique description of displacements can address a variety of edge conditions. The accuracy of these approaches is confirmed through the satisfaction of conserved power identity and through the reconstruction of matching condition with the truncated form of the solutions. In the modeled configuration, the vibrational energy propagates along the walls as well as through the fluid, and is affected by the variation of edge conditions. Moreover, the role of edge conditions is significant for structure-borne radiation only and is negligible for fluid-borne radiations. The contents of this chapter are submitted in Vibration and Control journal for possible publication.

Chapter 6: This chapter investigates the traveling waveform in a flexible waveguide bounded by elastic plates containing a wave-bearing expansion chamber with clamped or pin-jointed connections at the junctions, whereby the bridging

elastic plates are introduced to connect the inlet/outlet to the expansion chamber. The bridging elastic plates may comprise a variety of the edge conditions on the joints such as clamped, pin-jointed or pivoted. The configuration is exited with the structure as well as fluid-born mode to analyze the influence of the imposed edge conditions and interface conditions on attenuation. To model the response of bridging elastic plates a comparison analytical/semi-analytical technique is given. These techniques are mainly based upon the mode-matching procedure in connection with Galerkin concept with variation of priori assumptions. These priori solutions can be orthogonal as well non-orthogonal bases functions. The contents of this chapter are submitted in Journal of Acoustical Society of America journal for possible publication. Finally, a brief summary, concluding remarks and future work are presented in Chapter-7.

Chapter 2

Preliminaries

This chapter depicts the fundamental concepts that are relevant to understand the propagation and scattering of acoustic wave in waveguides containing flexible boundaries with different set of edge conditions. The acoustic problems are governed with linear acoustic wave equation and different types of boundary conditions. The boundary conditions are considered to be: rigid, elastic membrane and elastic plate. The physical problems are governed by Helmholtz's or Laplace equation and having boundary conditions rigid, soft or impedance type underlie SL category, thereby the appearing eigenfunctions are linearly independent and satisfy the standard orthogonality conditions (for more details, see for instance [125, 126]. The orthogonality conditions help to recast the differential system to linear algebraic system during the matching analysis which is discussed in ongoing chapters of the thesis. On the other hand if the problem is governed by Helmholtz's or Laplace equation and involve higher order boundary conditions such as membrane or plate, the governing eigenfunctions do not satisfy standard orthogonality conditions, and thus the generalized orthogonality conditions are discussed. In more general form the development of such orthogonality conditions is explained in [113]. The associated eigenfunctions are linearly dependent and satisfy the generalized orthogonality conditions. The detail of these conditions are explained in this chapter. This chapter is organized in the following manners as: Section 2.1 is dedicated to the mathematical derivation of the acoustic wave

equations. Non-dimensional settings are illustrated in Section 2.3. The different types of boundary conditions are presented in Section 2.2. and the travelling wave formulation is presented in Section 2.4. The generalized orthogonality relations for flexible boundaries such as elastic plate and membrane are derived in section 2.5. The Mode-Matching technique, Low-Frequency Approximation, energy fluxes and transmission loss are explained in Section 2.6, Section 2.7, Section 2.8 and Section 2.9, respectively.

2.1   Linear Acoustic Equation

The linear acoustic wave equation defines the propagation of pressure fluctuation in the fluid medium. The mathematical formulation of the acoustic wave equation in a fluid can be obtained with following assumptions [127].

- The fluid is stationary.

- Fluid is compressible.

- The fluid flows under adiabatic conditions.

Conservation of mass: The fluid mass is conserved and that can be found through continuity equation.

$$\frac{\partial \rho}{\partial t} + \nabla \cdot (\rho \mathbf{v}) = 0, \tag{2.1}$$

where ρ is the mass density and $\mathbf{v}$ be the velocity of moving mass.

Conservation of momentum: The linear momentum is conserved and can be obtained as

$$\rho \left(\frac{\partial \mathbf{v}}{\partial t} + (\mathbf{v} \cdot \nabla)\mathbf{v} \right) = -\nabla p, \tag{2.2}$$

where p represent the fluid pressure. The quantities ρ, v_0 and p have constant values when fluid is stationary such that $\rho = \rho_0$, $v = 0$ and $p = p_0$. For acoustic propagation we assume small perturbation in the fluid and write the linear

approximation of the quantities ρ, v and p as

$$\rho = \rho_0 + \rho' + \dots,$$

$$\mathbf{v} = \mathbf{v}' + \dots$$

$$p = p_0 + p' + \dots. \tag{2.3}$$

where the higher order product of fluctuation are neglected, linearized (2.1)-(2.2) with the aid of (2.3), differentiating partially the obtained equation of continuity with respect to t and taking gradient of linearized momentum equation then on subtraction, it is found as

$$\frac{\partial^2 \rho'}{\partial t^2} - \nabla^2 p' = 0. \tag{2.4}$$

Assuming the barotropic flow i.e., the flow in which pressure is function of density alone $p = p(\rho)$ and using the Taylor's series expansion, it is obtained as

$$p' = \frac{\partial p}{\partial \rho}(\rho_0)p' \tag{2.5}$$

where, $c^2 = \frac{\partial p}{\partial \rho}(\rho_0)$ is taken to be as speed of sound, substituting (2.5) into (2.4), we obtained

$$\frac{1}{c^2}\frac{\partial^2 p'}{\partial t^2} - \nabla^2 p' = 0. \tag{2.6}$$

The equation (2.6) is known as acoustic wave equation in term of pressure. Throughout this dissertation we are looking for steady harmonic solutions. It is useful to develop the wave, membrane and elastic plates equations in the above mentioned form.

For this purpose we assume that $p'(x,y,t) = p(x,y)e^{-i\omega t}$ and $V'(x,y,t)e^{-i\omega t}$, where ω is the radian frequency, using the above substitution in the wave equation (2.6), we obtained

$$\left(\frac{\partial^2}{\partial x^2} + \frac{\partial^2}{\partial y^2} + k^2 \right) p = 0. \tag{2.7}$$

The equation (2.7) is known as Helmholtz's equation, it is useful to express pressure in form of field potential $\Psi(x,y,t) = \psi(x,y)e^{-i\omega t}$, where

$$p = -\rho_0 \frac{\partial \Psi}{\partial t} \quad \text{and} \quad v = \nabla \Psi \tag{2.8}$$

Substituting (2.8) into (2.7), we get

$$\left(\frac{\partial^2}{\partial x^2} + \frac{\partial^2}{\partial y^2} + k^2 \right) \psi = 0, \tag{2.9}$$

the equation (2.9) is known as Helmholtz's equation in the form of field potential.

2.2 Boundary Conditions

The boundary conditions play an important role in determining the mathematical solutions of physical problems. The nature and types of boundary conditions depend on the conditions assumed while modeling the physical problems. In acoustic, "reaction of the surface to sound" can be expressed in terms of boundary conditions and that describes the behavior of sound in the neighborhood of a bounding surface. The present study describes acoustic analysis of waveguides having different geometrical and bounding characteristics. Following types of boundary conditions are considered.

2.2.1 Rigid Boundary Condition:

In acoustic if a boundary Ω do not support support vibration is known as rigid boundary. The given surface is acoustically rigid if $Z \to \infty$, and that reveals from (2.6), that can be written as

$$\hat{n}.v = 0 \qquad \text{on } \Omega \tag{2.10}$$

where $\hat{n}$ is out ward drawn normal to boundary Ω. The rigid boundary conditions (2.15) in the form of field potential using harmonic time dependence can be expressed as

$$\frac{\partial \psi}{\partial y} = 0, \tag{2.11}$$

where ψ is harmonic time dependence field potential.

2.2.2 Flexible Boundary Condition

In acoustic if a boundary Ω support vibrations along the surface, the boundary is known as flexible boundary. In this dissertation, we have considered elastic membrane and elastic plate boundaries both of these support vibrations. Also the membrane and plates walls are considered horizontal and vertical direction

- **Membrane Boundary**

To formulate the elastic membrane condition it is assumed that the tensile stress is same at every point on the membrane and at every orientation of the line element perpendicular to the membrane surface. Such membranes are deformable like a sheet of rubber and that contain wave behavior similar to the waves on assemblage of flexible strings. Therefore, the tensile stress of the membrane can be referred as tension (T), and the wave equation for membrane can be found in many text, for instance [127]. For membrane condition coupled with compressible fluid, the dimensional displacement $W(x, y, t)$ satisfies the equation of motion.

$$\frac{\partial^2 W}{\partial \zeta^2} - \frac{1}{c_m^2} \frac{\partial^2 W}{\partial t^2} = \frac{1}{T} [p]_-^+, \tag{2.12}$$

where ζ is either replaced by variable x or y, if $\zeta = x$ then (2.12) represent the horizontal elastic membrane boundary, whereas in case when $\zeta = y$ the equation (2.12) denotes the vertical elastic membrane boundary. Also here $c_m = \sqrt{T/\rho_m}$ specifies the sound's speed on membrane having mass density ρ_m. The quantity $[p]_-^+ = [p]^+ - [p]^-$ on the right hand side of the (2.12) denotes the fluid pressure difference across the membrane surface. Using the harmonic time dependence as addressed in section 2.1 the harmonic time dependent membrane boundary conditions in the form of field potential can be expressed as

$$\left[\frac{\partial^2}{\partial x^2} + \frac{\omega^2}{c_m^2} \right] \frac{\partial \psi}{\partial y} = \frac{\omega^2 \rho_0}{T} [\psi]_-^+, \tag{2.13}$$

where c_m is speed of sound on membrane boundary and T denotes the membrane tension. The quantities ρ_0 represents the density of membrane.

- **Elastic Plate Boundary**

A plate is a solid body bounded by two surfaces. The distance between the two surfaces defines the thickness of the plate, which is assumed to be small compared to the lateral dimensions, such as the length and width in the case of a rectangular plate and the diameter in the case of a circular plate. The vibration of plates play an important role in the study of structural acoustic. The theory of elastic plates is an approximation of the three-dimensional elasticity theory to two dimensions, and that permits a description of the deformation in the plate along the mid plane of the plate. Moreover, it is assumed that Young's modulus, Poisson ratio and area density vary across the plate in one direction. The governing equation of the plate in the form of dimensional plate displacement $W_1(\zeta, t)$ coupled with compressible fluid is expressed below while the details pertaining to the derivation of the plate equation is given in [124].

$$\frac{\partial^4 W_1}{\partial \zeta^4} + \frac{2B'(\zeta)}{B(\zeta)} \frac{\partial^3 W_1}{\partial \zeta^3} + \frac{B''(\zeta)}{B(\zeta)} \frac{\partial^2 W_1}{\partial \zeta^2} + \frac{\rho_p}{B(\zeta)} \frac{\partial^2 W_1}{\partial t^2} = -[p]_-^+, \qquad (2.14)$$

where ρ_p is the mass density of the plate, $[p]_-^+$ is the fluid pressure difference across the plate and B is the bending stiffness. For constant bending stiffness and area density, (2.14) leads to

$$\frac{\partial^4 W_1}{\partial \zeta^4} + \frac{\rho_p}{B(\zeta)} \frac{\partial^2 W_1}{\partial t^2} = -[p]_-^+. \qquad (2.15)$$

Here, in above equations the quantity ζ is either x or y, $\zeta = x$ is horizontal elastic plate boundary and $\zeta = y$ represents vertical elastic plate boundary. The elastic plate boundary condition in the form of field potential with the aid of harmonic time dependence can be written as

$$\left[\frac{\partial^4}{\partial x^4} + \frac{\rho_p \omega^2}{B(x)} \right] \frac{\partial \psi}{\partial y} = \frac{\omega^2 \rho_0}{B(x)} \psi, \qquad (2.16)$$

where the quantities ρ_p and B represents the density and the bending stiffness of elastic plate that is express as $B = Eh^3/12(1 - \nu^2)$, in which E and ν are Young's modulus and Poisson's ratio respectively.

2.3 Non-Dimensional Setting

The governing Helmholtz equation and the boundary conditions such as rigid, membrane and elastic plates in dimensional setting can be expressed as

$$(\frac{\partial^2}{\partial \bar{x}^2} + \frac{\partial^2}{\partial \bar{y}^2} + k^2)\bar{\Psi} = 0, \tag{2.17}$$

$$\left[\frac{\partial^2}{\partial \bar{x}^2} + \frac{\omega^2}{c_m^2}\right] \frac{\partial \bar{\Psi}}{\partial \bar{y}} = \frac{\omega^2 \rho_0}{T} \left[\bar{\Psi}\right]_{-}^{+}, \tag{2.18}$$

and

$$\left[\frac{\partial^4}{\partial \bar{x}^4} + \frac{\rho_p \omega^2}{B(\bar{x})}\right] \frac{\partial \bar{\Psi}}{\partial \bar{y}} = \frac{\omega^2 \rho_0}{B(\bar{x})} \bar{\Psi} \tag{2.19}$$

respectively. With the non-dimensional setting, the equations and boundary conditions of the boundary value problems are appeared in dimensionless form, where all mathematical laws and rules are easily applicable.

Thus, for making the physical quantities dimensionless in the mathematical modeling of the physical problems, the dimensionless settings, with respect to the typical scale k^{-1} (length scale) and ω^{-1} (time scale), are framed in the following way

$$x = k\bar{x}, \qquad y = k\bar{y} \qquad \text{and} \qquad t = \omega \bar{t}. \tag{2.20}$$

On using the above transformation, we have

$$\frac{\partial^2}{\partial \bar{x}^2} = k^2 \frac{\partial^2}{\partial x^2}, \quad \frac{\partial^2}{\partial \bar{y}^2} = k^2 \frac{\partial^2}{\partial y^2} \quad \text{and} \quad \bar{\Psi}(\bar{x}, \bar{y}) = \frac{\omega^2}{k^2} \psi(x, y). \tag{2.21}$$

By using non-dimensional settings, Helmholtz's equation (2.17) can be expressed in dimensionless

$$\left(\nabla^2 + 1\right) \psi(x, y) = 0. \tag{2.22}$$

Any solution of this equation has to comply with the acoustical properties of the boundary. Similarly, the non-dimensionalized form of the rigid, elastic membrane and elastic plate boundaries can be obtained from (2.20)-(2.21) as under

$$\frac{\partial \psi}{\partial y} = 0 \tag{2.23}$$

$$\left[\frac{\partial^2}{\partial x^2} + \mu^2\right] \frac{\partial \psi}{\partial y} = \alpha \left[\bar{\psi}\right]_-^+, \tag{2.24}$$

and

$$\left[\frac{\partial^4}{\partial x^4} - \mu_1\right] \frac{\partial \psi}{\partial y} = \alpha_1 \psi^- \tag{2.25}$$

respectively. Where, the parameters α, α_1, μ and μ_1 represent the fluid loading parameter and the in *vacuo* wavenumber for both membrane and plate respectively, here $\mu = c/c_m$ and $\alpha = c^2\rho_0/(kT)$ are the expressions for the elastic membrane parameters. The value of the elastic plates parameters μ_1 and α_1 can be expressed as under

$$\mu_1 = 4\sqrt{\frac{c^2 h \rho_p}{Bk^2}} \qquad \alpha_1 = \frac{c^2 \rho}{Bk^3}. \tag{2.26}$$

2.4 Travelling Wave Formulation

The solution of non-dimensional Helmholtz's equation (2.22) by separation of variable method is known as travelling wave solution that can be expressed as

$$\psi(x,y) = \sum_{n=0}^{\infty} \mathcal{B}_n Y_n(y) e^{\pm i\nu_n x}, \tag{2.27}$$

where $Y_n(y); n = 0, 1, 2...$ denote the eigenfunction expansions, $\mathcal{B}_n$ are the amplitudes of that n^{th} mode and ν_n is the wavenumber of nth propagating mode.

2.5   Orthogonality Relations

The physical problems considered in this thesis are solved by the matching techniques. These techniques rely on the formulation of field potentials in terms of eigenfunction expansions and then utilizing the orthogonal characteristics underlying eigen subsystems.

The eigenfunctions of the problems governed with Helmholtz's equation and having conditions to be Dirichlet, Neumann or Robin's types undergoes Strum-Lioullie (SL) category and satisfy usual orthogonality conditions.

However, if the problem governed by Helmholtz's equation and comprises higher order boundary conditions the eigen system is of non- Strum-Lioullie type and satisfies generalized orthogonality conditions. To determine the form of generalize orthogonality relation used in this thesis we assume the eigenfunction ansatz (2.27)

2.5.1   Orthogonality Relation for Membrane

For a duct bounded between walls, with rigid condition at $y = a$ and having membrane boundary conditions at $y = b$ the eigen subsystem can be found as

$$Y_n^{''}(y) - s_n^2 Y_n(y) = 0, \tag{2.28}$$

$$Y_n^{'}(a) = 0, \tag{2.29}$$

$$(s_n^2 + 1 - \mu^2)Y_n^{'}(b) - \alpha Y_n(b) = 0, \tag{2.30}$$

To established the generalized orthogonality relation for underlying eigen system we multiplying (2.28) by $Y_m(y)$ and integrating from a to b gives:

$$\int_a^b Y_n(y)Y_n^{''}(y)dy = s_n^2 \int_a^b Y_n(y)Y_m(y)dy, \tag{2.31}$$

after integrating left hand side of (2.31) using by parts rule, we obtain

$$\int_a^b Y_n^{''}(y)Y_m(y)dy = \left[Y_n^{'}(y)Y_m(y)\right] - \left[Y_n(y)Y_m^{'}(y)\right] + \int_a^b Y_m^{''}(y)Y_n(y)dy$$

$$= Y_m(b)Y_n^{'}(b) - Y_m^{'}(b)Y_n(b) + \int_a^b Y_m^{''}(y)Y_n(y)dy$$

$$= \frac{Y_n^{'}(b)Y_m^{'}(b)}{\alpha}\left(s_m^2 - s_n^2\right) + s_m^2\int_a^b Y_n(y)Y_m(y)dy. \qquad (2.32)$$

Substituting (2.32) into (2.31) gives:

$$(s_n^2 - s_m^2)Y_n^{'}(b)Y_m^{'}(b) + \alpha(s_n^2 - s_m^2)\int_a^b Y_n(y)Y_m(y)dy = 0 \qquad (2.33)$$

If $m \neq n$ then the above equation implies that

$$Y_n^{'}(b)Y_m^{'}(b) + \alpha\int_a^b Y_n(y)Y_m(y)dy = 0 \qquad (2.34)$$

Consequently, if $m = n$ then (2.33) yields

$$En = [Y_n^{'}(')]^2 + \alpha\int_a^b Y_n^2(y)dy. \qquad (2.35)$$

On combining (2.34) and (2.35), we have

$$Y_n^{'}(b)Y_m^{'}(b) + \alpha\int_a^b Y_n(y)Y_m(y)dy = \delta_{mn}E_n, \qquad (2.36)$$

Hence, the property (2.35) and (2.36) is concluded to generalized orthogonality relation for the flexible waveguide bounded by membrane.

2.5.2 Orthogonality Relation for Elastic Plate

In this section, we consider a flexible waveguide model that is bounded above by an elastic plate and bounded below by a rigid wall. The model problem is governed by Helmholtz's equation (2.22) together with boundary conditions (2.23) and (2.25) which yields

$$Y_n^{''}(y) - s_n^2 Y_n(y) = 0, \tag{2.37}$$

$$Y_n^{'}(a) = 0, \tag{2.38}$$

$$\{(s_n^2 + 1)^2 - \mu_1^4\}Y_n^{'}(b) - \alpha_1 Y_n(b) = 0. \tag{2.39}$$

To develop the generalized orthogonality relation for plate bounded duct we proceed as. On multiplying (2.37) with $Y_m(y)$, we get

$$\int_a^b Y_n(y)Y_n^{''}(y)dy = s_n^2 \int_a^b Y_n(y)Y_m(y)dy, \tag{2.40}$$

after integrating by parts the left hand side of of (2.40), we find

$$\int_a^b Y_n^{''}(y)Y_m(y)dy = \left[Y_n^{'}(y)Y_m(y)\right] - \left[Y_n(y)Y_m^{'}(y)\right] + \int_a^b Y_m^{''}(y)Y_n(y)dy$$

$$= Y_m(b)Y_n^{'}(b) - Y_m^{'}(b)Y_n(b) + \int_a^b Y_m^{''}(y)Y_n(y)dy$$

$$= \frac{Y_n^{'}(b)Y_m^{'}(b)}{\alpha}\left(s_m^2 - s_n^2\right) + s_m^2 \int_a^b Y_n(y)Y_m(y)dy. \tag{2.41}$$

Substituting (2.32) into (2.31) gives:

$$(s_n^2 - s_m^2)Y_n^{'}(b)Y_m^{'}(b) + \alpha(s_n^2 - s_m^2)\int_a^b Y_n(y)Y_m(y)dy = 0 \tag{2.42}$$

If $m \neq n$ then the above equation implies that

$$Y_n^{'}(b)Y_m^{'}(b) + \alpha \int_a^b Y_n(y)Y_m(y)dy = 0 \tag{2.43}$$

Consequently, if $m = n$ then (2.33) yields

$$En = [Y_n^{'}(')]^2 + \alpha \int_a^b Y_n^2(y)dy. \tag{2.44}$$

On combining (2.43) and (2.44), we have

$$Y_n^{'}(b)Y_m^{'}(b) + \alpha \int_a^b Y_n(y)Y_m(y)dy = \delta_{mn}E_n, \tag{2.45}$$

Hence, the property (2.44) and (2.45) is concluded to generalized orthogonality relation for the flexible waveguide bounded by elastic plate.

2.5.3 Properties of Eigenfunctions for Elastic Membrane

The eigen system in case of flexible membrane has well recognized properties [45] that are explained as

- The eigenfunctions $Y_n(y)$, $n = 0, 1, 2, 3...$, for flexible duct bounded by membrane are linearly dependent that satisfy

$$\sum_{n=0}^{\infty} \frac{Y_n'(b)Y_n(y)}{E_n} = 0, \qquad a \leq y \leq b. \tag{2.46}$$

  It is important to note that the number of linearly dependent sum is taken half of the order of the membrane partial differential equation.

- The eigenfunctions also satisfy the identities for membrane bounded duct, that is

$$\sum_{n=0}^{\infty} \frac{[Y_n'(b)]^2}{E_n} = 1. \tag{2.47}$$

2.5.4 Properties of Eigenfunctions for Elastic Plate

The eigenfunctions $Y_j(\varrho_q, y)$, $j = 1, 2$ are linearly dependent and their properties are mentioned below [45]

$$\sum_{q=0}^{\infty} \Delta_{jq} Y_j(\varrho_q, y) = \sum_{q=0}^{\infty} \varrho_q^2 \Delta_j Y_j(\varrho_q, y) = 0, \qquad 0 \leq y \leq u \tag{2.48}$$

and

$$\sum_{q=0}^{\infty} \Delta_{jq}^2 \kappa_q = 0, \quad \sum_{q=0}^{\infty} \varrho_q^2 \Delta_{jq}^2 \kappa_q = 1, \qquad 0 \leq y \leq u, \tag{2.49}$$

where

$$\Delta_{jq} = \frac{Y_j'(\varrho_q, u)}{\kappa_q}. \tag{2.50}$$

The Green's function for the eigenfunctions can be constructed as [45]

$$\alpha_1 \sum_{q=0}^{\infty} \frac{Y_{jq}(\varrho_q, \upsilon) Y_{jq}(\varrho_q, y)}{\kappa_q} = \delta(y - \upsilon) + \delta(y + \upsilon) + \delta(y + \upsilon - 2u), \qquad -u \le \upsilon, \ y \le u,$$

(2.51)

where $\delta(y)$ is the usual Dirac delta function and this result shows that the eigenfunction expansion representation of a suitably smooth function, say $f(y)$, converges point-wise to that functions. In order to obtain the solution of acoustic scattering problems in ducts or channels, Mode-Matching technique is presented in next section.

2.6   Mode Matching Technique

Modal representation is generally opt to obtain the solution of acoustic waveguide problems. A single modal representation is only possible in segments of a duct with constant properties (diameter, wall impedance). When two segments of different properties are connected to each other, a modal representation can be used in each segment, but since the modes are different we have to reformulate the expansion of the incident field into an expansion of the transmitted field in the neighboring segment, using conditions of continuity of pressure and velocity.

This is called: "MM". Furthermore, these continuity conditions cannot be satisfied with a transmission field only, and a part of the incident field is reflected. Each mode is scattered into a modal spectrum of transmitted and reflected modes. The first step in the MM method entails the eigenfunction expansion of unknown fields in the individual duct-regions in terms of their respective modes. Since the functional form of the modes is known, the problem reduces to that of obtaining modal amplitudes related with the field expansions in different duct-regions of waveguide. The modal representation is followed by the implementation of the continuity conditions for the fields at the interfaces in the junction regions. This method, in conjunction with the standard or generalized orthogonality relations of the modes, eventually leads to an infinite system of linear simultaneous equations

for the unknown modal amplitudes. For further details on MM, we refer to [20]. In next section, we discuss the Low-Frequency Approximation technique.

2.7 Low Frequency Approximation

The low frequency approximation (LFA) is found useful but valid only in low frequency regime. In this technique, we consider only a finite number of modes and the resulting finite systems can be solved simultaneously through inversion. The complete methodology of this method is presented in Chapters 4, 5 and 6.

2.8 Energy Flux

The energy flux or power (P) provides the understanding about the physical aspect of scattering as well as a check on the accuracy of obtained solution. The formula to obtain energy flux through fluid medium is given in [38] as

$$P\rfloor_{\text{fluid}} = \text{Re}\left\{ i \int_a^b \psi \left(\frac{\partial \psi}{\partial x} \right)^* dy \right\}, \tag{2.52}$$

where superposed asterisk ($*$) specifies for complex conjugate. Accordingly, the mathematical form of energy flux propagating via elastic membrane and plate are given by

$$P\rfloor_{\text{memb}} = \text{Re}\left\{ \frac{i}{\alpha} \left(\frac{\partial \psi}{\partial y} \right) \left(\frac{\partial^2 \psi}{\partial x \partial y} \right)^* \right\} \tag{2.53}$$

and

$$P\rfloor_{\text{plate}} = \text{Re}\left\{ \frac{i}{\alpha_1} \left[\left(\frac{\partial^2 \psi}{\partial x \partial y} \right) \left(\frac{\partial^3 \psi}{\partial x^2 \partial y} \right)^* - \left(\frac{\partial \psi}{\partial y} \right) \left(\frac{\partial^4 \psi}{\partial^3 x \partial y} \right)^* \right] \right\}, \tag{2.54}$$

respectively. Note that by using (2.52)-(2.54), we may construct a conserve power identity based upon the law of conservation of energy and that may serve as a physical check on the accuracy of truncated solution. As well, the accuracy of the

silencer or waveguide are measured by transmission-loss (TL) that is expressed mathematically in next section.

2.9   Transmission Loss

The performance of any acoustic waveguide is generally testified with the opt of transmission-loss [113], that is

$$\text{TL} = -10 \log_{10} \left(\frac{P_t}{P_i} \right), \tag{2.55}$$

where, P_t stands for power transmitted, whilst P_i is for incident power through fluid.

Chapter 3

On the Extension of Mode Matching Procedure for Modeling a Wave-bearing Cavity

3.1   Introduction

The problem of rectangular wave-bearing cavity is presented in this chapter. The study describes a versatile form of tailored-Galerkin approach along with MM method to analyze the acoustic scattering through the rectangular flexible cavity containing different conditions on joints in rigid channel, with simpler and computationally more effective way. The cavity is composed of one finite flexible wall along x- direction and two finite flexible strips along the y-direction. The analytical expression depending upon the eigenvalues/eigenfunctions incorporates the fluid-structure interaction between the horizontal flexible component and inside fluid. However, to encounter the vibrational response of vertical flexible components, the tailored-Galerkin process is introduced. The displacements of vertical flexible components are defined in such a way that their homogeneous parts involve the material properties of elastic components, whilst their integral parts link the cavity vibrations. On the other hand, the Galerkin approach relies upon a

priori solution along vertical elastic components, that is chosen herein to be the orthogonal basis eigenfunctions. Both Galerkin and tailored-Galerkin solutions are obtained for the silencer containing wave-bearing cavity and rigid inlet/outlet.

This chapter is arranged in following sections.

The problem formulation is described in Section 1. The mode-matching solution accompanying with Galerkin and tailored-Galerkin approaches has been discussed in Sections 2 and 3. Numerical results and discussion on results are presented in Section 4. Finally, the concluding remarks are specified in Section 5.

3.2   Problem Formulation

A two-dimensional waveguide containing a wave-bearing chamber cavity and rigid extended inlet and outlet is assumed. The inside of the waveguide is filled with compressible fluid having mass density ρ and sound speed c. The physical configuration of the waveguide is shown in Fig. 3.1. In dimensional setting of coordinates
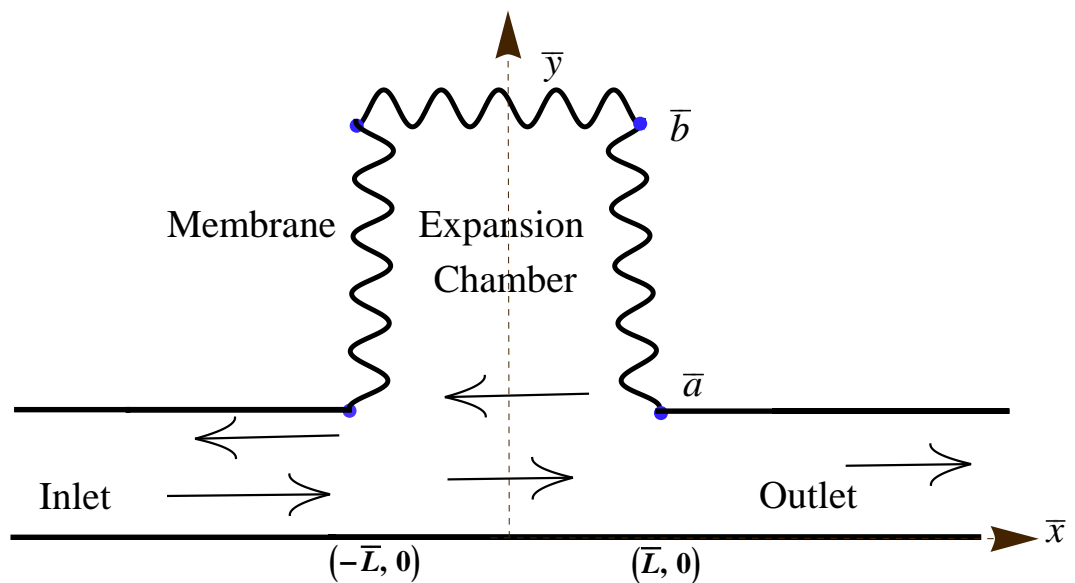
FIGURE 3.1: The physical configuration of waveguide.

the rigid surfaces are situated at $\bar{y} = \bar{0}$ and $\bar{y} = \bar{a}$, whereas, the elastic membrane located at $\bar{y} = \bar{b}$, $|\bar{x}| < \bar{L}$ is connected from its ends to vertical membranes lying along $\bar{x} = \pm\bar{L}$, $\bar{a} \leq \bar{y} \leq \bar{b}$. The other ends of the vertical membranes are connected to rigid horizontal surfaces at $(\bar{x}, \bar{y}) = (\pm\bar{L}, \bar{a})$. Note that overbars with variables here and henceforth denote the dimensional setting of coordinates.

The waveguide is radiated with the fundamental duct mode of extended inlet $\bar{x} < \bar{L}$ and the response is observed in the term of fluid potential $\bar{\Phi}(\bar{x}, \bar{y}, \bar{t})$. The harmonic time dependence $\exp(-i\omega\bar{t})$, where $\omega = ck$ is radial frequency in which k is wavenumber, is suppressed throughout, and the boundary value problem is non-dimensionalized with respect to the length scale k^{-1} and time scale ω^{-1}.

In waveguide regions the non-dimensional harmonic fluid potential $\psi(x, y)$ satisfy the Helmholtz equation

$$(\nabla^2 + 1)\psi(x, y) = 0, \tag{3.1}$$

where

$$\psi(x, y) = \begin{cases} \psi_1(x, y), & x < -L, \quad 0 \leqslant y \leqslant a \\ \psi_2(x, y), & |x| < L, \quad 0 \leqslant y \leqslant b. \\ \psi_3(x, y), & x > L, \quad 0 \leqslant y \leqslant a \end{cases} \tag{3.2}$$

The fluid potentials $\psi_1(x, y)$ and $\psi_3(x, y)$ in extended inlet and outlet, respectively, satisfy the acoustically rigid surfaces:

$$\frac{\partial \psi_1}{\partial y} = 0, \quad y = 0, a, \quad x < -L, \tag{3.3}$$

$$\frac{\partial \psi_3}{\partial y} = 0, \quad y = 0, a, \quad x > L. \tag{3.4}$$

The traveling wave solutions of extended inlet and extended inlet govern respectively the eigenfunction expansions

$$\psi_1(x, y) = e^{i(x+L)} + \sum_{n=0}^{\infty} A_n \cos(\frac{n\pi}{a}y)e^{-i\eta_n(x+L)} \tag{3.5}$$

and

$$\psi_3(x, y) = \sum_{n=0}^{\infty} D_n \cos(\frac{n\pi}{a}y)e^{i\eta_n(x-L)}, \tag{3.6}$$

where $\eta_n = \sqrt{1 - (n^2\pi^2)/a^2}$ be the wave number of nth propagating duct mode in extended inlet/outlet. Note that the first term in (3.5) denotes incident radiation, which is assumed to be the fundamental duct mode with unit amplitude. The eigenfunctions $\{\cos(\frac{n\pi}{a}y)\}$; $n = 0, 1, 2, \ldots$ in extended inlet/outlet are orthogonal and satisfy the usual orthogonality relation:

$$\int_0^a \cos(\frac{n\pi}{a}y)\cos(\frac{m\pi}{a}y)dy = \frac{a}{2}\delta_{mn}\epsilon_n, \qquad (3.7)$$

where δ_{mn} is the Kronecker delta and $\epsilon_n = 2$ if $n = 0$ and $\epsilon_n = 1$ otherwise. The wave-bearing cavity is bounded above with elastic membranes and below with acoustically rigid surface, that give

$$\frac{\partial\psi_2}{\partial y} = 0, \qquad\qquad y = 0, \quad |x| < L, \qquad (3.8)$$

$$\left(\frac{\partial^2}{\partial x^2} + \mu^2\right)\frac{\partial\psi_2}{\partial y} + \alpha\psi_2 = 0, \quad y = b, \quad |x| < L, \qquad (3.9)$$

$$\left(\frac{\partial^2}{\partial y^2} + \mu^2\right)\frac{\partial\psi_2}{\partial x} \pm \alpha\psi_2 = 0, \quad x = \pm L, \quad a \leqslant y \leqslant b. \qquad (3.10)$$

where $\mu = c/c_m$ in which c_m the sound speed on membrane and $\alpha = \omega^2\rho/(Tk^3)$ in which T the membrane tension are the dimensionless membrane wave number and the fluid loading parameter, respectively. In addition to the boundary conditions as stated in (3.8)-(3.10), edge conditions at the finite ends of horizontal and vertical membranes are imposed. These conditions define the physical behavior of membranes at joints as well as ensure the uniqueness of the solution. Their choices may be of fixed, free, spring-like edges or else depending upon the considered physical model and the aims of investigation. These conditions are stated in later sections. Equation (5.1) together with (3.8) and (3.9), yields the eigenfunction expansion of chamber cavity region as

$$\psi_2(x, y) = \sum_{n=0}^{\infty}(B_n e^{is_n x} + C_n e^{-is_n x})\cosh(\gamma_n y), \qquad (3.11)$$

where $s_n = \sqrt{\gamma_n^2 + 1}$ represents the wave number of nth duct mode of chamber cavity. Here the quantity γ be the roots of dispersion relation:

$$(\gamma^2 + 1 - \mu^2)\gamma \sinh(\gamma b) - \alpha \cosh(\gamma b) = 0. \tag{3.12}$$

There are infinite many values for which (3.12) holds, therefore, $\gamma \equiv \gamma_n$; $n = 0, 1, 2, \ldots$. These roots are found numerically and contain following properties [113]:

(i) For every γ_n, there is $-\gamma_n$.

(ii) There is a finite number of real roots (having $\text{Re}(\gamma) \neq 0$ and $\text{Im}(\gamma) = 0$) depending upon the polynomial factor involving (3.12).

(iii) There is an infinite number of imaginary roots (having $\text{Re}(\gamma) = 0$ and $\text{Im}(\gamma) \neq 0$.)

In order that eigenfunction expansion (3.11) converges, we consider only the real positive roots (i.e. $\text{Re}(\gamma) > 0$ and $\text{Im}(\gamma) = 0$ in complex $\gamma - plane$) and the imaginary positive roots (i.e. $\text{Re}(\gamma) = 0$ and $\text{Im}(\gamma) > 0$ in complex $\gamma - plane$).

These roots are arranged in such a way that the positive real roots appear first with descending order, and then the imaginary positive roots occur with increasing value of the imaginary part (ascending order with respect to imaginary part).

The eigenfunctions $Z_n(y) = \cosh(\gamma_n y), n = 0, 1, 2, \ldots$ associated with the eigenvalues γ_n; $n = 0, 1, 2, \ldots$ are non-orthogonal in nature and satisfy the following generalized orthogonality relation [113]:

$$\alpha \int_0^b \cosh(\gamma_m y) \cosh(\gamma_n y) dy = \delta_{mn} E_m - \gamma_m \gamma_n \sinh(\gamma_n b) \sinh(\gamma_m b), \tag{3.13}$$

where

$$E_m = \frac{\alpha b}{2} + \left(\frac{3\gamma_m^2 + 1 - \mu^2}{2\gamma_m^2} \right) (\gamma_m \sinh(\gamma_m b))^2. \tag{3.14}$$

Moreover, the eigenfunctions $Z_n(y), n = 0, 1, 2, \ldots$ are linearly dependent and their properties are mentioned below [25].

$$\sum_{n=0}^{\infty} \frac{[Z_n'(b)]^2}{E_n} = 0, \qquad \sum_{n=0}^{\infty} \frac{\gamma_n^2[Z_n'(b)]^2}{E_n} = 1. \tag{3.15}$$

In addition, the Greens function is constructed to ensure the convergence of emerging sums, that is

$$\alpha \sum_{n=0}^{\infty} \frac{Z_n(y)Z_n(\nu)}{E_n} = \delta(y - \nu) + \delta(y + \nu) + \delta(y + \nu - 2b), \qquad 0 \le \nu, \ y \le b, \tag{3.16}$$

where $\delta(.)$ is the Dirac delta function. These results are crucial to proving the point wise convergence of eigenfunction expansion representation (3.11). Note that the model amplitudes $\{A_m, B_m, C_m, D_m\}$; $m = 0, 1, 2, \ldots$ in the eigenfunction expansions defined by (3.5), (3.6) and (3.11), are unknowns. These are determined after using the matching conditions at the interfaces $x = \pm L$.

3.3 Mode Matching Formulation

Here the pressure and normal velocity modes are matched to determine the unknown modal coefficients. At interfaces $x = \pm L$, the continuity of pressures reveals

$$\int_0^a \psi_1(-L, y) \cos(\frac{m\pi}{a}y) dy = \int_0^a \psi_2(-L, y) \cos(\frac{m\pi}{a}y) dy, \tag{3.17}$$

$$\int_0^a \psi_3(L, y) \cos(\frac{m\pi}{a}y) dy = \int_0^a \psi_2(L, y) \cos(\frac{m\pi}{a}y) dy, . \tag{3.18}$$

On substituting the eigenfunction expansions (3.5)-(3.6) and (3.11) into (3.17) and (3.18), then by simplifying the emerging equations with the aid of respective orthogonality relations, after some rearrangements it is found that

$$\Phi_m^+ = -\delta_{m0} + \frac{4}{a\epsilon_m} \sum_{n=0}^{\infty} \chi_m^+ \cos(s_n L) R_{mn}, \tag{3.19}$$

$$\Phi_m^- = -\delta_{m0} - \frac{4i}{a\epsilon_m} \sum_{n=0}^{\infty} \chi_m^- \sin(s_n L) R_{mn}, \tag{3.20}$$

where $\Phi_m^{\pm} = A_m \pm D_m$ and $\chi_m^{\pm} = B_m \pm C_m$ for $m = 0, 1, 2, \ldots$ represent the amplitudes of symmetric/anti-symmetric modes propagating in extended inlet and outlet, respectively.

The quantity R_{mn} reveals the interaction of inlet/outlet modes with expansion chamber modes at interfaces and is defined by

$$R_{mn} = \int_0^a \cos(\frac{m\pi}{a}y) \cosh(\gamma_n y) dy. \tag{3.21}$$

Now the matching of the normal velocity modes is discussed. To incorporate the vibrational effects of vertical elastic membranes lying along $a \leq y \leq b$ at $x = \pm L$ two methods are developed in accompanying subsections.

3.3.1 Tailored-Galerkin Method

The fundamentals of this approach are linked with the assortment of trial functions which determine the response along the vertical boundaries and their edges. The dimensionless membrane displacements $w_1(y)$ and $w_2(y)$ satisfy

$$\frac{\partial^2 w_1}{\partial y^2} + \mu^2 w_1 = \alpha\psi_2, \quad x = -L, \quad a \leq y \leq b, \tag{3.22}$$

and

$$\frac{\partial^2 w_2}{\partial y^2} + \mu^2 w_2 = -\alpha\psi_2, \quad x = L, \quad a \leq y \leq b, \tag{3.23}$$

respectively. By solving (3.22) and (3.23) the membrane displacements are obtained as

$$w_1(y) = a_1 \cos(\mu y) + a_2 \sin(\mu y) + \alpha \sum_{n=0}^{\infty} \frac{\left(B_n e^{-is_n L} + C_n e^{is_n L}\right) \cosh(\gamma_n y)}{\gamma_n^2 + \mu^2}, \tag{3.24}$$

$$w_2(y) = a_3 \cos(\mu y) + a_4 \sin(\mu y) - \alpha \sum_{n=0}^{\infty} \frac{\left(B_n e^{is_n L} + C_n e^{-is_n L}\right) \cosh(\gamma_n y)}{\gamma_n^2 + \mu^2}. \tag{3.25}$$

Here quantities a_j, $j = 1, 2, 3, 4$ are unknown constants and that determine the physical behavior of vertical membranes at edges. These edges can be fixed, free

or spring-like. Here we calculate the solution by considering the spring-like edge conditions at $y = a$ and $y = b$ only, whereas, the solution with other combinations of edge conditions can be obtained through variation in the coupling constants ξ_1 and ξ_2.

Spring-like Edge Conditions at $y = a$

The spring-like edge conditions at $y = a$ with coupling constant $\xi_1 = k\bar{\xi}_1$ are defined by

$$\xi_1 w_1 + \frac{\partial w_1}{\partial y} = 0, \quad x = -L, \tag{3.26}$$

$$\xi_1 w_2 + \frac{\partial w_2}{\partial y} = 0, \quad x = L. \tag{3.27}$$

On invoking (3.24)–(3.25) into (3.26)-(3.27), and then the addition and subtraction of the resulting equations result

$$a_{13}^+(\xi_1 \cos(\mu a) - \mu \sin(\mu a)) + a_{24}^+(\xi_1 \sin(\mu a) + \mu \cos(\mu a))$$
$$= 2i\alpha \sum_{n=0}^{\infty} \frac{\chi_n^- \sin(s_n L)(\xi_1 \cosh(\gamma_n a) + \gamma_n \sinh(\gamma_n a))}{\gamma_n^2 + \mu^2}, \tag{3.28}$$

$$a_{13}^-(\xi_1 \cos(\mu a) - \mu \sin(\mu a)) + a_{24}^-(\xi_1 \sin(\mu a) + \mu \cos(\mu a))$$
$$= -2\alpha \sum_{n=0}^{\infty} \frac{\chi_n^+ \cos(s_n L)(\xi_1 \cosh(\gamma_n a) + \gamma_n \sinh(\gamma_n a))}{\gamma_n^2 + \mu^2}, \tag{3.29}$$

where $a_{13}^\pm = a_1 \pm a_3$ and $a_{24}^\pm = a_2 \pm a_4$ are constants.

Spring-like Edge Conditions at $y = b$

The spring-like edge conditions at $y = b$ containing coupling constant $\xi_2 = k\bar{\xi}_2$ are given by

$$\xi_2 w_1 + \frac{\partial w_1}{\partial y} = 0, \quad x = -L, \tag{3.30}$$

$$\xi_2 w_2 + \frac{\partial w_2}{\partial y} = 0, \quad x = L. \tag{3.31}$$

By substituting (3.24)–(3.25) into (3.30)-(3.31), and then by adding and subtracting the governing equations reveal

$$a_{13}^+(\xi_2 \cos(\mu b) - \mu \sin(\mu b)) + a_{24}^+(\xi_2 \sin(\mu b) + \mu \cos(\mu b))$$
$$= 2i\alpha \sum_{n=0}^{\infty} \frac{\chi_n^- \sin(s_n L)(\xi_2 \cosh(\gamma_n b) + \gamma_n \sinh(\gamma_n b))}{\gamma_n^2 + \mu^2}, \tag{3.32}$$

$$a_{13}^-(\xi_2 \cos(\mu b) - \mu \sin(\mu b)) + a_{24}^-(\xi_2 \sin(\mu b) + \mu \cos(\mu b))$$
$$= -2\alpha \sum_{n=0}^{\infty} \frac{\chi_n^+ \cos(s_n L)(\xi_2 \cosh(\gamma_n b) + \gamma_n \sinh(\gamma_n b))}{\gamma_n^2 + \mu^2}. \tag{3.33}$$

Now by solving (3.28), (3.29), (3.32) and (3.33) simultaneously, the values of unknowns $\{a_{13}^\pm, a_{24}^\pm\}$ are achieved. Once these quantities become known, the constants a_j, $j = 1, 2, 3, 4$ are obtained in straightforward way from the expressions:

$$a_1 = \frac{1}{2}(a_{13}^+ + a_{13}^-), \quad a_3 = \frac{1}{2}(a_{13}^+ - a_{13}^-), \tag{3.34}$$

$$a_2 = \frac{1}{2}(a_{24}^+ + a_{24}^-), \quad a_4 = \frac{1}{2}(a_{24}^+ - a_{24}^-). \tag{3.35}$$

From (3.28), (3.29), (3.32) and (3.33), it is noted that one can get the results with fixed, free and spring-like edges by setting $\xi_j \to \infty$, $\xi_j \to 0$ and $\xi_j \to 1$, respectively, where $j = 1, 2$.

In this way the contribution of different physical conditions at the joints may be incorporated in the responses of the vertical elastic boundaries. Whereas, to assimilate these responses in the guiding structure, the continuity of normal

velocities at $x = \pm L$ take the form

$$\frac{\partial \psi_2}{\partial x}(-L, y) = \begin{cases} \frac{\partial \psi_1}{\partial x}(-L, y), & 0 \leqslant y \leqslant a, \\ \\ w_1(y), & a \leqslant y \leqslant b, \end{cases} \tag{3.36}$$

$$\frac{\partial \psi_2}{\partial x}(L, y) = \begin{cases} \frac{\partial \psi_3}{\partial x}(L, y), & 0 \leqslant y \leqslant a, \\ \\ w_2(y), & a \leqslant y \leqslant b. \end{cases} \tag{3.37}$$

On substituting (3.5), (3.6), (3.11) and (3.24)-(3.25) into (3.36) and (3.37), and then by using the orthogonality relation (3.13), after some rearrangements it is found that:

$$\begin{aligned} \chi_m^- = &\frac{1}{2s_m G_m \cos(s_m L)} \{\gamma_m \sinh(\gamma_m b) E_{24}^+ + \alpha R_{0m}\} - \\ &\frac{1}{2s_m G_m \cos(s_m L)} \{\alpha \sum_{n=0}^{\infty} \Phi_n^- \eta_n R_{nm} - i\alpha a_{13}^+ P_{1m} - i\alpha a_{24}^+ P_{2m}\} \\ &- \frac{\alpha^2}{s_m E_m \cos(s_m L)} \sum_{n=0}^{\infty} \frac{\chi_n^- \sin(s_n L) T_{nm}}{\gamma_n^2 + \mu^2}, \end{aligned} \tag{3.38}$$

$$\begin{aligned} \chi_m^+ = &\frac{i}{2s_m G_m \sin(s_m L)} \{\gamma_m \sinh(\gamma_m b) E_{24}^- + \alpha R_{0m}\} - \\ &\frac{i}{2s_m G_m \sin(s_m L)} \{\alpha \sum_{n=0}^{\infty} \Phi_n^+ \eta_n R_{nm} - i\alpha a_{13}^- P_{1m} - i\alpha a_{24}^- P_{2m}\} \\ &+ \frac{\alpha^2}{s_m E_m \sin(s_m L)} \sum_{n=0}^{\infty} \frac{\chi_n^+ \cos(s_n L) T_{nm}}{\gamma_n^2 + \mu^2}, \end{aligned} \tag{3.39}$$

where

$$P_{1m} = \int_a^b \cos(\mu y) \cosh(\gamma_m y) dy, \tag{3.40}$$

$$P_{2m} = \int_a^b \sin(\mu y) \cosh(\gamma_m y) dy, \tag{3.41}$$

and

$$T_{nm} = \int_a^b \cos(\gamma_n y) \cosh(\gamma_m y) dy. \tag{3.42}$$

Here the quantities $E_{24}^{\pm} = E_2 \pm E_4$ are constants in which E_2 and E_4 appeared with the implication of orthogonality relation, and their values depend upon the

conditions on the edges of horizontal membrane and that for fixed edges comprise

$$\frac{\partial \psi_2}{\partial y}(\pm L, b) = 0. \tag{3.43}$$

By using these edge conditions and then rearranging the resulting equations lead to

$$
\begin{aligned}
E_{24}^+ S_1 =& \alpha \sum_{m=0}^{\infty} \frac{\gamma_m \sinh(\gamma_m b) \tan(s_m L)}{2 s_m E_m} \left[-R_{0m} + \sum_{n=0}^{\infty} \Phi_n^- \eta_n R_{nm} \right] \\
&+ \alpha \sum_{m=0}^{\infty} \frac{\gamma_m \sinh(\gamma_m b) \tan(s_m L)}{2 s_m E_m} \left[i a_{13}^+ P_{1m} + i a_{24}^+ P_{2m} \right] \\
&+ \alpha^2 \sum_{m=0}^{\infty} \frac{\gamma_m \sinh(\gamma_m b) \tan(s_m L)}{s_m E_m} \left[\sum_{n=0}^{\infty} \frac{\chi_n^- \sin(s_n L) T_{mn}}{\gamma_n^2 + \mu^2} \right],
\end{aligned} \tag{3.44}
$$

$$
\begin{aligned}
E_{24}^- S_2 =& \alpha \sum_{m=0}^{\infty} \frac{\gamma_m \sinh(\gamma_m b) \cot(s_m L)}{2 i s_m E_m} \left[-R_{0m} + \sum_{n=0}^{\infty} \Phi_n^+ \eta_n R_{nm} \right] \\
&+ \alpha \sum_{m=0}^{\infty} \frac{\gamma_m \sinh(\gamma_m b) \cot(s_m L)}{2 s_m E_m} \left[i a_{13}^- P_{1m} + i a_{24}^- P_{2m} \right] \\
&+ \alpha^2 \sum_{m=0}^{\infty} \frac{\gamma_m \sinh(\gamma_m b) \cot(s_m L)}{s_m E_m} \left[\sum_{n=0}^{\infty} \frac{\chi_n^+ \cos(s_n L) T_{mn}}{\gamma_n^2 + \mu^2} \right],
\end{aligned} \tag{3.45}
$$

where S_1 and S_2 are

$$S_1 = \sum_{m=0}^{\infty} \frac{[\gamma_m \sinh(\gamma_m b)]^2 \tan(s_m L)}{2 s_m E_m}, \tag{3.46}$$

and

$$S_2 = \sum_{m=0}^{\infty} \frac{[\gamma_m \sinh(\gamma_m b)]^2 \cot(s_m L)}{2 s_m E_m}. \tag{3.47}$$

Thus, for membrane vertical strips the mode-matching tailored-Galarekin (MMTG) approach yields two systems of equations defined by (3.19)-(3.20) and (3.38)-(3.39) along with (3.44)-(3.45). These are truncated and inverted for $\{\Phi_m^\pm, \chi_m^\pm\}$ and that finally yield the unknown amplitudes through the expressions:

$$A_m = \frac{1}{2}\{\Phi_m^+ + \Phi_m^-\}, \qquad D_m = \frac{1}{2}\{\Phi_m^+ - \Phi_m^-\}, \tag{3.48}$$

$$B_m = \frac{1}{2}\{\chi_m^+ + \chi_m^-\}, \qquad C_m = \frac{1}{2}\{\chi_m^+ - \chi_m^-\}. \qquad (3.49)$$

3.4 Galerkin Approach

In preceding analysis the MMTG approach is used to solve the boundary value problem, but herein the mode-matching Galerkin (MMG) procedure is developed to obtain the solution. It would be interesting to compare the results obtained via MMTG and MMG methods.

The Galerkin approach basically relies on the determinations of a priori solutions to express the responses along vertical membrane boundaries, and the values of priori solutions change with variations of physical conditions at the joints or connections of the vertical membranes.

The fundamentals of the technique has been briefly discussed in [72]. We express the vertical membrane displacements $w_1(y)$ and $w_2(y)$ at $x = -L$ and $x = L$, respectively, in terms of Fourier series by

$$w_1(y) = \sum_{n=0}^{\infty} G_{1n} Y_n(y), \qquad (3.50)$$

$$w_2(y) = \sum_{n=0}^{\infty} G_{2n} Y_n(y). \qquad (3.51)$$

Here G_{1n} and G_{2n} for $n = 0, 1, 2, \ldots$ are the unknown Fourier coefficients, and $Y_n(y)$ represents the nth eigenfunction that satisfies the eigen equation

$$\frac{d^2 Y_n}{dy^2} + \lambda_n^2 Y_n(y) = 0, \quad x = \pm L, \quad a < y < b. \qquad (3.52)$$

The exact formulation of eigenfunctions and corresponding eigenvalues satisfying (3.52) depend upon the conditions at boundaries or joints, which for the problem discussed herein are assumed fixed, free or spring-like and their possible combinations are explained in accompanying subsections.

Fixed Edges at $y = a$

First we consider the case whereby the edges of vertical membranes at $y = a$, $x = \pm L$ comprise zero displacement, and thus satisfy

$$Y_n(y) = 0, \qquad y = a. \tag{3.53}$$

The eigenfunction satisfying (3.52) and (3.53) takes form $Y_n(y) = \sin[\lambda_n(y - a)]$ which includes the nth eigenvalue λ_n and that are determined from the edge conditions at $y = b$, $x = \pm L$. These conditions include:

• Fixed edges at $y = b$ which reveal the condition $Y_n(b) = 0$, which yields eigenvalues

$$\lambda_n = \frac{n\pi}{b - a}, \ n = 1, 2, 3 \ldots. \tag{3.54}$$

• Free edges at $y = b$ that lead to the condition $Y_n'(b) = 0$, (where prime here and henceforth denotes differentiation with respect to y) which yields eigenvalues

$$\lambda_n = \frac{(n + \frac{1}{2})\pi}{b - a}, \qquad n = 0, 1, 2 \ldots. \tag{3.55}$$

• Spring-like edges at $y = b$ which satisfy the condition $\xi_2 Y_n(b) + Y_n'(b) = 0$, and the eigenvalues are the roots of characteristic equation

$$\xi_2 \sin[\lambda_n(b - a)] + \lambda_n \cos[\lambda_n(b - a)] = 0, \qquad n = 0, 1, 2 \ldots. \tag{3.56}$$

These roots are found numerically.

Free Edges at $y = a$

At free edges the gradient is zero, that gives

$$\frac{dY_n}{dy} = 0, \qquad y = a. \tag{3.57}$$

From (3.52) and (3.57), the eigenfunction $Y_n(y) = \cos[\lambda_n(y-a)]$ is found, whereas, for the nth eigenvalue λ_n following edge conditions at $y = b$, $x = \pm L$ are considered.

• Fixed edges at $y = b$ reveal the condition $Y_n(b) = 0$, which yields eigenvalues

$$\lambda_n = \frac{(n + \frac{1}{2})\pi}{b - a}, \quad n = 0, 1, 2 \ldots. \tag{3.58}$$

• Free edges at $y = b$ and that lead to the condition $Y_n'(b) = 0$, which yields eigenvalues

$$\lambda_n = \frac{n\pi}{b - a}, \quad n = 0, 1, 2, \ldots. \tag{3.59}$$

• Spring-like edges at $y = b$ satisfy the condition $\xi_2 Y_n(b) + Y_n'(b) = 0$, and the eigenvalues are the roots of characteristic equation

$$\xi_2 \cos[\lambda_n(b - a)] - \lambda_n \sin[\lambda_n(b - a)] = 0 \quad n = 0, 1, 2 \ldots. \tag{3.60}$$

These roots are found numerically.

Spring-like Edges at $y = a$

The spring-like edges satisfy the condition

$$\xi_1 Y_n(a) + Y_n'(a) = 0, \quad y = a. \tag{3.61}$$

By solving (3.52) and (3.61) the eigenfunction $Y_n(y) = \xi_1 \sin[\lambda_n(y-a)] + \lambda_n \cos[\lambda_n(y-a)]$ is obtained and for eigenvalue λ_n following edge conditions at $y = b$, $x = \pm L$ apply:

• Fixed edges at $y = b$ result the condition $Y_n(b) = 0$, and that yields eigenvalues to be the roots of characteristic equation

$$\xi_1 \sin[\lambda_n(b - a)] + \lambda_n \cos[\lambda_n(b - a)] = 0 \quad n = 0, 1, 2 \ldots. \tag{3.62}$$

• Free edges at $y = b$ specify the condition $Y_n'(b) = 0$, and that result eigenvalues are roots of equation

$$\xi_1 \lambda_n \cos[\lambda_n(b-a)] - \lambda_n^2 \sin[\lambda_n(b-a)] = 0 \quad n = 0, 1, 2 \dots. \tag{3.63}$$

• Spring-like edges at $y = b$ satisfy the condition $\xi_2 Y_n(b) + Y_n'(b) = 0$, and the eigenvalues are the roots of characteristic equation

$$(\xi_1\xi_2 - \lambda_n^2)\sin[\lambda_n(b-a)] + (\xi_1 + \xi_2)\lambda_n \cos[\lambda_n(b-a)] = 0, \quad n = 0, 1, 2 \dots. \tag{3.64}$$

These roots can be found numerically and their properties can be found in [44].

Note that the eigenfunctions Y_n, $n = 0, 1, 2, ..$ in each case are orthogonal and satisfy the orthogonality relation

$$\int_a^b Y_n(y) Y_m(y) dy = \delta_{mn} H_n, \tag{3.65}$$

where

$$H_n = \int_a^b Y_n^2(y) dy. \tag{3.66}$$

From the preceding cases, we have determined the formulation of eigenfunctions and their corresponding eigenvalues for different set of edge conditions. But the Fourier coefficients G_{1n} and G_{2n} are still unknowns. By substituting (3.50) and (3.51) into (3.22) and (3.23), the value of Fourier coefficients G_{1n} and G_{2n} can be expressed in terms of model amplitudes B_n and $C_n, n = 0, 1, 2, \ldots$ as follows:

$$\sum_{n=0}^{\infty} G_{1n}(\mu^2 - \lambda_n^2) Y_n(y) = \alpha \sum_{n=0}^{\infty} (B_n e^{-is_n L} + C_n e^{is_n L}) \cosh(\gamma_n y), \tag{3.67}$$

$$\sum_{n=0}^{\infty} G_{2n}(\mu^2 - \lambda_n^2) Y_n(y) = -\alpha \sum_{n=0}^{\infty} (B_n e^{is_n L} + C_n e^{-is_n L}) \cosh(\gamma_n y). \tag{3.68}$$

On multiplying (5.20) and (3.68) by $Y_m(y)$, integrating over a to b and using OR (5.15), it is found after some rearrangements that:

$$G_{1m} + G_{2m} = -\frac{2i\alpha}{H_m(\mu^2 - \lambda_m^2)} \sum_{n=0}^{\infty} \chi_n^+ \sin(s_n L) P_{mn}, \qquad (3.69)$$

and

$$G_{1m} - G_{2m} = \frac{4\alpha}{H_m(\mu^2 - \lambda_m^2)} \sum_{n=0}^{\infty} \chi_n^- \cos(s_n L) P_{mn}. \qquad (3.70)$$

where

$$P_{mn} = \int_a^b Y_m(y) \cosh(\gamma_n y) dy. \qquad (3.71)$$

By substituting (3.5), (3.6), (3.11) and (3.50)-(3.51) into (3.36) and (3.37), multiplying with $\alpha \cosh(\gamma_m y)$, integrating from 0 to b and then on using the generalized OR (3.13), after some rearrangements of the resulting equations with the aid of (3.69) and (3.70), we reached that:

$$\chi_m^- = \frac{\gamma_m \sinh(\gamma_m b) E_{24}^+}{2 s_m E_m \cos(s_m L)} + \frac{\alpha}{2 s_m E_m \cos(s_m L)} \left\{ R_{0m} - \sum_{n=0}^{\infty} \Phi_m^- \eta_n R_{nm} \right\}$$
$$- \frac{2\alpha^2}{s_m E_m \cos(s_m L)} \sum_{j=0}^{\infty} \sum_{q=0}^{\infty} \frac{\chi_q^- \cos(s_q L) P_{qm} P_{jm}}{H_j(\mu^2 - \lambda_j^2)}, \qquad (3.72)$$

and

$$\chi_m^+ = \frac{\gamma_m \sinh(\gamma_m b) E_{24}^-}{2 i s_m E_m \sin(s_m L)} + \frac{\alpha}{2 i s_m E_m \sin(s_m L)} \left\{ R_{0m} - \sum_{n=0}^{\infty} \Phi_n^+ \eta_n R_{nm} \right\}$$
$$- \frac{2\alpha^2}{s_m E_m \sin(s_m L)} \sum_{j=0}^{\infty} \sum_{q=0}^{\infty} \frac{\chi_q^+ \cos(s_q L) P_{qm} P_{jm}}{H_j(\mu^2 - \lambda_j^2)} \qquad (3.73)$$

where $E_{24}^{\pm}$ are unknown constants which are governed by the implication of orthogonality relation. To evaluate that constants, the conditions at the joints of horizontal membrane are already stated in (3.43). Thus, the computation of $E_{24}^{\pm}$ by using (3.43) yields:

$$E_{24}^+ S_1 = \alpha \sum_{m=0}^{\infty} \frac{\gamma_m \sinh(\gamma_m b) \tan(s_m L)}{2 s_m E_m} \left\{ -R_{0m} + \sum_{n=0}^{\infty} \Phi_n^- \eta_n R_{nm} \right\}$$
$$+ 2\alpha^2 \sum_{j=0}^{\infty} \sum_{m=0}^{\infty} \sum_{q=0}^{\infty} \frac{\chi_q^- \sin(s_q L) \gamma_m \sinh(\gamma_m b) \tan(s_m L) P_{qj} P_{jq}}{s_m E_m H_j(\mu^2 - \lambda_j^2)(\gamma_q^2 + \mu^2)}, \qquad (3.74)$$

and

$$E_{24}^- S_2 = \alpha \sum_{m=0}^{\infty} \frac{\gamma_m \sinh(\gamma_m b) \cot(s_m L)}{2 s_m E_m} \left\{ -R_{0m} + \sum_{n=0}^{\infty} \Phi_n^+ \eta_n R_{nm} \right\}$$
$$+ 2i\alpha^2 \sum_{j=0}^{\infty} \sum_{m=0}^{\infty} \sum_{q=0}^{\infty} \frac{\chi_q^+ \gamma_m \sin(s_q L) \sinh(\gamma_m b) \cot(s_m L) P_{qj} P_{jq}}{s_m E_m H_j (\mu^2 - \lambda_j^2)(\gamma_q^2 + \mu^2)}. \tag{3.75}$$

In this way mode-matching Galerkin (MMG) approach yields two systems of equations defined by (3.72)-(3.75) together with (3.19)-(3.20). These are truncated and inverted for $\{\Psi_m^\pm, \chi_m^\pm\}$ that finally yield the unknown amplitudes by using (3.48) and (3.49).

3.5   Numerical Results and Discussion

Here the validity of mode-matching tailored-Galerkin (MMTG) and mode-matching Galerkin (MMG) methods is analyzed numerically, after truncating the linear algebraic systems retained against these methods up to N terms.

Without loss of generality, the truncated solutions are used to investigate the effects of edge conditions on the scattering energies, and transmission loss versus frequency. On using the definition given in [93], the reflected energy flux or power in inlet and transmitted energy flux or power in outlet can be found

$$\mathcal{E}_{\mathrm{r}} = \frac{1}{2} \sum_{m=0}^{\mathcal{K}-1} |A_m|^2 \epsilon_m \eta_m \tag{3.76}$$

and

$$\mathcal{E}_{\mathrm{t}} = \frac{1}{2} \sum_{m=0}^{\mathcal{K}-1} |D_m|^2 \epsilon_m \eta_m, \tag{3.77}$$

respectively, where the incident energy flux or power is scaled at unity and $\mathcal{K}$ denotes the number of cut-on modes in extended inlet/outlet region. The conservation of energy flux of confined system can be expressed through the conserve power identity, that is

$$\mathcal{E}_r + \mathcal{E}_t = 1. \tag{3.78}$$

It shows that the incident power, that is unity herein, fed into the system is equal to the sum of the reflected power ($\mathcal{E}_r$) and transmitted power ($\mathcal{E}_t$).

For numerical computation attention is restricted to the cavity chamber of a stainless steel membrane of mass density $0.2 \mathrm{kgm}^{-2}$ and of tension $T = 3250 \, \mathrm{Nm}^{-1}$. The density of air ρ and sound speed c are assumed $1.2 \mathrm{kgm}^{-3}$ and $344 \mathrm{ms}^{-1}$, respectively. The dimensional height and half length of chamber region respectively are $\bar{b} = 0.3$m and $\bar{L} = 0.17$m, whereas, the dimensional height of extended inlet/outlet $\bar{a} = 0.15$m is assumed. Note that the mentioned parameters are consistent with the parameters as used by Lawrie and Guled [101].

In Figs. 3.2–3.4, the reflected power ($\mathcal{E}_r$) and transmitted power ($\mathcal{E}_t$) against frequency with different sets of edge conditions are shown. The curves with symbols (▲,■,●) are obtained by using MMTG solution whilst the dashed curves represent MMG solution.

The systems of equations achieved with MMTG and MMG techniques are truncated by taking $N = 60$ terms, and then are inverted for nine different sets of edge conditions. These edge conditions are imposed on the joints of vertical membranes at $(x, y) = (\pm L, a)$ and $(x, y) = (\pm L, b)$ and define the characteristics of joints. The following three groups express the nine sets of edge conditions:

Group-1: Having zero displacement conditions at $(x, y) = (\pm L, a)$, whereas, zero displacement, spring-like edge or zero gradient conditions at $(x, y) = (\pm L, b)$.

Group-2: Having spring-like conditions at $(x, y) = (\pm L, a)$, whereas, zero displacement, spring-like or zero gradient edge conditions at $(x, y) = (\pm L, b)$.

Group-3: Having zero gradient conditions at $(x, y) = (\pm L, a)$, whereas, zero displacement, spring-like or zero gradient edge conditions at $(x, y) = (\pm L, b)$.

Fig. 3.2 depicts the curves of reflected and transmitted powers against frequency for three sets of edge conditions that are listed in Group-1. The first set comprises zero displacement edge conditions ($\xi_1 = \infty$) at both $(x, y) = (\pm L, a)$ and

$(x, y) = (\pm L, b)$ and the resulting curve with this set of edge conditions is expressed through symbol '▲' in Fig. 3.2; the second set of edge conditions contains zero displacement conditions ($\xi_1 = \infty$) at $(x, y) = (\pm L, a)$ and spring-like conditions ($\xi_1 = 1$) at $(x, y) = (\pm L, b)$ and the resulting curve with this set of edge conditions is denoted with symbol '■' and; the third set of edge conditions have zero displacement conditions ($\xi_1 = \infty$) at $(x, y) = (\pm L, a)$ and zero gradient conditions ($\xi_1 = 0$) at $(x, y) = (\pm L, b)$ and the resulting curve with this set of edge conditions is expressed through symbol '●'. From Fig. 3.2 it can be seen that at $f = 1$Hz, the majority of the radiated energy goes on transmission which decreases by increasing frequency, and reaches to its decremented value before the point whereby the second mode of the chamber cavity starts propagating, whereas, the reflected powers behave conversely such that the sum of reflected and transmitted powers for each set of edge conditions is unity (which is being the incident power). Nevertheless, by changing the edge conditions of the vertical flexible walls at $(x, y) = (\pm L, b)$, a variation in scattering energies is evident. This behavior is more significant about the points whereby the cuts-on of the chamber cavity are occurred.

(a) Reflected power versus frequency. (b) Transmitted power versus frequency.
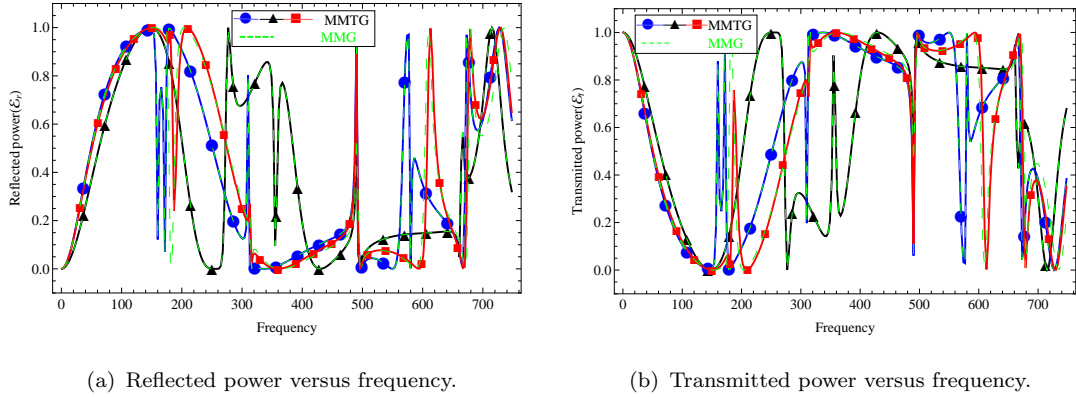
FIGURE 3.2: Zero displacement edge conditions at $(x, y) = (\pm L, a)$ and zero displacement (▲), spring-like (■) or zero gradient (●) edge conditions at $(x, y) = (\pm L, b)$.

Note that the fundamental mode ($n = 0$) of extended inlet/outlet is always cut-on due to the presence of zero eigenvalue, which results the propagation of plane acoustic wave in the duct having rigid boundary conditions. The next energy propagating modes appear on higher frequencies; such as the second cut-on mode

TABLE 3.1: Propagating Modes

Cut-on f(Hz)	Inlet-Outlet Region	Expansion Chamber Region
191	1	2
657	1	3
1146	2	3
1194	2	4
1752	2	5
2291	3	5
2316	3	6
2884	3	7
3436	4	7
3453	4	8
4730	4	9

of extended inlet/outlet occurs at $f = 1146$Hz, however, lies out of the frequency regime considered herein for analysis. Likewise, in the cavity containing duct region, which is bounded below with rigid wall and upper with elastic membrane, a fundamental duct mode remains propagating throughout the frequency regime due to the presence of one real root of dispersion relation (3.12). Whereas, the cut-on frequencies of second and third duct modes of this region are 191Hz and 657Hz, respectively, and thus, such modes affect the scattering energies. The list of cut-on modes frequencies is as shown in Table:1.

In Fig. 3.3, three curves of reflected and transmitted powers associated with three sets of edge conditions as listed in Group-2 are shown. The curve with symbol '▲' is achieved by setting spring-like edge conditions ($\xi_1 = 1$) at $(x,y) = (\pm L, a)$ and zero displacement conditions ($\xi_1 = \infty$) at $(x,y) = (\pm L, b)$, the curve with symbol '■' is found by keeping spring-like conditions ($\xi_1 = 1$) at both $(x,y) = (\pm L, a)$ and $(x,y) = (\pm L, b)$ and, the curve with symbol '●' is obtained by fixing spring-like edge conditions ($\xi_1 = 1$) at $(x,y) = (\pm L, a)$ and zero gradient conditions ($\xi_1 = 0$) at $(x,y) = (\pm L, b)$. From the graphs shown in Fig. 3.3, it can be seen

that in start majority of the excited power goes on reflection while transmitted power behave conversely. The scattering behavior seems opposite at the starting frequency to the curves as shown in Fig. 3.2. Moreover, a significant deviation in scattering powers is evident with the variation of edge conditions on the vertical membranes. Accordingly in Fig. 3.4, the scattering powers associated with three

(a) Reflected power versus frequency.

(b) Transmitted power versus frequency.
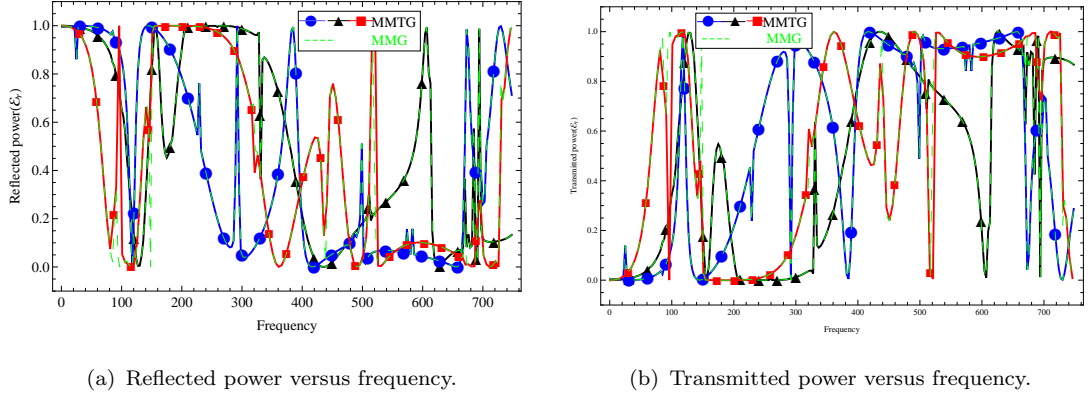
FIGURE 3.3: Spring-like edge conditions at $(x, y) = (\pm L, a)$ and zero displacement ($\blacktriangle$), spring-like ($\blacksquare$) or zero gradient ($\bullet$) edge conditions at $(x, y) = (\pm L, b)$.

sets of edge conditions as listed in Group-3 are shown. The curve with symbol '$\blacktriangle$' is achieved by setting zero gradient edge conditions ($\xi_1 = 0$) at $(x, y) = (\pm L, a)$ and zero displacement conditions ($\xi_1 = \infty$) at $(x, y) = (\pm L, b)$, the curve with symbol '$\blacksquare$' is found by keeping zero gradient edge conditions ($\xi_1 = 0$) at $(x, y) = (\pm L, a)$ and spring-like conditions conditions ($\xi_1 = 1$) at $(x, y) = (\pm L, b)$ and, the curve with symbol '$\bullet$' is obtained by fixing zero gradient conditions ($\xi_1 = 0$) at both $(x, y) = (\pm L, a)$ and $(x, y) = (\pm L, b)$. From Fig. 3.4 it is seen that initially majority of the radiated power goes on reflection, except the case having zero gradient edge conditions ($\xi_1 = 0$) at $(x, y) = (\pm L, a)$ and zero displacement conditions ($\xi_1 = \infty$) at $(x, y) = (\pm L, b)$ (see curve with symbol $\blacktriangle$). In the later case, initially majority of the radiated power goes on transmission instead of reflection as is found in Fig. 3.2 with a little variability of pattern. Moreover, from Figs. 3.2–3.4 it is found that the results obtained via MMTG and MMG methods match closely. However, some dissimilarities in spring-like edges graphs are found. These variations are because of the numerical computation of the eigenvalues from the dispersion relations defined by (3.56), (3.60) and (3.62)-(3.64). Furthermore, the reflected power ($\mathcal{E}_r$) and transmitted power ($\mathcal{E}_t$) achieved via MMTG and MMG

(a) Reflected power versus frequency.

(b) Transmitted power versus frequency.
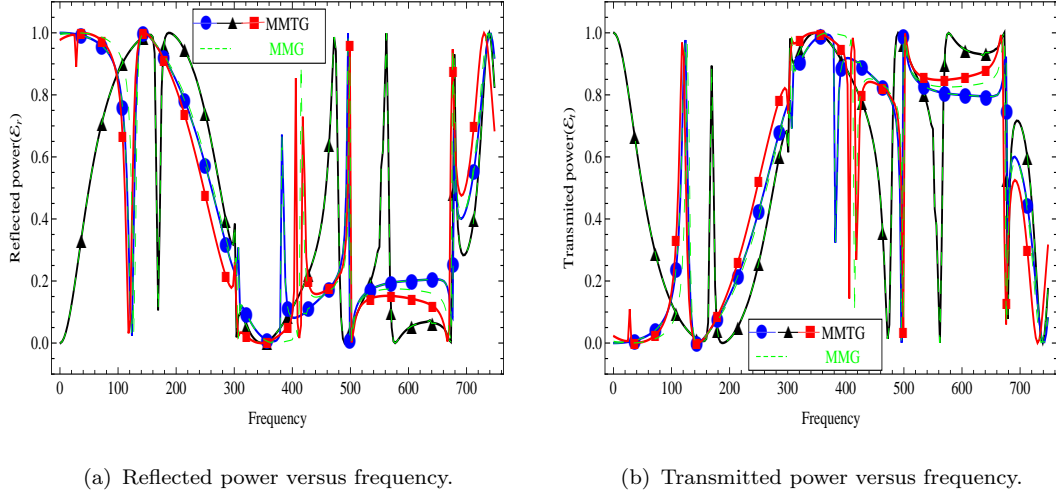
FIGURE 3.4: Zero gradient edge conditions at $(x, y) = (\pm L, a)$ and zero displacement (▲), spring-like (■) or zero gradient (●) edge conditions at $(x, y) = (\pm L, b)$.

methods obey the conservation law as defined by (6.129). The performance of a reactive device is usually measured with the help of transmission loss (TL), and that for unit incident power can be defined by [101].

$$\text{TL} = -10 \log_{10}(\mathcal{E}_t). \tag{3.79}$$

The aspect ratio of the silencing device can be calculated by using the formula [101, 111]: $\mathcal{R} = 2L/(b-a)$. Huang [111] has shown that the stopbands produced with the high aspect ratios are wide. Nevertheless, too large value of aspect ratio drops the resonant peaks of TL below 10 dB. On the other hand, the stopbands produced by the low aspect ratios are high and narrow. Therefore, to be of practical use of reactive device in HVAC system, the parametric settings of chamber cavity are assumed with lower aspect ratios.

In Figs. 3.5–3.7, the TL against frequency is shown. The systems are truncated to $N = 60$ terms, whereas, all other involving parameters are kept same as assumed earlier while producing the results of scattering energies. The curves having symbols (▲,■,●) represent the outcomes of MMTG method whilst the results with MMG are depicted with dashing curves.

Fig. 3.5 refers the TL versus frequency with the sets of edge edge conditions listed

in Group-1. The curve with symbol '▲' represents the setting having zero displacement edge conditions ($\xi_1 = \infty$) at both $(x,y) = (\pm L, a)$ and $(x,y) = (\pm L, b)$, the curve with symbol '■' denotes the case with zero displacement conditions ($\xi_1 = \infty$) at $(x,y) = (\pm L, a)$ and spring-like conditions ($\xi_1 = 1$) at $(x,y) = (\pm L, b)$ and curve with symbol '●' expresses zero displacement conditions ($\xi_1 = \infty$) at $(x,y) = (\pm L, a)$ and zero gradient conditions ($\xi_1 = 0$) at $(x,y) = (\pm L, b)$. The peak value of TL with zero displacement conditions on both edges (see curves with ▲) is 59.57dB which appears at $f = 148$Hz in frequency regime $1\text{Hz} \leq f \leq 750\text{Hz}$ including passbands and stopbands. The major stopband in frequency range $(115-174)$Hz with a bandwidth of 1.51 is produced. For spring-like conditions at $y = b$ as shown by curves with symbol ■ in Fig. 3.5, the maximum TL is 52.6 dB which appear at 151 Hz, and two stopbands with aspect ratios of 1.51 and 1.42 are produced in frequency ranges (103-156) Hz and (176-201) Hz, respectively. However, by changing the conditions at $(x,y) = (\pm L, b)$ to zero gradient, the maximum TL of 37.63dB appears at $f = 723$Hz (see curves having ● in Fig. 3.5). Two stopbands with aspect ratios 1.51 and 1.42 are produced in frequency ranges (103-156) Hz and 176-201 Hz, respectively.
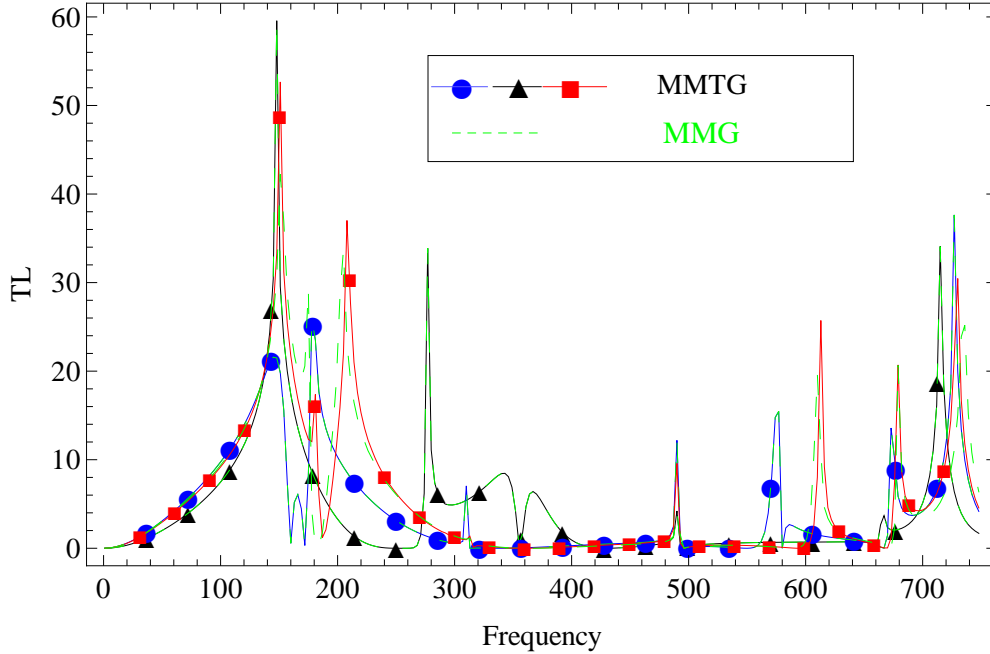
FIGURE 3.5: Transmission loss against frequency with zero displacement edge conditions at $(x,y) = (\pm L, a)$ and zero displacement (▲), spring-like (■) or zero gradient (●) edge conditions at $(x,y) = (\pm L, b)$.

Fig. 3.6 depicts TL against frequency with sets of edge conditions that are listed in Group-2. The curve with symbol '▲' is achieved by setting spring-like edge conditions ($\xi_1 = 1$) at $(x,y) = (\pm L, a)$ and zero displacement conditions ($\xi_1 = \infty$) at $(x,y) = (\pm L, b)$, the curve with symbol '■' is found by keeping spring-like conditions ($\xi_1 = 1$) at both $(x,y) = (\pm L, a)$ and $(x,y) = (\pm L, b)$ and, the curve with symbol '●' is obtained by fixing spring-like edge conditions ($\xi_1 = 1$) at $(x,y) = (\pm L, a)$ and zero gradient conditions ($\xi_1 = 0$) at $(x,y) = (\pm L, b)$.

The peak value of TL with spring-like conditions at $y = a$ and zero displacement conditions at $y = b$ (see curve with ▲) is 48.2dB which arises at $f = 223$Hz and a stopband in frequency range (200-330) Hz with aspect ratio of 1.65 is revealed. However, by considering the spring-like edge conditions at both $(x,y) = (\pm L, a)$ and $(x,y) = (\pm L, b)$, the maximum TL of 81.29 dB governs at 181 Hz, and a stopband in frequency range (150-290) Hz with aspect ratio of 1.93 is achieved (see curve with symbol ■ in Fig. 6). Whereas, by replacing the conditions at $y = b$ from spring-like to zero gradient, the maximum TL of 44.36 dB appears at 145 Hz and a stopband in frequency range (130-183) Hz with aspect ratio of 1.41 is produced (see curves having ● in Fig. 3.6).
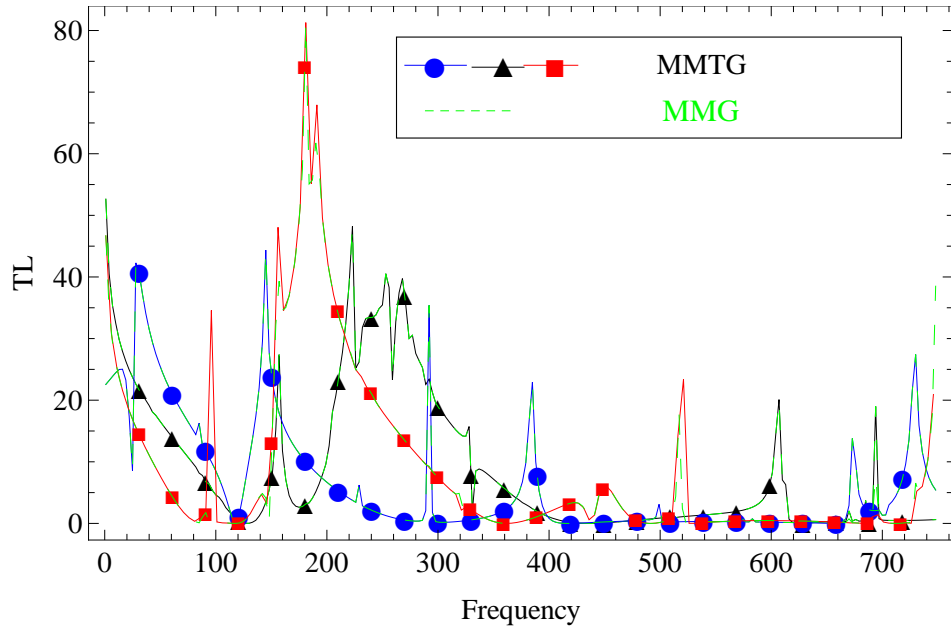
FIGURE 3.6: Transmission loss against frequency with spring-like edge conditions at $(x,y) = (\pm L, a)$ and zero displacement (▲), spring-like (■) or zero gradient (●) edge conditions at $(x,y) = (\pm L, b)$.

Fig. 3.7 displays TL versus frequency with sets of edge condition which are listed in Group-3. The curve with symbol '▲' is achieved by setting zero gradient edge conditions ($\xi_1 = 0$) at $(x, y) = (\pm L, a)$ and zero displacement conditions ($\xi_1 = \infty$) at $(x, y) = (\pm L, b)$, the curve with symbol '■' is found by keeping zero gradient edge conditions ($\xi_1 = 0$) at $(x, y) = (\pm L, a)$ and spring-like conditions conditions ($\xi_1 = 1$) at $(x, y) = (\pm L, b)$ and, the curve with symbol '●' is obtained by fixing zero gradient conditions ($\xi_1 = 0$) at both $(x, y) = (\pm L, a)$ and $(x, y) = (\pm L, b)$. The peak value of TL with zero gradient conditions at $(x, y) = (\pm L, a)$ and zero displacement conditions at $(x, y) = (\pm L, b)$ (see curves comprising ▲) is 38.6dB which appears at $f = 187$Hz in frequency regime 1Hz $\leq f \leq$ 750Hz and two stopbands with aspect ratios of 1.52 and 1.27 are produced in frequency ranges (108-164) Hz and (177-225) Hz, respectively. Accordingly, for spring-like conditions at $(x, y) = (\pm L, b)$ as shown by the curve with symbol ■ in Fig. 3.7, the maximum TL of 53 dB occurs at 145 Hz, and a stopband in the frequency range (132-183) Hz with aspect ratio of 1.4 appears. Whereas, by changing the conditions at $(x, y) = (\pm L, b)$ from spring-like to zero gradient, the maximum TL is 56.04 dB occurs at 145 Hz, and a stopband in frequency range (134-186) Hz with bandwidth of 1.39 is produced (see curves having ● in Fig. 3.7). Furthermore, the behavior of TL versus frequency depicted in Figs. 3.5 to 3.7 is respectively compatible with the transmitted powers shown in Figs. 3.2 to 3.4. It can be seen that the behavior of TL curves is consistent with the associated transmitted power components.

Accordingly, from Figs. 3.5–3.7 it is found that the MMTG and MMG curves almost overlap in whole frequency regime for all the three sets of edge conditions. Nevertheless, some dissimilarities in the curves whereby involving spring-like conditions occur. These variations in fact appear in MMG solutions, and are due to the usage of roots of dispersion relations (3.56), (3.60) and (3.62)-(3.64), that are calculated by using Newton's method. An augmented principle to retrieve all roots in the specified region is applied, for details see [45]. In addition, the matching conditions at $x = \pm L$ are reconstructed by using the truncated form of MMTG and MMG solutions at $f = 1000$Hz where truncation parameter is kept $N = 60$
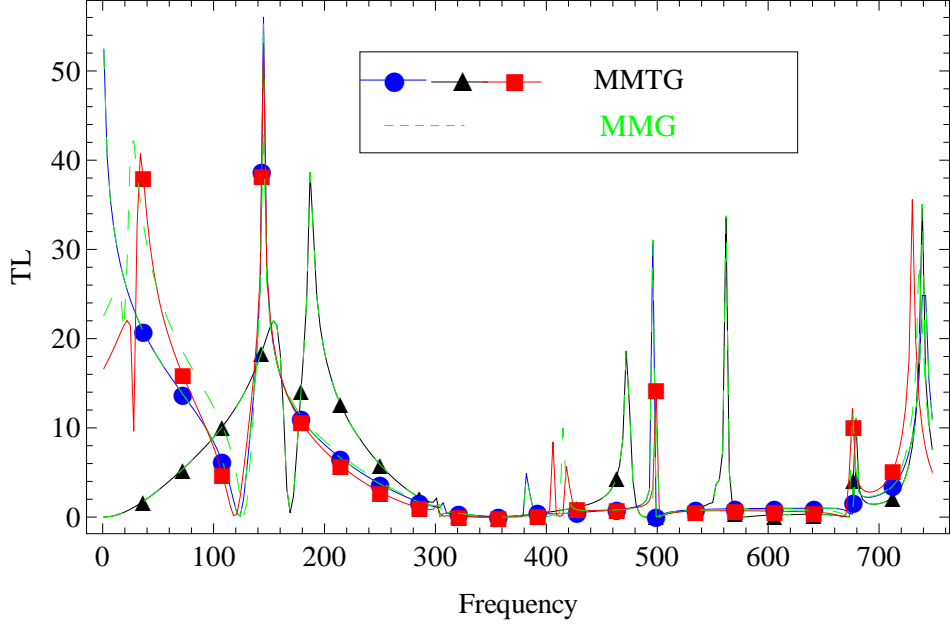
FIGURE 3.7: Transmission loss against frequency with zero gradient edge conditions at $(x, y) = (\pm L, a)$ and zero displacement (▲), spring-like (■) or zero gradient (●) edge conditions at $(x, y) = (\pm L, b)$.
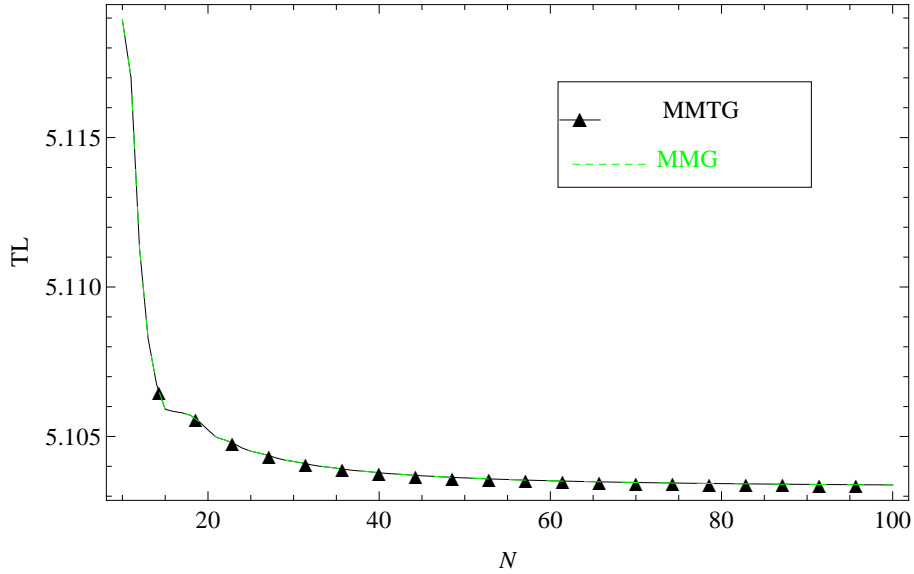
FIGURE 3.8: Transmission loss against number of terms N via MMTG and MMG approaches with $\bar{a} = 0.15$m, $\bar{b} = 0.3$m, $\bar{L} = 0.17$m and $f = 1000Hz$.

terms. In Fig. 3.9 the matching of real and imaginary parts of pressures are shown with MMTG and MMG techniques, while the zero displacement conditions $(\xi_1 = \infty, \xi_2 = \infty)$ on the edges of vertical flexible walls are considered. In Fig. 3.9(a) and 3.9(b) the real parts of pressure in extended inlet $(\psi_1(-L, y))$ obtained respectively, through MMTG and MMG methods are matched with respective real

parts of cavity pressure $(\psi_2(-L, y))$, wherein a good agreement exists. Likewise matching is evident in imaginary parts of pressure obtained via MMTG and MMG approaches see Fig. 3.10. In Figs. 3.11 and 3.12 the real and imaginary parts
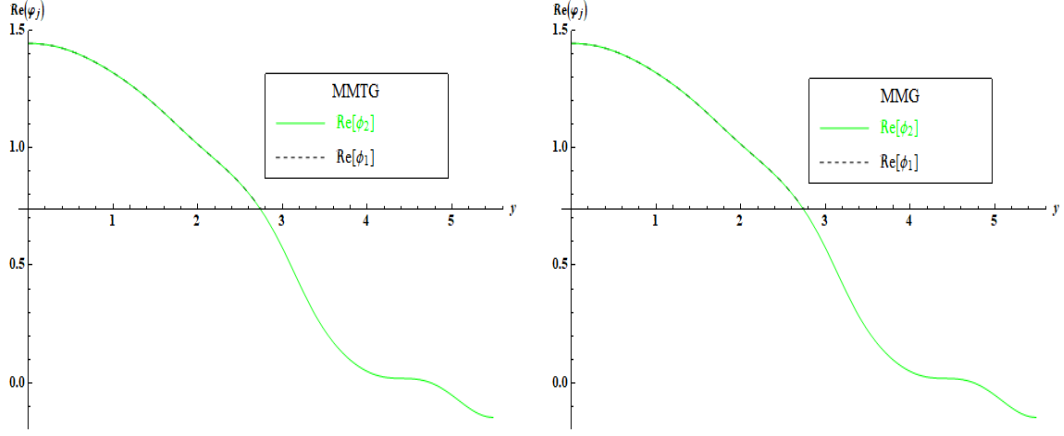
(a) Real parts of pressures (MMTG).

(b) Real parts of pressures(MMG).

FIGURE 3.9: The real parts of acoustic pressure against duct height obtained via MMTG and MMG approaches with $\bar{a} = 0.15\text{m}$, $\bar{b} = 0.3\text{m}$, $\bar{L} = 0.17\text{m}$ and $N = 60$.
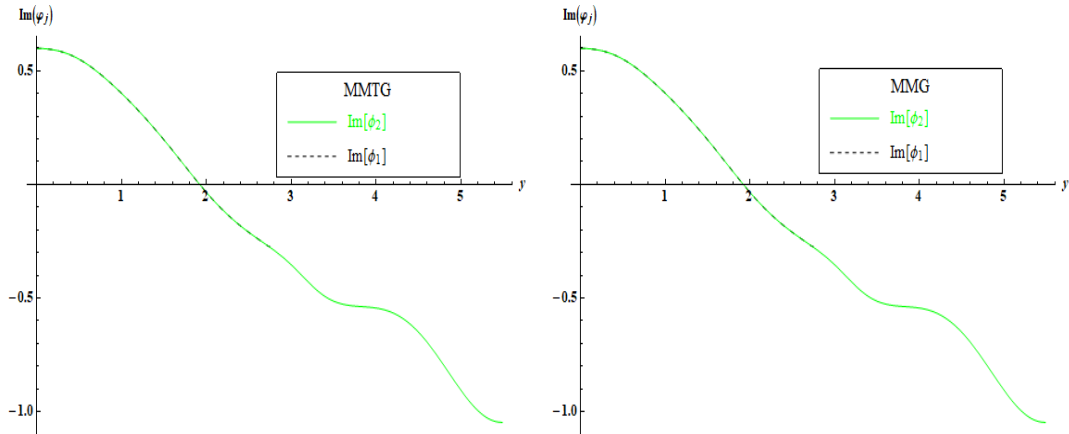
(a) Imagnary parts of pressures(MMTG).

(b) imagnary parts of pressures (MMG).

FIGURE 3.10: The imaginary parts of acoustic pressure against duct height obtained via MMTG and MMG approaches with $\bar{a} = 0.15\text{m}$, $\bar{b} = 0.3\text{m}$, $\bar{L} = 0.17\text{m}$ and $N = 60$.

of normal velocities achieved with truncated form of MMTG and MMG methods are displayed. It can be seen that the normal velocity curves of extended inlet and cavity chamber coincide at $x = -L$. In this way the matching conditions considered in (3.18) and (3.36) are fully reconstructed. Likewise, the matching

conditions (3.19) and (3.37), can be reformulated by using the truncated velocity formulations of cavity chamber and extended outlet achieved through MMTG and MMG methods. Furthermore, the transmission loss against truncation parameter N with MMG and MMTG is shown in Fig. 3.8. It can be seen that by increasing the number of terms the solution converges adequately when $N > 40$.

Therefore, the attention is restricted to $N = 60$ while producing the numerical results.

(a) Real parts of velocities (MMTG).

(b) Real parts of velocities (MMG).
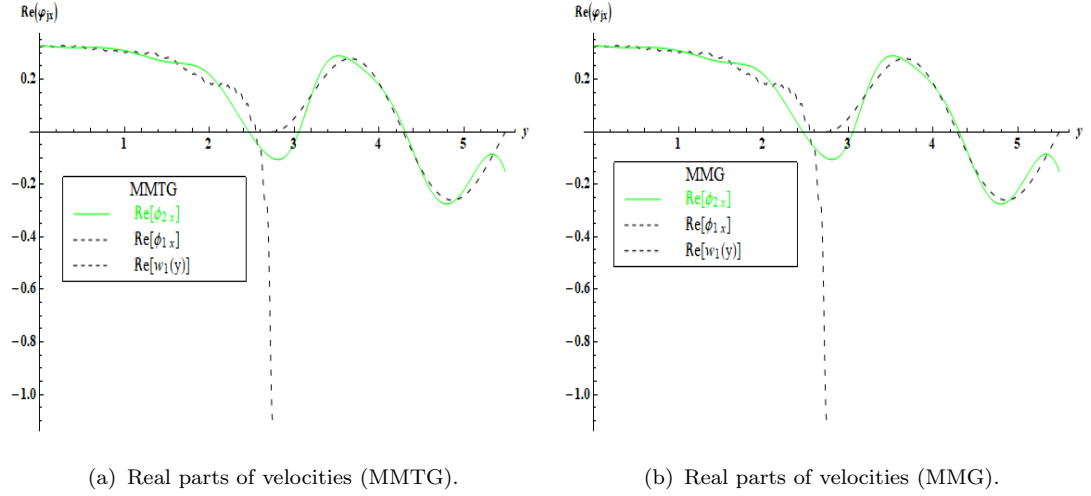
FIGURE 3.11: The real parts of normal velocities against duct height obtained via MMTG and MMG approaches with $\bar{a} = 0.15$m, $\bar{b} = 0.3$m, $\bar{L} = 0.17$m and $N = 60$.

(a) Imagnary parts of velocities (MMTG).

(b) Imagnary part of velocities (MMG).
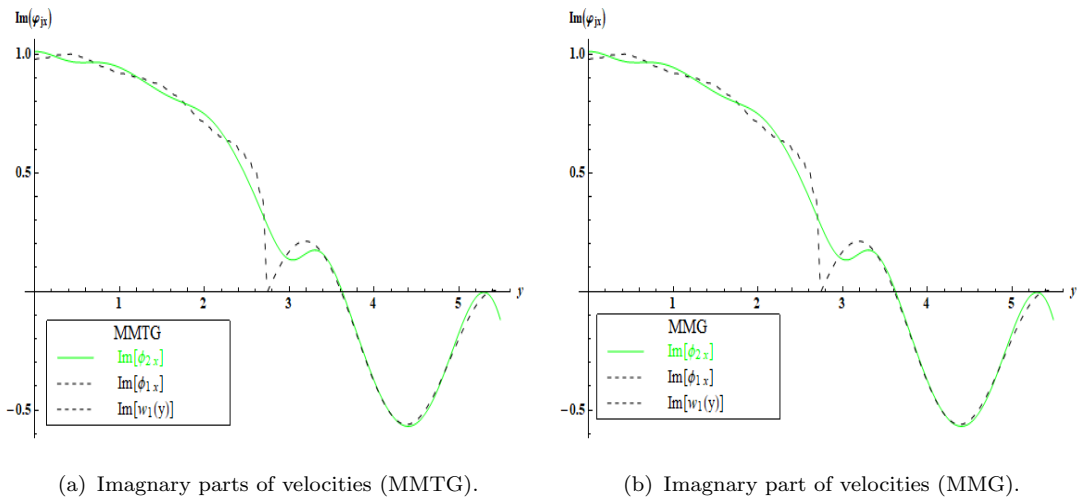
FIGURE 3.12: The imaginary parts of normal velocities against duct height obtained via MMTG and MMG approaches with $\bar{a} = 0.15$m, $\bar{b} = 0.3$m, $\bar{L} = 0.17$m and $N = 60$.

The reformulation of matching conditions with truncated solutions as well as the satisfaction of the conservation laws confirm that the performed algebra is correct. The TL against number of terms depicts that the retained systems when $N > 40$ reveal an adequate convergent solutions.

Chapter 4

Reflection and Transmission of Acoustic Wave through the Bridging Membrane Junctions

4.1 Introduction

The analysis of fluid-structure coupled waves in non-planar ducts or channels is challenging as well as important subject with a diverse range of applications in structural acoustics, water wave theory, seismological waves through lyres of rocks, and noise reduction problems etc. The motivation behind is the necessity to model and understand the scattering behavior, in channels or guiding structures, with the help of which the structural vibrations and related issues could be addressed.

The aims of current study are; first, to analyze the scattering effects of vertical membranes or rigid plates of a flexible cavity subject to different conditions on the joints of vertical membranes and second, to develop a solution procedure that provides a unique description of basis functions to apply the variety of edge conditions on vertical flexible components. The new approach has a variation of Glarekin procedure and is different from the already existing approach [119].

The displacements of the vertical membranes are expressed such that their homogeneous parts contain material properties of the boundaries while their integral parts include cavity vibrations. The variation of basis functions associated with different edge conditions can be computed directly with less computational cost. Further, the proposed formulation avoids root finding algorithm.

The present study is different from [119] in the following directions. The geometrical configuration involves cavity in a flexible infinite waveguide which makes the problem more physical. The proposed configuration seems like an HVAC component having expansion chamber to attenuate noise. With the assumed setting the problem includes more interface conditions which result multiple linear algebraic systems to solve. Further, it includes two bridging flexible height discontinuities instead of a bridging flexible height as assumed by Lawrie and Afzal [119]. They introduced the Galerkin and the tailored-Galerkin procedures to encounter the vibrational response of single bridging flexible height. In the first approach the vibrational modes of bridging flexible height are expressed in terms of orthogonal basis functions while the later relies on the non-orthogonal modes of semi-infinite regions. The main disadvantage of first technique is the assumption of appropriate orthogonal basis that changes with the variation of edge conditions on the bridging height. On the other hand, the second approach contains a unique description for all set of edge conditions but has high computational cost. The reason behind the computational cost is the slow convergence rate of sums which appear with the imposition of edge conditions and that depend upon the non-orthogonal modes of semi-infinite region. Moreover, the modeled problem is solved by using the Low Frequency Approximation (LFA). This approach is well known, see for example [114] and [101, 102], especially in low frequency regime, wherein the contributions from the fundamental and/or next mode are significant.

The chapter is arranged as follows: The mathematical formulation and related theoretical background are explained in Section 2. The MM solution is provided in Section 3. The MM procedure used in traditional way to the BVP with rigid vertical strips is elucidated in sub-section 3.1, whilst, the MM in conjunction with tailored Galerkin approach for the BVP with membrane vertical strips is provided

in sub-section 3.2. The LFA is detailed in Section 4. Numerical results, and discussion on results are given in Section 5. Finally, the concluding remarks are contained in Section 6.

4.2   Formulation of the Physical Model

The boundary value problem is governed by considering an infinite, two dimensional rectangular waveguide stretched along $\bar{x}-$direction in dimensional coordinate plane $(\bar{x}, \bar{y})$, where over bars denote the dimensional setting of coordinates. The inside of the waveguide is filled with compressible fluid of density ρ and sound speed c, whereas the outside of it is set into *vacou*. The lower horizontal wall of the waveguide is assumed to be acoustically rigid, whilst, the upper horizontal walls of it are elastic membranes. Two vertical strips lying along $\bar{x} = \pm L$, $\bar{a} \leqslant \bar{y} \leqslant \bar{b}$ divide the waveguide into three duct regions i.e., the inlet, the expansion chamber and the outlet. The material properties of the vertical strips are assumed to be; a) acoustically rigid or b) elastic membranes. The physical configuration of the waveguide is shown in Fig.4.1

Let $\bar{\Phi}(\bar{x}, \bar{y}, \bar{t})$ represents the dimensional time dependent velocity potential in waveguide, which after suppressing the harmonic time dependent $e^{i\omega\bar{t}}$ throughout the BVP, can be termed as $\bar{\Phi}(\bar{x}, \bar{y}, \bar{t}) = \bar{\psi}(\bar{x}, \bar{y})e^{i\omega\bar{t}}$. Moreover, the BVP is non-dimensionalized with respect to the length scale k^{-1} and time scale ω^{-1}. The non-dimensional form of the Helmholtz's equation along with the rigid and membrane boundary conditions are respectively given by:

$$(\nabla^2 + 1)\psi_j(x,y) = 0, \quad j = 1, 2, 3, \tag{4.1}$$

$$\frac{\partial \psi_j}{\partial y}(x,y) = 0, \quad j = 1, 2, 3 \quad y = 0, \quad -\infty < x < \infty, \tag{4.2}$$

and

$$\left(\frac{\partial^2}{\partial x^2} + \mu_h^2\right)\frac{\partial \psi_1}{\partial y} + \alpha_h \psi_1 = 0, \qquad y = a, \quad x < -L, \tag{4.3}$$
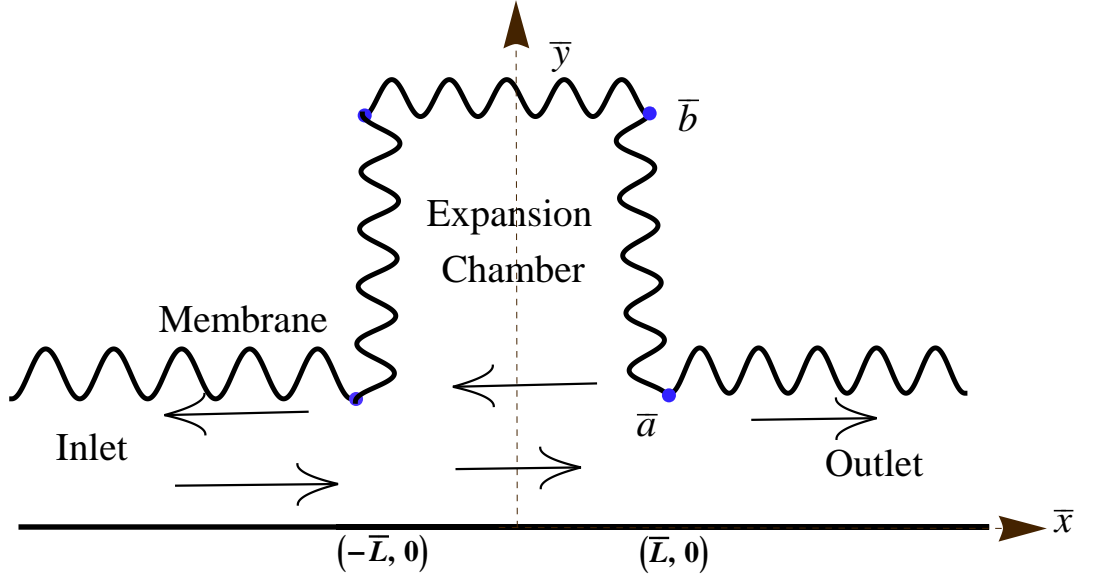
FIGURE 4.1: The physical configuration of waveguide.

$$(\frac{\partial^2}{\partial x^2} + \mu_h^2)\frac{\partial \psi_2}{\partial y} + \alpha_h \psi_2 = 0, \qquad y = b, \quad |x| < L, \tag{4.4}$$

$$(\frac{\partial^2}{\partial x^2} + \mu_h^2)\frac{\partial \psi_3}{\partial y} + \alpha_h \psi_3 = 0, \qquad y = a, \quad x > L, \tag{4.5}$$

for instance see [101]. Clearly, $\psi_j(x,y)$ for j=1,2 and 3 stand for the non-dimensional velocity potentials in the inlet region ($x \leqslant -L, 0 \leqslant y \leqslant a$), expansion chamber ($|x| < L, 0 \leqslant y \leqslant b$) and outlet region ($x \geq L, 0 \leqslant y \leqslant a$), respectively. The quantities $\mu_h = c/c_h$ and $\alpha_h = \rho\omega/(T_h k^3)$ are the membrane wave number and the fluid loading parameter, respectively containing horizontal membrane mass density c_h and tension T_h.

The bounding characteristic of the vertical strips lying along $x = \pm L, a \leqslant y \leqslant b$ can be rigid or membrane, that will be defined later.

Consider an incident wave of inlet duct mode enters from negative $x-$direction to an expansion chamber wherein it scatters in to infinite number of reflected and transmitted modes. The eigenfunction expansion form of velocity potentials in the

inlet, the expansion chamber and the outlet regions is found as:

$$\psi_1(x, y) = F_\ell \cosh(\tau_\ell y) e^{i\eta_\ell (x+L)} + \sum_{n=0}^{\infty} A_n \cosh(\gamma_n y) e^{i\eta_n (x+L)}, \qquad (4.6)$$

$$\psi_2(x, y) = \sum_{n=0}^{\infty} \left\{ B_n e^{is_n x} + C_n e^{-is_n x} \right\} \cosh(\gamma_n y), \qquad (4.7)$$

and

$$\psi_3(x, y) = \sum_{n=0}^{\infty} D_n \cosh(\gamma_n y) e^{i\eta_n (x-L)}, \qquad (4.8)$$

respectively. Note that the first term on the right hand side of equation (4.6) stands for incident wave with forcing $F_\ell = \sqrt{\alpha_h / E_\ell \eta_\ell}$, with $\ell = 0, 1$ (E_ℓ will be defined later). The quantities $\eta_n = \sqrt{1 + \tau_n^2}$ and $s_n = \sqrt{1 + \gamma_n^2}$ are the wave numbers of the nth mode propagating in the inlet/outlet and the expansion chamber, respectively. The eigenvalues τ_n; $n = 0, 1, 2, \ldots$ in the inlet/outlet regions are the roots of the dispersion relation, $N(\tau) = 0$, where

$$N(\tau) = (\tau^2 + 1 - \mu_h^2)\tau \sinh(\tau a) - \alpha_h \cosh(\tau a). \qquad (4.9)$$

These roots can be found numerically and contain following properties [114]:

- For every τ_n, there is τ_n^* (note that the asterisk stands for complex conjugate).

- The real roots ($\mathrm{Re}(\tau) \neq 0$ and $\mathrm{Im}(\tau) = 0$) are finite depending upon the approximated polynomial dispersion relation (9).

- There is an infinite number of imaginary roots (having $\mathrm{Re}(\tau) = 0$ and $\mathrm{Im}(\tau) \neq 0$).

To ensure the convergence of series solution (7), only real positive roots (i.e. for τ roots $\mathrm{Re}(\tau) > 0$ and $\mathrm{Im}(\tau) = 0$ in complex τ-plane) and the imaginary positive roots (i.e. τ roots $\mathrm{Re}(\tau) = 0$ and $\mathrm{Im}(\tau) > 0$ in complex τ-plane) are considered. All these roots are arranged such that the positive real roots appear first with descending order, and then the imaginary positive roots appear with ascending

order of imaginary part. Further, the eigenfunctions $\{\cosh(\tau_n y); n = 0, 1, 2, \}$ having eigenvalues $\{\tau_n; n = 0, 1, 2, \}$ are linearly dependent and satisfy the generalized orthogonal properties as given in [39].

The corresponding eigenfunctions satisfy generalized orthogonality relation (OR) that is,

$$\alpha_h \int_0^a \cosh(\tau_m y)\cosh(\tau_n y)dy = \delta_{mn}E_m - \tau_m\tau_n \sinh(\tau_n a)\sinh(\tau_m a), \qquad (4.10)$$

where, δ_{mn} is the Kronecker delta and

$$E_m = \frac{\alpha_h a}{2} + \left(\frac{3\tau_m^2 + 1 - \mu^2}{2\tau_m^2}\right)[\tau_m \sinh(\tau_m a)]^2. \qquad (4.11)$$

Likewise the eigenvalues γ_n; $n = 0, 1, 2\ldots$ in the expansion chamber satisfy the dispersion relation $M(\gamma) = 0$, where

$$M(\gamma) = (\gamma^2 + 1 - \mu_h^2)\gamma \sinh(\gamma b) - \alpha_h \cosh(\gamma b). \qquad (4.12)$$

The corresponding eigenfunctions satisfy the generalized OR

$$\alpha_h \int_0^b \cosh(\gamma_m y)\cosh(\gamma_n y)dy = \delta_{mn}G_m - \gamma_m\gamma_n \sinh(\gamma_n b)\sinh(\gamma_m b), \qquad (4.13)$$

where
$$G_m = \frac{\alpha_h b}{2} + \left(\frac{3\gamma_m^2 + 1 - \mu_h^2}{2\gamma_m^2}\right)[\gamma_m \sinh(\gamma_m b)]^2. \qquad (4.14)$$

Note that the coefficients $\{A_m, B_m, C_m, D_m\}$; $m = 0, 1, 2\ldots$ in the eigenfunction expansions defined by (6)-(8) are the modal amplitudes and are unknowns. These are determined after using the matching conditions at the interfaces $x = \pm L$.

4.3   Mode Matching Solution

Here we use the continuity of pressures and normal velocities across the regions at interfaces to determine the unknowns modal amplitudes. At matching interfaces

$x = \pm L$, the continuity conditions of pressures are defined by:

$$\psi_1(-L, y) = \psi_2(-L, y), \quad 0 \leqslant y \leqslant a, \tag{4.15}$$

$$\psi_3(L, y) = \psi_2(L, y), \quad 0 \leqslant y \leqslant a. \tag{4.16}$$

On using (4.6)-(4.8) into (4.15) and (4.16), multiplying with $\alpha_h \cosh(\tau_m y)$, integrating from $0 \leqslant y \leqslant a$ and then simplifying the resulting with the aid of OR (4.10), we get

$$\Phi_m^+ = \frac{1}{E_m}\{-F_\ell \delta_{m\ell}E_\ell + \tau_m \sinh(\tau_m a)J_{13}^+ + 2\alpha_h \sum_{n=0}^{\infty} \chi_n^+ \cos(s_n L)R_{mn}\}, \tag{4.17}$$

$$\Phi_m^- = \frac{1}{E_m}\{-F_\ell \delta_{m\ell}E_\ell + \tau_m \sinh(\tau_m a)J_{13}^- - 2i\alpha_h \sum_{n=0}^{\infty} \chi_n^- \sin(s_n L)R_{mn}\}, \tag{4.18}$$

where $\Phi_m^\pm = A_m \pm D_m$ and $\chi_m^\pm = B_m \pm C_m$ for $m = 0, 1, 2, ...$ represent the amplitudes of symmetric/anti-symmetric modes propagating in inlet/outlet and the expansion chamber, respectively.

The quantity R_{mn} reveals the interaction of inlet/outlet modes with expansion chamber modes at interfaces and is defined by

$$R_{mn} = \int_0^a \cosh(\tau_m y)\cosh(\gamma_n y)dy, \tag{4.19}$$

whereas, $J_{13}^\pm = J_1 \pm J_3$ are constants in which

$$J_1 = \frac{\partial \psi_1}{\partial y}(-L, a) \qquad \text{and} \qquad J_3 = \frac{\partial \psi_3}{\partial y}(L, a). \tag{4.20}$$

These constants describe the physical behavior of horizontal membranes bounding the inlet/outlet ducts on finite edges $(\pm L, a)$. For fixed membrane edges, we assume zero displacement conditions at finite edges i.e.,

$$\frac{\partial \psi_1}{\partial y}(-L, a) = 0 \qquad \text{and} \qquad \frac{\partial \psi_3}{\partial y}(L, a) = 0. \tag{4.21}$$

which yields $J_{13}^\pm = 0$.

Now to determine the explicit relations of the amplitudes of expansion chamber modes $\chi_m^\pm, m = 0, 1, 2, ...$, the continuity conditions of normal velocities at interfaces are used.

There are two cases in this regard depending upon the properties of vertical strips which are discussed in subsequent subsections.

4.3.1 Rigid Strips

First we assume that the surfaces lying along $x = \pm L$, $a \leqslant y \leqslant b$ to be acoustically rigid that is

$$\frac{\partial \psi_2}{\partial x}(\pm L, y) = 0, \qquad a \leqslant y \leqslant b. \tag{4.22}$$

Thus the appropriate conditions of normal velocities at interfaces, after multiplied by $\alpha_h \cosh(\gamma_m y)$ and integrated over 0 to b, can be written as

$$\int_0^b \alpha_h \cosh(\gamma_m y) \frac{\partial \psi_2}{\partial x}(-L, y) dy = \int_0^a \alpha_h \cosh(\gamma_m y) \frac{\partial \psi_1}{\partial x}(-L, y) dy \tag{4.23}$$

$$\int_0^b \alpha_h \cosh(\gamma_m y) \frac{\partial \psi_2}{\partial x}(L, y) dy = \int_0^a \alpha_h \cosh(\gamma_m y) \frac{\partial \psi_3}{\partial x}(L, y) dy. \tag{4.24}$$

On substituting (4.6)-(4.8) into (4.23) and (4.24), using the OR (4.13) and then rearranging the resulting equations, we obtain

$$\chi_m^- = \frac{1}{2 s_m G_m \cos(s_m L)} \left\{ \gamma_m \sinh(\gamma_m b) J_{24}^+ + \alpha_h F_\ell \eta_\ell R_{\ell m} - \alpha_h \sum_{n=0}^\infty \Phi_m^- \eta_n R_{nm} \right\}, \tag{4.25}$$

$$\chi_m^+ = \frac{i}{2 s_m G_m \sin(s_m L)} \left\{ \gamma_m \sinh(\gamma_m b) J_{24}^- + \alpha_h F_\ell \eta_\ell R_{\ell m} - \alpha_h \sum_{n=0}^\infty \Phi_m^+ \eta_n R_{nm} \right\}, \tag{4.26}$$

where $J_{24}^\pm = J_2 \pm J_4$ are constants in which

$$J_2 = -i \frac{\partial^2 \psi_2}{\partial x \partial y}(-L, b) \qquad \text{and} \qquad J_4 = -i \frac{\partial^2 \psi_2}{\partial x \partial y}(L, b). \tag{4.27}$$

These constants determine the behavior of membrane bounding the expansion chamber at edge $(\pm L, b)$. For physically fixed edges, the membrane displacement

is zero, that is

$$\frac{\partial \psi_2}{\partial y}(-L, b) = 0 \qquad \text{and} \qquad \frac{\partial \psi_2}{\partial y}(L, b) = 0, \tag{4.28}$$

which after using (4.7) lead to

$$\sum_{n=0}^{\infty} \chi_m^+ \cos(s_m L) \gamma_n \sinh(\gamma_n b) = 0, \tag{4.29}$$

$$\sum_{n=0}^{\infty} \chi_m^- \sin(s_m L) \gamma_n \sinh(\gamma_n b) = 0. \tag{4.30}$$

On multiplying (4.25) by $\sin(s_m L)\gamma_m \sinh(\gamma_m y)$ and (4.26) by $\cos(s_m L)\gamma_m \sinh(\gamma_n b)$, summing over m, and then simplifying with the help of (4.29)-(4.30), we find

$$J_{24}^+ = \frac{\alpha_h}{S_1} \sum_{m=0}^{\infty} \frac{\gamma_m \sinh(\gamma_m b) \tan(s_m L)}{2 s_m G_m} \Big\{ -F_\ell \eta_\ell R_{\ell m} + \sum_{n=0}^{\infty} \Phi_n^- \eta_n R_{nm} \Big\}, \tag{4.31}$$

$$J_{24}^- = \frac{\alpha_h}{S_2} \sum_{m=0}^{\infty} \frac{\gamma_m \sinh(\gamma_m b) \cot(s_m L)}{2 s_m G_m} \Big\{ -F_\ell \eta_\ell R_{\ell m} + \sum_{n=0}^{\infty} \Phi_n^+ \eta_n R_{nm} \Big\}, \tag{4.32}$$

where

$$S_1 = \sum_{m=0}^{\infty} \frac{[\gamma_m \sinh(\gamma_m b) \tan(s_m L)]^2}{2 s_m G_m} \tag{4.33}$$

and

$$S_2 = \sum_{m=0}^{\infty} \frac{[\gamma_m \sinh(\gamma_m b) \cot(s_m L)]^2}{2 s_m G_m}. \tag{4.34}$$

In this way, for rigid vertical strips the Mode-Matching procedure yields two systems of equations defined by (4.17)-(4.18) and (4.25)-(4.26) along with (4.31)-(4.32) containing infinite unknowns in each system. Now these systems can be truncated and solved numerically for unknown amplitudes.

4.3.2 Membrane Strips –a tailored-Galerkin Approach

Here the vertical strips at interfaces lying along $x = \pm L$, $a \leqslant y \leqslant b$ are assumed elastic membranes. This alteration replaces the Neumann's type boundary conditions along the vertical strips with the higher order boundary conditions, for

which the use of traditional Mode-Matching procedure is inappropriate. There-
fore, a tailored Galerkin approach is developed. This approach is different from
the approaches already adopted by Lawrie and Afzal [81] and it provides compet-
itively a more convenient and flexible way of imposing extra edge conditions. The
set of basis functions for the displacements of vertical membranes are determined
from the given conditions at interfaces. Then the extra conditions are imposed
to determine the particular shape of propagating modes. The displacement of
vertical membranes satisfy the equations:

$$\frac{\partial^2 w_1}{\partial y^2} + \mu_v^2 w_1 = \alpha_v \psi_2, \quad x = -L, \quad a \leqslant y \leqslant b, \tag{4.35}$$

$$\frac{\partial^2 w_2}{\partial y^2} + \mu_v^2 w_2 = -\alpha_v \psi_2, \quad x = L, \quad a \leqslant y \leqslant b, \tag{4.36}$$

where $\mu_v = c/c_v$ and $\alpha_v = \rho\omega/(T_v k^3)$ are the membrane wave number and the
fluid loading parameters, respectively. On solving the differential equation (4.35)
and (4.36), the membrane displacement are found to be:

$$w_1(y) = a_1 \cos(\mu_v y) + a_2 \sin(\mu_v y) + \alpha_v \sum_{n=0}^{\infty} \frac{(B_n e^{-is_n L} + C_n e^{is_n L}) \cosh(\gamma_n y)}{\gamma_n^2 + \mu_v^2}, \tag{4.37}$$

$$w_2(y) = a_3 \cos(\mu_v y) + a_4 \sin(\mu_v y) - \alpha_v \sum_{n=0}^{\infty} \frac{(B_n e^{is_n L} + C_n e^{-is_n L}) \cosh(\gamma_n y)}{\gamma_n^2 + \mu_v^2}, \tag{4.38}$$

where the quantities $a_j, j = 1, 2, 3, 4$ are constants whose values will be found
through edge conditions. On adding and subtracting (4.37) and (4.38), the sym-
metric and anti-symmetric modes are found as

$$W^-(y) = a_{13}^- \cos(\mu_v y) + a_{24}^- \sin(\mu_v y) - 2i\alpha_v \sum_{n=0}^{\infty} \frac{\chi_n^- \sin(s_n L) \cosh(\gamma_n y)}{\gamma_n^2 + \mu_v^2}, \tag{4.39}$$

$$W^+(y) = a_{13}^+ \cos(\mu_v y) + a_{24}^+ \sin(\mu_v y) + 2\alpha_v \sum_{n=0}^{\infty} \frac{\chi_n^+ \cos(s_n L) \cosh(\gamma_n y)}{\gamma_n^2 + \mu_v^2}, \tag{4.40}$$

where $a_{13}^\pm = a_1 \mp a_3$, $a_{24}^\pm = a_2 \mp a_4$ and $W^\pm(y) = w_1(y) \mp w_2(y)$. Now we impose
extra edge conditions which not only define the type of connection of vertical
membranes having at finite edges $y = a$ and $y = b$ but also ensure the uniqueness

of the solution. In order to explain the versatility of approach three different types of such conditions are discussed in the subsequent subsections.

i) Fixed Edges

In case of fixed edges the displacements are zero, thus satisfy

$$W^{\pm}(a) = 0 = W^{\pm}(b). \tag{4.41}$$

On using into (4.39)-(4.40) into (4.41), the matrix forms of unknown constants are obtained as:

$$
\begin{bmatrix} a_{13}^- \\ \\ a_{24}^- \end{bmatrix} = U_1^{-1}
\begin{bmatrix} 2i\alpha_v \sum_{n=0}^{\infty} \dfrac{\chi_n^- \sin(s_n L)\cosh(\gamma_n a)}{\gamma_n^2 + \mu_v^2} \\ 2i\alpha_v \sum_{n=0}^{\infty} \dfrac{\chi_n^- \sin(s_n L)\cosh(\gamma_n b)}{\gamma_n^2 + \mu_v^2} \end{bmatrix} \tag{4.42}
$$

and

$$
\begin{bmatrix} a_{13}^+ \\ \\ a_{24}^+ \end{bmatrix} = U_1^{-1}
\begin{bmatrix} -2\alpha_v \sum_{n=0}^{\infty} \dfrac{\chi_n^+ \cos(s_n L)\cosh(\gamma_n a)}{\gamma_n^2 + \mu_v^2} \\ -2\alpha_v \sum_{n=0}^{\infty} \dfrac{\chi_n^+ \cos(s_n L)\cosh(\gamma_n b)}{\gamma_n^2 + \mu_v^2} \end{bmatrix}. \tag{4.43}
$$

where

$$
U_1 = \begin{bmatrix} \cos(\mu_v a) & \sin(\mu_v a) \\ \cos(\mu_v b) & \sin(\mu_v b) \end{bmatrix}. \tag{4.44}
$$

Now the constants $a_{13}^{\pm}$ and $a_{24}^{\pm}$ can easily be found from (4.42) and (4.43) which yield $a_j, j = 1, 2, 3, 4$.

ii) Free Edges

For free edges, the gradient is zero, that are

$$\frac{\partial W^{\pm}(a)}{\partial y} = 0 = \frac{\partial W^{\pm}(b)}{\partial y}, \tag{4.45}$$

On using (4.39)-(4.40) into (4.45), the suitable matrix forms of unknowns are found to be

$$
\begin{bmatrix} a_{13}^- \\ \\ a_{24}^- \end{bmatrix} = U_2^{-1} \begin{bmatrix} 2i\alpha_v \sum_{n=0}^{\infty} \dfrac{\chi_n^- \sin(s_n L)\gamma_n \sinh(\gamma_n a)}{\gamma_n^2 + \mu_v^2} \\ 2i\alpha_v \sum_{n=0}^{\infty} \dfrac{\chi_n^- \sin(s_n L)\gamma_n \sinh(\gamma_n b)}{\gamma_n^2 + \mu_v^2} \end{bmatrix}, \tag{4.46}
$$

$$
\begin{bmatrix} a_{13}^+ \\ \\ a_{24}^+ \end{bmatrix} = U_2^{-1} \begin{bmatrix} -2\alpha_v \sum_{n=0}^{\infty} \dfrac{\chi_n^+ \cos(s_n L)\gamma_n \sinh(\gamma_n a)}{\gamma_n^2 + \mu_v^2} \\ -2\alpha_v \sum_{n=0}^{\infty} \dfrac{\chi_n^+ \cos(s_n L)\gamma_n \sinh(\gamma_n b)}{\gamma_n^2 + \mu_v^2} \end{bmatrix}, \tag{4.47}
$$

where

$$
U_2 = \begin{bmatrix} -\mu_v \sin(\mu_v a) & \mu_v \cos(\mu_v a) \\ -\mu_v \sin(\mu_v b) & \mu_v \cos(\mu_v b) \end{bmatrix}, \tag{4.48}
$$

which yield constants $a_{13}^\pm$ and $a_{24}^\pm$.

iii) Spring-like Edges

The spring like conditions corresponds to a situation in which membrane is attached to a light spring which moves horizontally in the plane $y = a$ and $y = b$. The appropriate edge conditions in this case for the problem in hand are

$$
\xi_a w_1 + \frac{\partial w_1}{\partial y} = 0, \qquad y = a \tag{4.49}
$$

$$
\xi_b w_2 + \frac{\partial w_2}{\partial y} = 0, \qquad y = b \tag{4.50}
$$

where $\xi_a = \bar{\xi}_a/k$ and $\xi_b = \bar{\xi}_b/k$ in which $\bar{\xi}_a$ and $\bar{\xi}_b$ are coupling constants. On using (4.39)-(4.40) into (4.49)-(4.50) two systems containing unknowns $a_{13}^\pm$ and $a_{24}^\pm$ are obtained. The matrix form of these system are

$$
\begin{bmatrix} a_{13}^- \\ \\ a_{24}^- \end{bmatrix} = U_3^{-1} \begin{bmatrix} 2i\alpha_v \sum_{n=0}^{\infty} \dfrac{\chi_n^- \sin(s_n L)\{\xi_a \cosh(\gamma_n a) + \gamma_n \sinh(\gamma_n a)\}}{\gamma_n^2 + \mu_v^2} \\ 2i\alpha_v \sum_{n=0}^{\infty} \dfrac{\chi_n^- \sin(s_n L)\{\xi_b \cosh(\gamma_n b) + \gamma_n \sinh(\gamma_n b)\}}{\gamma_n^2 + \mu_v^2} \end{bmatrix}. \tag{4.51}
$$

and

$$\begin{bmatrix} a_{13}^+ \\ \\ a_{24}^+ \end{bmatrix} = U_3^{-1} \begin{bmatrix} -2\alpha_v \sum_{n=0}^{\infty} \dfrac{\chi_n^+ \cos(s_n L)\{\xi_a \cosh(\gamma_n a) + \gamma_n \sinh(\gamma_n a)\}}{\gamma_n^2 + \mu_v^2} \\ -2\alpha_v \sum_{n=0}^{\infty} \dfrac{\chi_n^+ \cos(s_n L)\{\xi_b \cosh(\gamma_n b) + \gamma_n \sinh(\gamma_n b)\}}{\gamma_n^2 + \mu_v^2} \end{bmatrix}. \quad (4.52)$$

where

$$U_3 = \begin{bmatrix} \xi_a \cos(\mu_v a) - \mu_v \sin(\mu_v a) & \xi_a \sin(\mu_v a) + \mu_v \cos(\mu_v a) \\ \xi_b \cos(\mu_v b) - \mu_v \sin(\mu_v b) & \xi_b \sin(\mu_v b) + \mu_v \cos(\mu_v b) \end{bmatrix} \quad (4.53)$$

Now from (4.51)-(4.52) the constants $a_{13}^{\pm}$ and $a_{24}^{\pm}$ can be found in a straightforward way.

Now we assume the continuity of normal velocities at $x = \pm L$. The appropriate velocity conditions for membrane strip when multiplied by $\alpha_h \cosh(\gamma_n y)$ and integrated from 0 to b takes the form:

$$\int_0^b \alpha_h \cosh(\gamma_m y) \frac{\partial \psi_2}{\partial x}(-L, y) dy = \int_0^a \alpha_h \cosh(\gamma_m y) \frac{\partial \psi_1}{\partial x}(-L, y) dy$$
$$+ \int_a^b \alpha_h \cosh(\gamma_m y) w_1(y) dy \quad (4.54)$$

and

$$\int_0^b \alpha_h \cosh(\gamma_m y) \frac{\partial \psi_2}{\partial x}(L, y) dy = \int_0^a \alpha_h \cosh(\gamma_m y) \frac{\partial \psi_3}{\partial x}(L, y) dy$$
$$+ \int_a^b \alpha_h \cosh(\gamma_m y) w_2(y) dy. \quad (4.55)$$

On invoking (4.6)-(4.8) into (4.54) and (4.55), using the OR (4.13) and then simplifying the resulting equations, we find

$$\chi_m^- = \frac{1}{2s_m G_m \cos(s_m L)}\{\gamma_m \sinh(\gamma_m b) J_{24}^+ + \alpha_h F_\ell \eta_\ell R_{\ell m} - \alpha_h \sum_{n=0}^{\infty} \Phi_n^- \eta_n R_{nm}\}$$
$$- \frac{\alpha_h}{2s_m G_m \cos(s_m L)}\{i a_{13}^+ P_{1m} + i a_{24}^+ P_{2m} - 2\alpha_v \sum_{n=0}^{\infty} \frac{\chi_n^- \sin(s_n L) T_{mn}}{\gamma_n^2 + \mu_v^2}\},$$
$$(4.56)$$

$$\chi_m^+ = \frac{i}{2s_mG_m\sin(s_mL)}\{\gamma_m\sinh(\gamma_m b)J_{24}^- + \alpha_h F_\ell \eta_\ell R_{\ell m} - \alpha_h \sum_{n=0}^{\infty} \Phi_n^+ \eta_n R_{nm}\}$$

$$+ \frac{\alpha_h}{2s_mG_m\sin(s_mL)}\{a_{13}^- P_{1m} + a_{24}^- P_{2m} + 2\alpha_v \sum_{n=0}^{\infty} \frac{\chi_n^+ \cos(s_nL)T_{mn}}{\gamma_n^2 + \mu_v^2}\}, \tag{4.57}$$

where

$$P_{1m} = \int_a^b \cos(\mu_v y)\cosh(\gamma_m y)dy, \tag{4.58}$$

$$P_{2m} = \int_a^b \sin(\mu_v y)\cosh(\gamma_m y)dy, \tag{4.59}$$

and

$$T_{mn} = \int_a^b \cos(\gamma_n y)\cosh(\gamma_m y)dy. \tag{4.60}$$

Note that there appear constants $J_{24}^{\pm}$ in (4.56) and (4.57). These constants describe the behavior of horizontal membrane of expansion chamber on edges and are found from the edge conditions. For fixed edges conditions (4.28), it is found that

$$J_{24}^+ = \frac{\alpha_h}{S_1} \sum_{m=0}^{\infty} \frac{\gamma_m \sinh(\gamma_m b)\tan(s_mL)}{2s_mG_m}\{-F_\ell \eta_\ell R_{\ell m} + ia_{13}^+ P_{1m} + ia_{24}^+ P_{2m}\}$$

$$+ \frac{\alpha_h}{S_1} \sum_{n=0}^{\infty}\sum_{m=0}^{\infty} \frac{\gamma_m \sinh(\gamma_m b)\tan(s_mL)}{2s_mG_m}\{\Phi_n^- \eta_n R_{nm} - \frac{2\alpha_v \chi_n^- \sin(s_nL)T_{mn}}{(\gamma_n^2 + \mu_v^2)}\} \tag{4.61}$$

and

$$J_{24}^- = \frac{\alpha_h}{S_2} \sum_{m=0}^{\infty} \frac{\gamma_m \sinh(\gamma_m b)\cot(s_mL)}{2s_mG_m}\{-F_\ell \eta_\ell R_{\ell m} + ia_{13}^- P_{1m} + ia_{24}^- P_{2m}\}$$

$$+ \frac{\alpha_h}{S_2} \sum_{n=0}^{\infty}\sum_{m=0}^{\infty} \frac{\gamma_m \sinh(\gamma_m b)\cot(s_mL)}{2s_mG_m}\{\Phi_n^+ \eta_n R_{nm} + \frac{2i\alpha_v \chi_n^+ \cos(s_nL)T_{mn}}{(\gamma_n^2 + \mu_v^2)}\}. \tag{4.62}$$

Thus, for membrane vertical strips the Mode-Matching procedure in conjunction with tailored-Galerkin approach yields two systems of equations defined by (4.17)-(4.18) and (4.56)-(4.57) along with (4.61)-(4.62).

These are truncated first and then solved numerically by considering different set of

edge conditions imposed on vertical membrane strips to get unknown amplitudes.

4.4 Low Frequency Approximation

Here the modeled problem is solved by using the Low-frequency approximation (LFA). The approach is useful especially in low frequency regime wherein only limited number of modes are important to analyze energy scattering. The usual LFA discussed in [101], for an unmodified expansion chamber, is derived by approximating the velocity potentials to the fundamental plane wave modes of duct regions. However, for the current geometry the velocity potentials of inlet/outlet and expansion chamber are truncated to M and N modes respectively.

Thus, $M+1$ modes in inlet/outlet and $N+1$ modes in expansion chamber will be taken into consideration. But the total number of modes $2M+N+3$, are consistent with number the physical conditions applied on the configuration. Therefore, the eigenfunction expansions of field potentials are approximated as:

$$\psi_1(x,y) \approx F_\ell \cosh(\tau_\ell y)e^{i\eta_\ell(x+L)} + \sum_{n=0}^{M} A_n \cosh(\tau_n y)e^{-i\eta_n(x+L)}, \quad x < -L, \quad (4.63)$$

$$\psi_2(x,y) \approx \sum_{n=0}^{N}(B_n e^{is_n x} + C_n e^{-is_n x})\cosh(\gamma_n y), \qquad x > -L, \quad (4.64)$$

$$\psi_3(x,y) \approx \sum_{n=0}^{M} D_n \cosh(\tau_n y)e^{i\eta_n(x-L)}, \quad x < L, \quad (4.65)$$

where A_n, $\{B_n, C_n\}$ and D_n are the approximated amplitudes of scattering waves in the inlet, expansion chamber and outlet regions, respectively.

Now to determine these approximated amplitudes following conditions are applicable by using low frequency approximation. The continuity of pressures and normal

velocities reveal

$$\int_0^a \psi_1(-L, y)dy = \int_0^a \psi_2(-L, y)dy, \tag{4.66}$$

$$\int_0^a \psi_3(L, y)dy = \int_0^a \psi_2(L, y)dy, \tag{4.67}$$

and

$$\int_0^a \frac{\partial \psi_2}{\partial x}(-L, y)dy = \int_0^a \frac{\partial \psi_1}{\partial x}(-L, y)dy, \tag{4.68}$$

$$\int_0^a \frac{\partial \psi_2}{\partial x}(L, y)dy = \int_0^a \frac{\partial \psi_3}{\partial x}(L, y)dy, \tag{4.69}$$

respectively. Now on invoking (4.63)-(4.65) into (4.66)-(4.69), which after some rearrangements of the resulting equations lead to

$$\sum_{n=0}^{M} \frac{\Phi_n^+ \sinh(\tau_n a)}{\tau_n} = -\frac{F_\ell \sinh(\tau_\ell a)}{\tau_\ell} + \sum_{n=0}^{N} \frac{2\chi_n^+ \cos(s_n L) \sinh(\gamma_n a)}{\gamma_n} \tag{4.70}$$

$$\sum_{n=0}^{M} \frac{\Phi_n^- \sinh(\tau_n a)}{\tau_n} = -\frac{F_\ell \sinh(\tau_\ell a)}{\tau_\ell} + \sum_{n=0}^{N} \frac{2i\chi_n^- \sin(s_n L) \sinh(\gamma_n a)}{\gamma_n} \tag{4.71}$$

and

$$\sum_{n=0}^{N} \frac{2\chi_n^+ s_n \cos(s_n L) \sinh(\gamma_n a)}{\gamma_n} = \frac{F_\ell \sinh(\tau_\ell a)}{\tau_\ell} - \sum_{n=0}^{M} \frac{\Phi_n^+ \eta_n \sinh(\tau_n a)}{\tau_n} \tag{4.72}$$

$$\sum_{n=0}^{N} \frac{2i\chi_n^- s_n \sin(s_n L) \sinh(\gamma_n a)}{\gamma_n} = -\frac{F_\ell \sinh(\tau_\ell a)}{\tau_\ell} - \sum_{n=0}^{M} \frac{\Phi_n^- \eta_n \sinh(\tau_n a)}{\tau_n}. \tag{4.73}$$

Furthermore, to consider the effects of edge conditions imposed on the finite edges of horizontal membranes we use (4.63)-(4.65) into (4.21) and (4.28), which after some manipulation yield

$$\sum_{n=0}^{M} \Phi_n^\pm \tau_n \sinh(\tau_n a) = -F_\ell \tau_\ell \sinh(\tau_\ell a), \tag{4.74}$$

$$\sum_{n=0}^{N} \chi_n^+ \gamma_n \sinh(\gamma_n b) \cos(s_n L) = 0, \tag{4.75}$$

and

$$\sum_{n=0}^{N} \chi_n^- \gamma_n \sinh(\gamma_n b) \sin(s_n L) = 0, \tag{4.76}$$

Moreover, some more modes in expansion chamber can be included by considering the properties of vertical strips at interfaces $x = \pm L$. Two cases are considered herein that are discussed in following subsections.

4.4.1 Rigid Strips

In this case the velocity flux along the strips $x = \pm L$, $a \leqslant y \leqslant b$ is assumed to be zero i.e.,

$$\int_a^b \frac{\partial \psi_2}{\partial x}(\pm L, y)dy = 0. \tag{4.77}$$

which lead to

$$\sum_{n=0}^{N} \frac{s_n \chi_n^- \cos(s_n L)\{\sinh(\gamma_n b) - \sinh(\gamma_n a)\}}{\gamma_n} = 0, \tag{4.78}$$

$$\sum_{n=0}^{N} \frac{s_n \chi_n^+ \sin(s_n L)\{\sinh(\gamma_n b) - \sinh(\gamma_n a)\}}{\gamma_n} = 0. \tag{4.79}$$

In this way two systems of equations defined by (4.70)-(4.76) and (4.78)-(4.79) are obtained. These can be solved for unknown amplitudes after fixing the truncating parameters $M = 1$ and $N = 2$.

4.4.2 Membrane Strips

Here we assume the case when vertical strips along $x = \pm L$, $a \leqslant y \leqslant b$ are taken to be elastic membranes. The appropriate velocity flux conditions at $x = \pm L$, $a \leqslant y \leqslant b$ can be given by

$$\int_a^b \frac{\partial \psi_2}{\partial x}(-L, y)dy = \int_a^b w_1(y)dy, \tag{4.80}$$

and

$$\int_a^b \frac{\partial \psi_2}{\partial x}(L, y)dy = \int_a^b w_2(y)dy. \tag{4.81}$$

On invoking (4.64) along with the truncated forms of (4.37) and (4.38) into (4.80) and (4.81), and after some algebraic manipulation it is found that

$$\sum_{n=0}^N \frac{2i\chi_n^- \{s_n \cos(s_n L)(\gamma_n^2 - \mu_v^2)) + \alpha_v \sin(s_n L)\}(\sinh(\gamma_n b) - \sinh(\gamma_n a))}{\gamma_n(\gamma_n^2 - \mu_v^2)} =$$

$$\frac{a_{13}^-}{\mu_v}\{\sin(\mu_v b) - \sin(\mu_v a)\} - \frac{a_{24}^-}{\mu_v}\{\cos(\mu_v b) - \cos(\mu_v a)\} \tag{4.82}$$

and

$$\sum_{n=0}^N \frac{2\chi_n^+ \{s_n \sin(s_n L)(\gamma_n^2 - \mu_v^2)) + \alpha_v \cos(s_n L)\}(\sinh(\gamma_n b) - \sinh(\gamma_n a))}{\gamma_n(\gamma_n^2 - \mu_v^2)} =$$

$$\frac{a_{13}^+}{\mu_v}\{\sin(\mu_v b) - \sin(\mu_v a)\} - \frac{a_{24}^+}{\mu_v}\{\cos(\mu_v b) - \cos(\mu_v a)\}. \tag{4.83}$$

Thus, we obtain two systems of equations defined by (4.70)-(4.76) and (4.82)-(4.83), that can be solved for unknown amplitudes after fixing $M = 1$ and $N = 2$.

4.5   Numerical Results and Discussion

The graphical results presented in this section are obtained from the truncated forms of Mode-Matching (MM) and Mode-Matching tailored Galerkin (MMTG) approaches. For the fundamental mode incident, the MM and MMTG results are shown in comparison with the Low Frequency Approximation (LFA). The numerical computations are performed after fixing the parameters as: membrane tension T = 3250 Nm^{-1}, membrane mass density $\rho_m = 0.2$ kgm^{-3}, the speed of sound in air $c = 344$ ms^{-1}, density of air $\rho = 1.2$ kgm^{-3}, and the dimensional duct heights $\bar{a} = 0.15$ m, $\bar{b} = 0.3$ m and $\bar{L} = 0.17$ m. The reflected energy flux in inlet

and the transmitted energy flux in outlet are found by using the definition given in [112] as

$$\mathcal{E}_{\mathrm{r}} = \frac{1}{\alpha} \sum_{m=0}^{\mathcal{K}-1} |A_m|^2 \eta_m E_m \tag{4.84}$$

and

$$\mathcal{E}_{\mathrm{t}} = \frac{1}{\alpha} \sum_{m=0}^{\mathcal{K}-1} |D_m|^2 \eta_m E_m, \tag{4.85}$$

respectively, where the incident energy flux/power is being scaled at unity and thus yields the conserve power identity $\mathcal{E}_{\mathrm{r}} + \mathcal{E}_{\mathrm{t}} = 1$. This identity states that if unit power is given to the system it will be equal to the sum of scattering powers in the inlet and outlet duct regions. Note that the quantity $\mathcal{K}$ denotes the number of cut-on in inlet/outlet ducts $|x| > L$.

For comparison purposes, the graphs with vertical rigid strips are depicted in Fig. 4.2 whilst the results with membrane vertical strips subjected to different edge conditions are shown in Figs. 4.3–4.5. Two different exciting modes are considered to get the scattering energies against frequency; the structural-borne mode (fundamental mode) incident Figs. 4.2(a)–4.5(a) and the fluid-borne mode (secondary mode) incident Figs. 4.2(b)–4.5(b). It is found that the results obtained via MM, MMTG techniques and LFA coincide for fundamental mode incident while for the higher order mode incident the matching is not good enough. Therefore the results obtained via MM, MMTG and LFA are compared for fundamental mode incident only. This is due to the fact that in LFA case a limited number of modes are allowed to propagate and it contains inability to account the contributions of higher order modes of propagation.

Note that the inlet/outlet and expansion chamber of heights $\bar{a} = 0.15$ m and $\bar{b} = 0.3$ m contain cut-on frequencies 301 Hz and 191 Hz, respectively. These cut-on frequencies have impact on the distribution of energy in frequency regime, see Fig 4.2. Clearly the transmission increases after cut-on of expansion chamber appeared at 191 Hz while the reflected energy becomes dominant after the first cut-on of inlet/ outlet which occurs at 301 Hz. Although the scattering energies have dips at 80 Hz, 260 Hz and 290 Hz. These dips are due to the trigonometric

term present in both the reflected and transmitted energies. Fig. 4.2(b) show the reflected and transmitted energies when the structure is radiated by the fluid-borne mode ($\ell = 1$) which cuts-on at 301 Hz. Clearly, for this case the reflected energy drops while the transmitting energy raises gradually below the second cut-on of the expansion chamber that occurs at 657 Hz. As maximum of the energy is transferring along the boundaries of the expansion chamber below this range. However when the secondary mode of the expansion chamber becomes cut-on the maximum of the energy is shifted to fluid and thus reflection is increased (a sudden inversion in Fig. 4.2(b) is evident).

(a) Structure-borne mode incident ($\ell = 0$).

(b) Fluid-borne mode incident ($\ell = 1$).
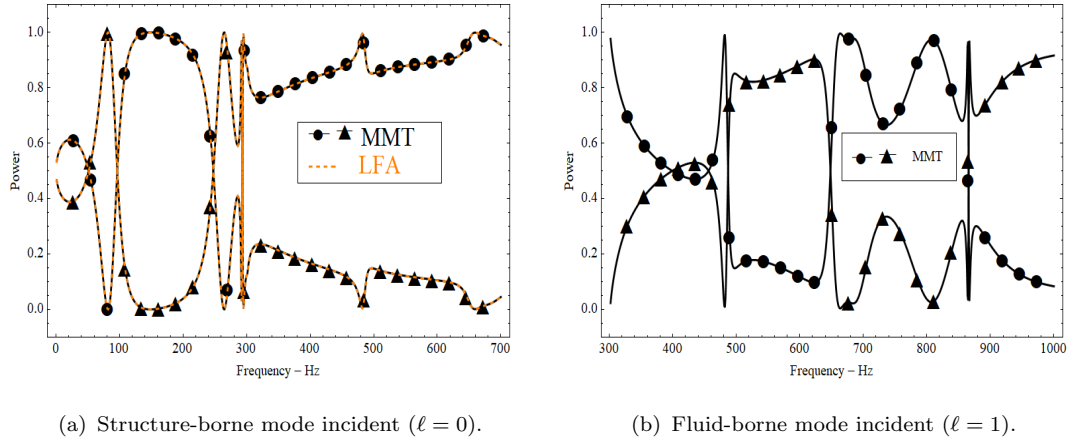
FIGURE 4.2: Rigid strips: The reflected energy flux $\mathcal{E}_\mathrm{r}$ (▲) and transmitted energy flux $\mathcal{E}_\mathrm{t}$ (●) against frequency with $\alpha_h = 3.308$ and $\mu_h = 2.695$.

The scattering of energies against frequency with membrane vertical strips are depicted in Figs. 4.3–4.5. Each of the figure is dissimilated by the edge conditions on vertical membranes. The results with MMTG are shown with symbols; the reflected energy flux (▲) and the transmitted energy flux (●) whilst the dashed curves delineates the outcomes with LFA. It can be seen that the conserved power identity is satisfied in whole frequency regime for each set of edge conditions and for both the structural-borne mode incident ($\ell = 0$) and the fluid-borne mode incident ($\ell = 1$). Fig. 4.3 shows the reflected and transmitted energies while the vertical membrane strips are being fixed tightly with the edges of horizontal membrane. It is found that when the structure is radiated with structure-born mode, a clear agreement between MMTG and LFA is in seen before the first cut-on frequency (301 Hz) of inlet/outlet duct. However this agreement is not good enough in the

range of second or higher order modes propagation. The fact that LFA deviates due to its inability to cater the information from the propagation of higher order modes. Similar behavior is prompted while the vertical membrane strips are being free (see Fig. 4.4(a)) or contain spring-like (see Fig. 4.5(a)) connections with horizontal membrane. Moreover, the overall scattering performance of vertical membrane strips in structure-born mode case resembles closely with the rigid vertical strips. However the presence of bridging membrane becomes apparent, when the structure is radiated with fluid-born mode. Note that this mode cuts-on at frequency 301 Hz. A significant variation in in scattering energies with change of edge conditions is noted which become more prominent after the secondary cut-on frequency of expansion chamber 657 Hz. The inversion of scattering energies with dips is evident which vary with variation of edge conditions.

(a) Structure-borne mode incident ($\ell = 0$). (b) Fluid-borne mode incident ($\ell = 1$).
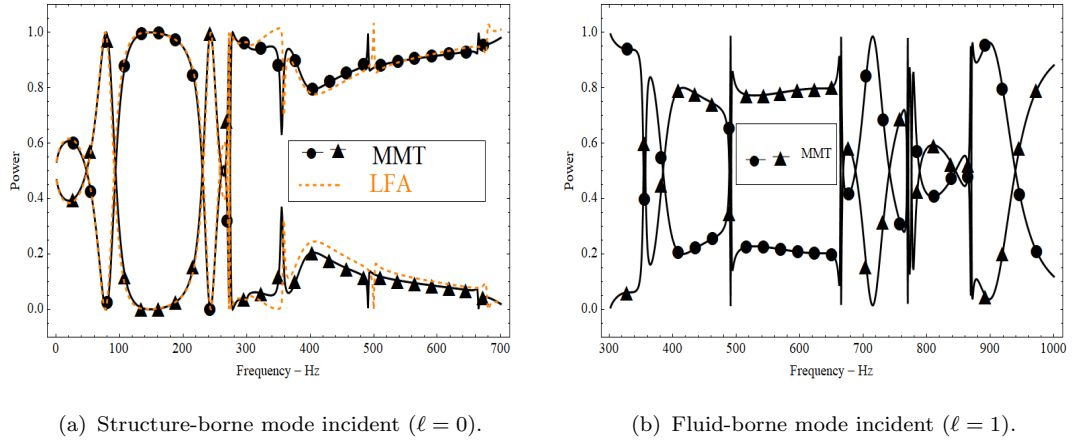
FIGURE 4.3: Membrane strips containing fixed edges: The reflected energy flux $\mathcal{E}_r$ (▲) and transmitted energy flux $\mathcal{E}_t$ (●) against frequency with $\alpha_h = 3.308$, $\mu_h = 2.695$, $\alpha_v = 3.308$ and $\mu_v = 2.695$.

The performance of an HVAC unit is usually measured in the term of transmission loss. The formula for transmission loss is: $\text{TL} = -10 \log_{10}(\mathcal{E}_t)$, where the incident power ($\mathcal{E}_i$) is being scaled at unity. Fig. 4.6 shows the transmission loss against frequency with rigid vertical strips. Both MM results (solid line with arrow) and LFA results (dashed line) are plotted together for structure-born mode incident. It is found that both the approaches show a good agreement (see Fig. 4.6(a)). A dome-like behavior is seen in frequency range 0-80 Hz and a stop-band is produced prior to the first cut-on of inlet/outlet in frequency range 82-265 Hz with band

(a) Structure-borne mode incident ($\ell = 0$).

(b) Fluid-borne mode incident ($\ell = 1$).
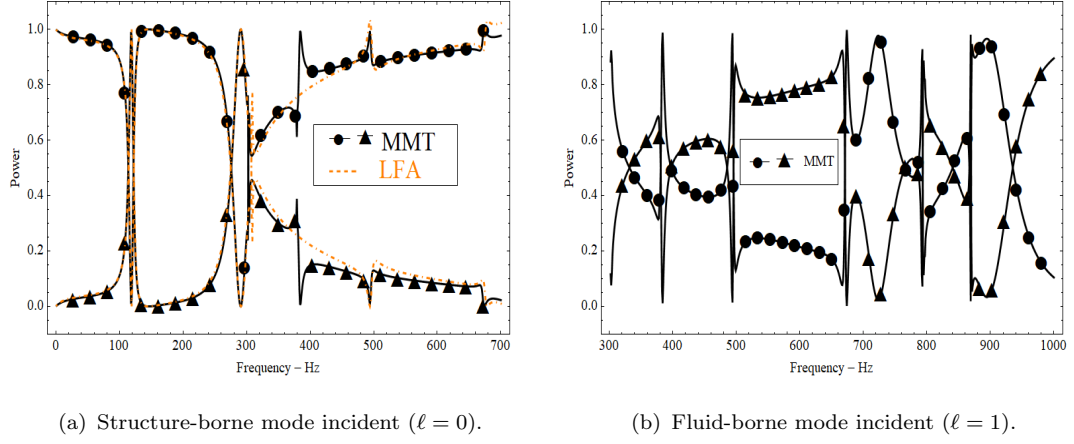
FIGURE 4.4: Membrane strips containing free edges: The reflected energy flux $\mathcal{E}_r$ (▲) and transmitted energy flux $\mathcal{E}_t$ (●) against frequency with $\alpha_h = 3.308$, $\mu_h = 2.695$, $\alpha_v = 3.308$ and $\mu_v = 2.695$.

(a) Structure-borne mode incident ($\ell = 0$).

(b) Fluid-borne mode incident ($\ell = 1$).
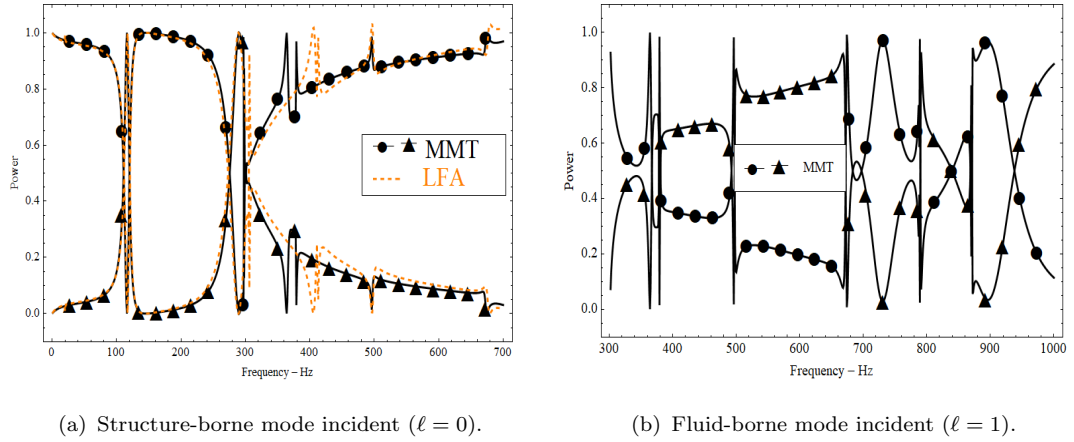
FIGURE 4.5: Membrane strips containing spring-like edges: The reflected energy flux $\mathcal{E}_r$ (▲) and transmitted energy flux $\mathcal{E}_t$ (●) against frequency with $\alpha_h = 3.308$, $\mu_h = 2.695$, $\alpha_v = 3.308$ and $\mu_v = 2.695$.

width 3.23. It clearly reveals a high transmission loss for low frequency range of noise. But once the new mode starts propagating the TL falls rapidly. Nevertheless, the TL peaks occur before the cut-on modes of the duct regions located at 191 Hz, 301 Hz and 657 Hz.

Fig. 4.6(b) indicates the TL against frequency when the considered configuration is radiated by the fluid-born mode. The stop-band produced here are in frequency range 468-492 Hz with a small band width of 1.05. It occurs before the new cut-on frequency of the expansion chamber. More stop-bands with small pass-band are produced after the new cut-on in the frequency range 623-860 Hz. Whereas,

the non-periodic variation in peaks at frequencies 482 Hz, 664 Hz, 812 Hz and 865 Hz represents the attenuation of the higher order modes, especially at high frequencies.

(a) Structure-borne mode incident ($\ell = 0$).

(b) Fluid-borne mode incident ($\ell = 1$).
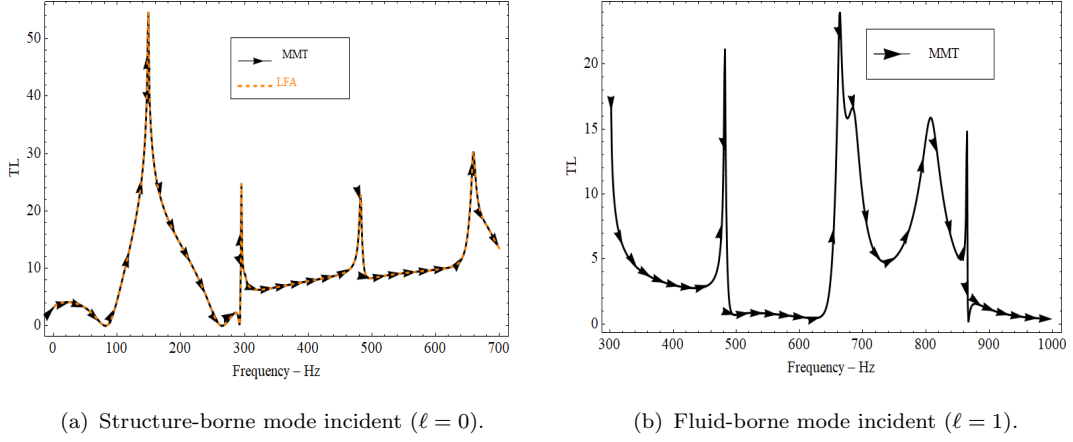
FIGURE 4.6: Rigid strips: Transmission loss against frequency with $\alpha_h = 3.308$ and $\mu_h = 2.695$.

TL through the wave-bearing cavity bridged by vertical membrane strips is shown in Figs. 4.7–4.12. The material properties of these vertical membranes and the membrane bounding the cavity horizontally are taken to be identical by using: $\alpha_h = \alpha_v = 3.308$ and $\mu_h = \mu_v = 2.695$ as well as different by considering: $\alpha_h = 3.308, \quad \alpha_v = 0.94$ and $\mu_h = 2.694, \quad \mu_v = 1.44$. Moreover, the edge conditions of vertical membranes are assumed to fixed, free or spring-like. The results obtained via MMTG (line with arrow head) are compared with LFA (dashed lining) for structure-born mode incident only, wherein a good agreement in results is observed in low frequency regime. Whereas, for higher frequencies the LFA deviates due to its inability to account the contribution from higher order modes of wave propagation.

Figs. 4.7 and 4.8 show TL against frequency with fixed edge conditions. A dome-like behavior in frequency range 0-79 Hz and a stop-band with band width of 3.076 in the frequency range 79-243 Hz is found, while the structure-borne mode is incident and material properties of bounding cavity are homogeneous (see Fig. 4.7(a)). However, by taking different material properties of horizontal and vertical membranes, a significant variation in attenuation is noted. More attenuation with heterogeneous properties of bounding cavity is revealed (see Figs. 4.7(a) and

4.8(a)). Likewise, behavior is evident for the case of fluid-borne mode incident (see Figs. 4.7(b) and 4.8(b)).

Also it is found that sound reduction in all the domes of frequencies of the vertical membranes placed at zero displacement is much more than the case of vertical rigid strips.

(a) Structure-borne mode incident ($\ell = 0$).

(b) Fluid-borne mode incident ($\ell = 1$).

FIGURE 4.7: Membrane strips containing fixed edges: Transmission loss against frequency for $\alpha_h = \alpha_v = 3.308$ and $\mu_h = \mu_v = 2.695$.

(a) Structure-borne mode incident ($\ell = 0$).

(b) Fluid-borne mode incident ($\ell = 1$).

FIGURE 4.8: Membrane strips containing fixed edges: Transmission loss against frequency for $\alpha_h = 3.308$, $\alpha_v = 0.94$, $\mu_h = 2.694$ and $\mu_v = 1.44$.

Figs. 4.9 and 4.10 show the graphical results when the vertical membranes of cavity are free to move at edges and the horizontal membranes are fixed tightly with edges. The material properties of both type of membranes are identical. In Figs. 9a and 10a, a wide stop-band with narrow pass-band in low frequency

regime < 300Hz is found, while the configuration is radiated through structure-borne mode. A leakage of compressional waves with free edges is evident (see Figs. 4.9(a) and 4.10(a)).

Furthermore, the highest TL peak with heterogeneous membranes (81.37 dB at 269 Hz in Fig 9b) is greater than that of homogeneous membranes (62.59 dB at 146 Hz in Fig 4.9(a)). However, when the configuration is radiated by the fluid-borne mode, the TL peaks of 19.38 dB, 18.52 dB and 27.24 dB respectively occur at 384 Hz, 494 Hz and 674 Hz for homogeneous membranes of cavity, whereas, these peaks are 22.42 dB, 24.98 dB and 18.96 dB at 535 Hz, 672 Hz and 718 Hz for heterogeneous case. These peaks are due to the harmonic resonance of the cavity.

(a) Structure-borne mode incident ($\ell = 0$).

(b) Fluid-borne mode incident ($\ell = 1$).
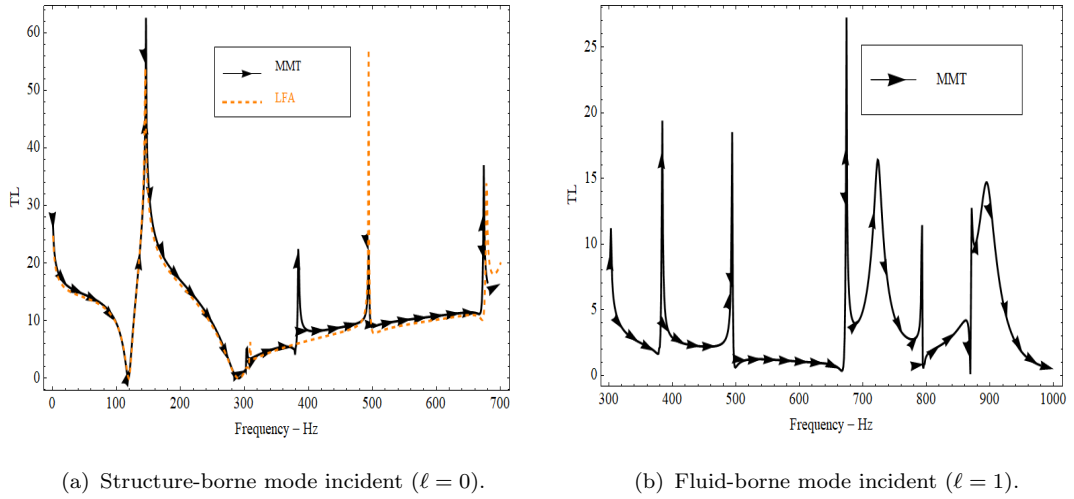
FIGURE 4.9: Membrane strips containing free edges: Transmission loss against frequency for $\alpha_h = \alpha_v = 3.308$ and $\mu_h = \mu_v = 2.695$.

The effects of spring like edge conditions of vertical membranes of cavity on TL against frequency are depicted in Figs. 4.11 and 4.12. The coupling constants $\bar{\xi}_a$ and $\bar{\xi}_b$ are assumed to be unity. The peaks in TL curve seen in Figs. 11a are 55.25 dB, 35 dB, 18.57 dB and 27.8 dB which occur at frequencies 146 Hz, 364 Hz, 496 Hz and 675 Hz, respectively. Nevertheless, such peak values are 31.9 dB, 18.1 dB, 17.45 dB and 21 dB with fluid-borne radiation (see Fig. 4.9(b)). However the results of spring like edges resemble closely with free edges because the compressional waves lose energy at the edges. Moreover, the tuning of the

(a) Structure-borne mode incident ($\ell = 0$).   (b) Fluid-borne mode incident ($\ell = 1$).
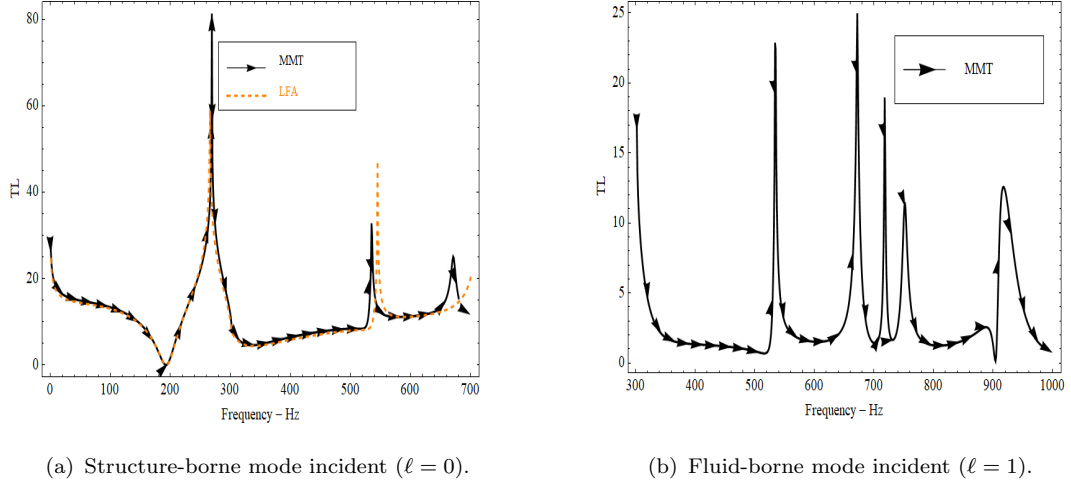
FIGURE 4.10: Membrane strips containing free edges: Transmission loss against frequency for $\alpha_h = 3.308$, $\alpha_v = 0.94$, $\mu_h = 2.695$ and $\mu_v = 1.44$.

component in given frequency regime can be adjusted by changing the material properties of walls. Furthermore, the MMTG and LFA curves contain a little variation at about every new cut-on of the cavity or expansion chamber. The fact leads to the inability of LFA to cater the contribution from every new propagating mode. Since the eigenvalues changes from imaginary to positive real value.

(a) Structure-borne mode incident ($\ell = 0$).   (b) Fluid-borne mode incident ($\ell = 1$).
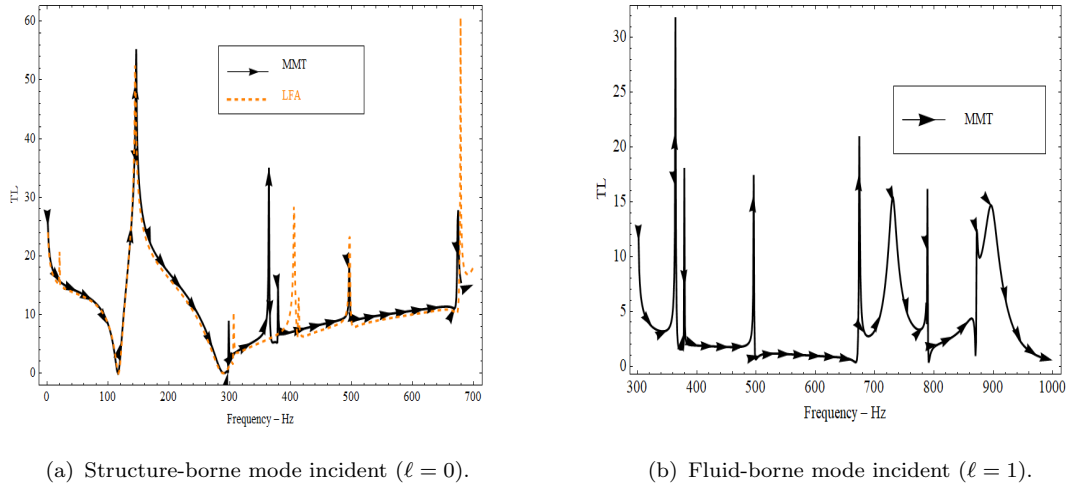
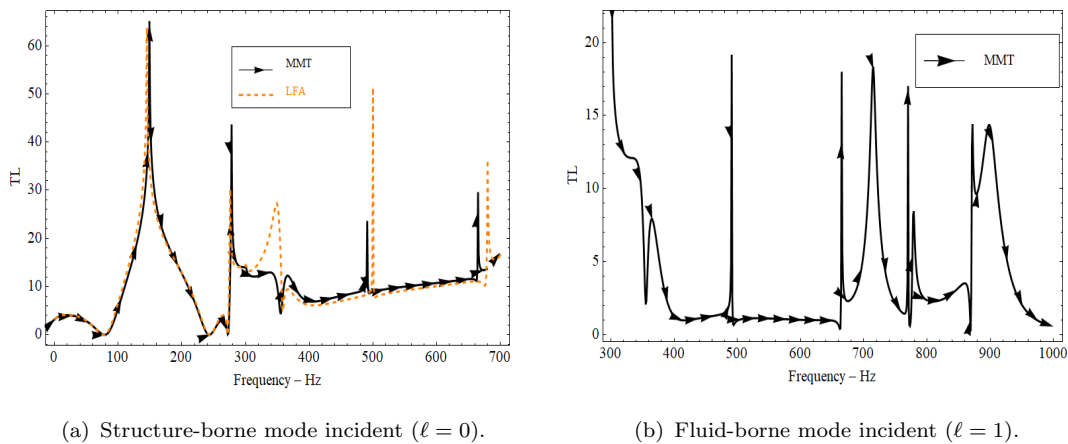FIGURE 4.11: Membrane strips containing spring like edges: Transmission loss against frequency for $\alpha_h = \alpha_v = 3.308$ and $\mu_h = \mu_v = 2.695$.

In next Figs. 4.13–4.14, the matching conditions are reconstructed form the truncated form Mode-Matching solution at $f = 350Hz$, while, the dimensional heights and half length of the chamber are fixed at $\bar{a} = 0.06$ m, $\bar{b} = 0.085$ m and

(a) Structure-borne mode incident ($\ell = 0$).

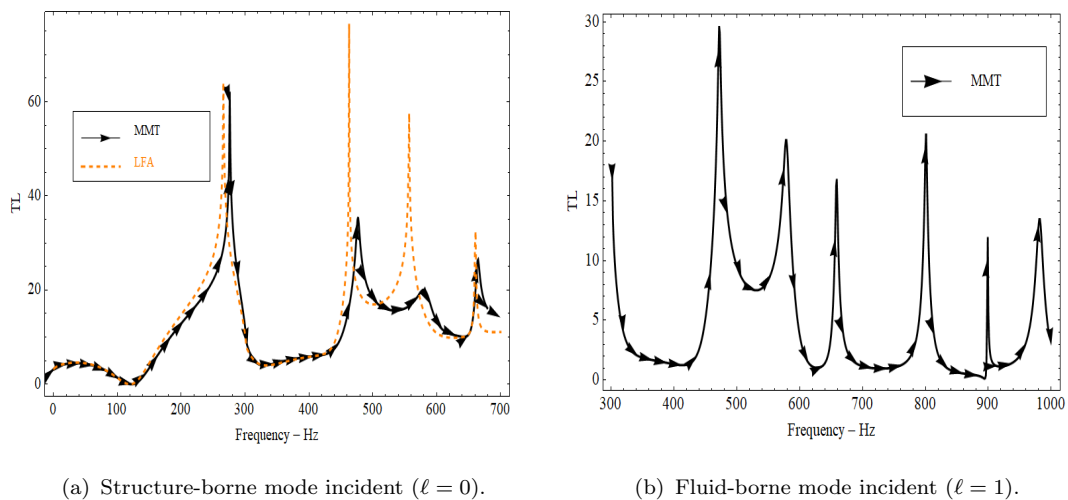(b) Fluid-borne mode incident ($\ell = 1$).
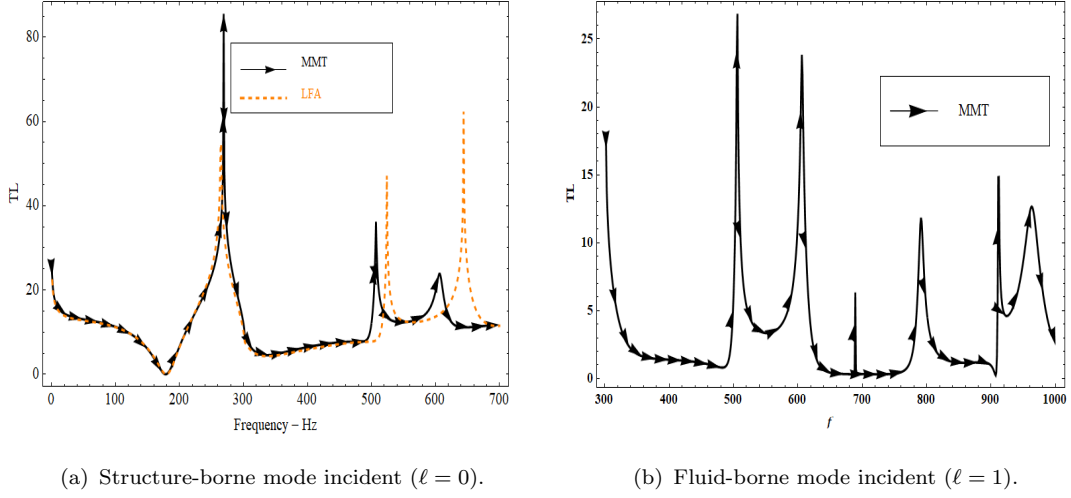
FIGURE 4.12: Membrane strips containing spring like edges: Transmission loss against frequency for $\alpha_h = 3.308$, $\alpha_v = 0.94$, $\mu_h = 2.695$ and $\mu_v = 1.44$.

(a) Real parts of pressure

(b) Imaginary parts of pressure
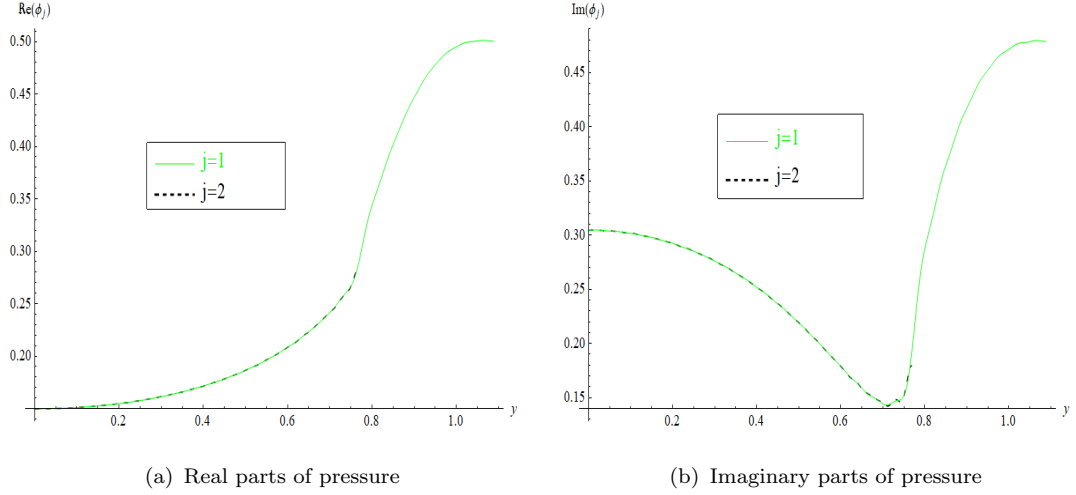
FIGURE 4.13: The real and imaginary parts of pressure against duct height with $N = 50$ terms.

$\bar{L} = 0.01$ m, respectively. It can seen that the real and imaginary parts of pressures of the inlet and expansion chamber match exactly at $x = -L$ as assumed in (4.15), see Fig. 4.13. Likewise, the matching of normal velocities perceived for vertical membrane case is shown in Fig. 4.14. Note that the displacement along the vertical membrane found through Galerkin procedure matches accurately with normal velocities at $x = -L$.

Similar observations for anti-symmetric case are obtained. It clearly validate the MM solution as well as authenticate the accuracy of performed algebra.

(a) Real parts of velocities

(b) Imaginary parts of velocities
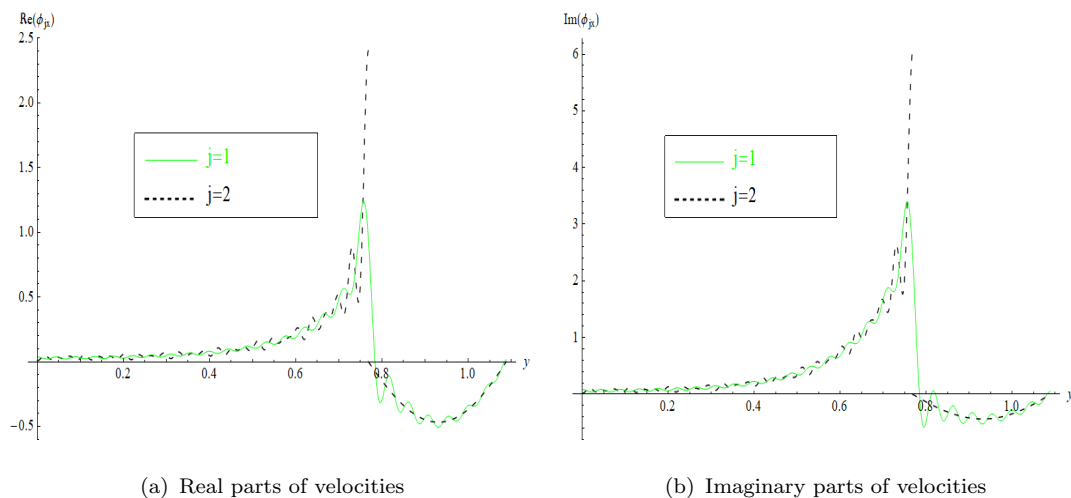
FIGURE 4.14: The real and imaginary parts of normal velocities against duct height with $N = 50$ terms.

Note that there appeared some oscillations in normal velocities curves due to Gibb's phenomenon [103]. We used Lanczos filter as given in [102], and then performed computations to get the plots of Figs. 4.13 and 4.14.

The issue is addressed comprehensively for elastic plate case [114] and then for membrane case in [119] and [102].

Chapter 5

Silencing Performance Analysis of a Membrane Cavity with Different Edge Conditions

5.1 Introduction

The modeling of fluid-structure coupled waves through the elastic structures bounding the fluid space and their scattering form geometric and material discontinuities is challenging as well as interesting, and have gained much attention of engineers and scholars. Such problems are commonly found in acoustics, elasticity, water wave theory, and aero-dynamics etc. The problems involving the interaction between the surface vibrations and sound field inside of cavity regions have application in noise control of heating, ventilation and air conditioning (HVAC) system of buildings, aero-engines and other engineering structures [104–110].

This chapter is concerned with the scattering analysis of the cavity region which has elastic membrane walls and contains compressible fluid. This flexible cavity is connected with extended inlet and outlet which are bounded by elastic plates. The particular interest of the authors is to establish a new form of Mode-Matching

tailored-Galerkin (MMTG) approach which comprises the general description to define a variety of edge conditions of bridging membranes. The proposed technique is a simple and computationally more effective way as compared with the technique as suggested in [120]. The response along the vertical components is taken such that the homogeneous part of the governing equations whereas their non-homogeneous parts link the fluid-space vibrations. To compare the results achieved with MMTG, the Mode-Matching Galerkin (MMG) approach as suggested by Lawrie and Afzal [120] is developed. The MMG basically relies on a priori solutions that can be chosen to be the orthogonal basis eigenfunctions along the vertical boundaries, for instance see [121–123].

The chapter is arranged as follows. The description of the physical problem and governing boundary value problem is given in Section 2. The Mode-Matching solution of the problem is stated in Section 3. The tailored Galerkin and Galerkin approaches are explained in Sections 4 and 5, respectively. The numerical results are explained in Section 5, whereas, the concluding remarks are portrayed in Section 6.

5.2   Problem Formulation

Consider a waveguide containing elastic plates bounded inlet/outlet and a membrane chamber membrane are lying along $\bar{y} = \bar{a}$, $|\bar{x}| > \bar{L}$ and $\bar{y} = \bar{b}$, $|\bar{x}| < \bar{L}$, respectively, in a dimensional setting (overbars represent dimensional variables). The lower surface of the waveguide located at $\bar{y} = \bar{0}$ is acoustically rigid. Two vertical elastic membranes lying along $\bar{x} = \pm\bar{L}$, $\bar{a} \leq \bar{y} \leq \bar{b}$ are connected to the horizontal membrane at $(\bar{x}, \bar{y}) = (\pm\bar{L}, \bar{b})$. The other ends of the membranes are connected to the elastic plates at $(\bar{x}, \bar{y}) = (\pm\bar{L}, \bar{a})$. Note that the bars on quantities here and henceforth express the dimensional setting of coordinates. A compressible fluid of mass density ρ and sound speed c is filled inside of the waveguide. The physical configuration of the waveguide is shown in Fig. 5.1 The harmonic time dependence $\exp{(-i\omega\bar{t})}$, where $\omega = 2\pi f$ is radiant frequency in which the
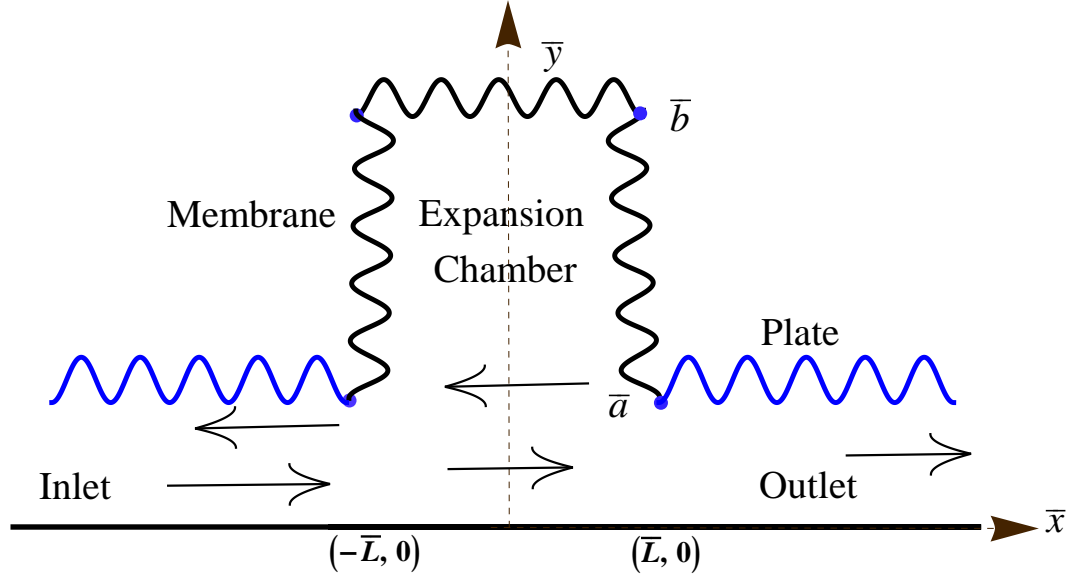
FIGURE 5.1: The physical configuration of waveguide.

frequency f is measured in Hz, is suppressed throughout and the boundary value problem, which is made dimensionless by using length scale k^{-1} and time scale ω^{-1}.

The non-dimensional fluid potential $\psi_j(x, y)$ satisfy the Helmholtz's equation

$$(\nabla^2 + 1)\psi_j(x, y) = 0, , \tag{5.1}$$

where $j = 1, 2, 3$ denote the fluid potential in extended inlet, outlet and expansion chamber. For rigid wall at $y = 0$, $\partial \psi_j / \partial y = 0$, whilst for the horizontal elastic membrane and plates surfaces, the conditions are:

$$\{\frac{\partial^2}{\partial x^2} + \mu_M^2\}\frac{\partial \psi_2}{\partial y} + \alpha_M \psi_2 = 0, \quad y = b, \tag{5.2}$$

$$\left(\frac{\partial^4}{\partial x^4} - \mu_p^4\right)\frac{\partial \psi_q}{\partial y} - \alpha_p \psi_q = 0, \quad y = a, \quad where \quad q = 1, 3. \tag{5.3}$$

Note that in (5.2) the quantities μ_M and α_M defined by

$$\mu_M = c/c_m \quad \text{and} \quad \alpha_M = \rho\omega/(TK^3),$$

are the dimensionless membrane wave number and the fluid loading parameter, respectively containing membrane mass density c_m and tension T. Accordingly, in (5.3) α_p and μ_p respectively, the plate wave number and fluid loading parameter are defined by

$$\alpha_p = \frac{12(1-\nu^2)c^2\rho}{k^3 h^3 E} \quad \text{and} \quad \mu_p = \frac{12(1-\nu^2)c^2\rho_p}{k^2 h^2 E}.$$

The quantity E represents the Young's modulus of plate having thickness h, density ρ_p and Poisson's ratio ν. Moreover, two bridging membranes situated at the junctions can be expressed by

$$\{\frac{\partial^2}{\partial y^2} + \mu_M^2\}\frac{\partial \psi}{\partial x} \pm \alpha_M \psi = 0, \quad x = \pm L, \ a \leqslant y \leqslant b. \tag{5.4}$$

Furthermore, some physical conditions are applied at the edges of the plates and membranes, such as clamped, pin-jointed etc., in elastic plate case and fixed free or spring-like in elastic membrane case. Lawrie in [62] proved that the number of edge conditions will be half of the even order derivatives present in the membrane or plate condition.

Therefore, there will be one edge condition on each finite membrane edge and two conditions on finite plate edge. These conditions will be defined later.

5.3 Problem Formulation

The physical configuration includes flexible surfaces that support energy propagation along the boundaries as well as through the fluid, and hence there exist a coupling between fluid and structure vibrations.

The eigenvalue problems associated with Helmholtz's equation together with rigid and plate or membrane boundaries govern eigenfunctions $\Psi_1(\beta_n, y) = \cosh(\beta_n y)$ in elastic plate bounding regions (extended inlet/outlet)and $\Psi_2(\gamma_n, y) = \cosh(\gamma_n y)$ in elastic membrane bounding region (central region or expansion chamber). The eigenvalues (β_n, γ_n) are the roots of dispersion relations:

$$\kappa_1(\beta) = (\beta^4 + 2\beta^2 + 1 - \mu_p^4)\beta \sinh(\beta a) - \alpha_p \cosh(\beta a) = 0. \tag{5.5}$$

$$\kappa_2(\gamma) = (\gamma^2 + 1 - \mu_M^2)\gamma \sinh(\gamma b) - \alpha_M \cosh(\gamma b) = 0. \tag{5.6}$$

These roots cab be found numerically and contain properties given in [113]. The corresponding eigenfunctions satisfy generalized orthogonality relations:

$$\alpha_p \int_0^a \Psi_1(\beta_m, y)\Psi_1(\beta_n, y)dy = \delta_{mn}E_m - (\beta_m^2 + \beta_n^2 + 2)\Psi_1^{'}(\beta_m, a)\Psi_1^{'}(\beta_n, a), \tag{5.7}$$

$$\alpha_M \int_0^b \Psi_2(\gamma_m, y)\Psi_2(\gamma_n, y)dy = \delta_{mn}H_m - \Psi_2^{'}(\gamma_m, b)\Psi_2^{'}(\gamma_n, b), \tag{5.8}$$

where δ_{mn} is the Kronecker delta function and:

$$E_m = 2(\beta_m^2 + 1)[\Psi_1^{'}(\beta_m, a)]^2 + \alpha_p \int_0^a \Psi_1^2(\beta_m, y)dy, \tag{5.9}$$

$$H_m = \frac{\alpha_M b}{2} + \left(\frac{3\gamma_m^2 + 1 - \mu_M^2}{2\gamma_m^2}\right)\left(\Psi_2^{'}(\gamma_m, b)\right)^2. \tag{5.10}$$

Now to include the response of the membranes lying at $Z = \pm L$ along $a < y < b$ one may adopt the 1) Galerkin approach, or 2) Tailored-Galerkin approch. Both techniques are discussed in subsequent subsection.

5.3.1 Galerkin Formulation

The fundamental of this approach is the assumption of the *priori solution* along the boundaries, and then the assortment of the complete solution with this solution. The membrane displacements $w^{\pm}(y)$ along the boundaries satisfy:

$$\{\frac{\partial^2}{\partial y^2} + \mu_M^2\}w^{\pm}(y) = \mp\alpha_M\psi_2, \quad x = \pm L, \ a \leqslant y \leqslant b. \tag{5.11}$$

One way to express the membrane displacements is by using the Fourier series assumption, that gives:

$$w^{\pm}(y) = \sum_{n=0}^{\infty} G_n^{\pm} Y_n(y), \tag{5.12}$$

where $Y_n(y)$, $n = 0, 1, 2 \ldots$ represent the eigenfunctions and $G_n^{\pm}$, $n = 0, 1, 2 \ldots$ are Fourier coefficients. The value of nth eigenfunction $Y_n(y)$ depends upon the physical conditions imposed at the edges of membranes lying along $a \leqslant y \leqslant b$. These edges can be fixed, free or spring like. The spring-like conditions on all edges is comparatively a general case and be expressed mathematically as:

$$\xi_1 Y_n(a) + Y_n'(a) = 0, \tag{5.13}$$

$$\xi_2 Y_n(b) + Y_n'(b) = 0. \tag{5.14}$$

On solving the eigenvalue equation of (5.11) subject to (5.13)-(5.14), we find $Y_n(y) = \xi_1 \sin[\lambda_n(y-a)] + \lambda_n \cos[\lambda_n(y-a)]$ having eigenvalues to be the roots of characteristic equation

$$(\xi_1\xi_2 - \lambda_n^2)\sin[\lambda_n(b-a)] + (\xi_1 + \xi_2)\lambda_n \cos[\lambda_n(b-a)] = 0, \quad n = 0, 1, 2 \ldots.$$

These roots can be found numerically. The associated eigenfunctions Y_n, $n = 0, 1, 2, ..$ are orthogonal and satisfy the orthogonality relation:

$$\int_a^b Y_n(y)Y_m(y)dy = \delta_{mn}H_n, \tag{5.15}$$

where

$$H_n = \int_a^b Y_n^2(y)dy. \tag{5.16}$$

Note that the Fourier coefficients $G_n^{\pm}$ are still unknowns. To determine these we match surface modes with cavity modes with the aid of (5.11). The propagating modes in duct regions can be expressed by:

$$\psi_1(x,y) = F_\ell \Psi_1(\beta_\ell, y)e^{i\eta_\ell(x+L)} + \sum_{n=0}^{\infty} A_n \Psi_1(\beta_n, y)e^{-i\eta_n(x+L)}, \quad x < -L, \tag{5.17}$$

$$\psi_2(x,y) = \sum_{n=0}^{\infty}(B_n e^{is_n x} + C_n e^{-is_n x})\Psi_2(\gamma_n, y), \quad |x| < L, \tag{5.18}$$

$$\psi_3(x,y) = \sum_{n=0}^{\infty} D_n \Psi_1(\beta_1, y)e^{i\eta_n(x-L)}, \quad x > L, \tag{5.19}$$

where $\eta_n = \sqrt{\beta_n^2 + 1}$ and $s_n = \sqrt{\gamma_n^2 + 1}$ are the wave numbers. Note that the first term in (5.17) represents incident wave having forcing $F_\ell = \sqrt{\alpha_p/(E_\ell \eta_\ell)}$. The counter ℓ is 0 or 1 to describe the fundamental mode or the secondary mode incident, respectively. Now to find Fourier coefficients $G_n^{\pm}$, we substitute (5.12) and (5.18) into (5.11), multiplying the resulting with $Y_m(y)$, integrating over $a < y < b$, and then applying (5.15), it is found that

$$G_m^{\pm} = \pm \frac{\pm \alpha_M}{H_m(\mu_M^2 - \lambda_m^2)} \sum_{n=0}^{\infty}(B_n e^{\mp is_n L} + C_n e^{\pm is_n L})I_{mn}, \tag{5.20}$$

where

$$I_{mn} = \int_a^b Y_m(y)\cosh(\gamma_n y)dy. \tag{5.21}$$

5.3.2 Tailored-Galerkin Formulation

In this approach, the surface modes of vertical membranes are found through the solution the membrane equations and satisfy the edge conditions. To determine the surface modes, we solve (5.11), to get

$$w^{\pm}(y) = a_1^{\pm}\cos(\mu_M y) + a_2^{\pm}\sin(\mu_M y) \pm \alpha_M \sum_{n=0}^{\infty} \frac{\left(B_n e^{\mp is_n L} + C_n e^{\pm is_n L}\right)\cosh(\gamma_n y)}{\gamma_n^2 + \mu_M^2}, \tag{5.22}$$

Here quantities $a_j^{\pm}$, $j = 1, 2$ are constants that will be found through the physical behavior of vertical membranes on edges $x = \pm L$, that for general setting are:

$$\xi_1 w^{\pm}(a) + \frac{\partial w^{\pm}}{\partial y}(a) = 0, \tag{5.23}$$

$$\xi_2 w^{\pm}(b) + \frac{\partial w^{\pm}}{\partial y}(b) = 0. \tag{5.24}$$

By substituting (5.22) into (5.23) and (5.24), a system of four equations is found. This system can be solved simultaneously for unknowns $a_j^{\pm}$, $j = 1, 2$.

Note that the modal amplitudes $\{A_m, B_m, C_m, D_m\}$; $m = 0, 1, 2, \ldots$ in the eigenfunction expansions defined by (5.17)–(5.19) are still unknowns. These are determined after using the matching conditions at the interfaces $x = \pm L$.

5.4 Mode Matching Solutions

To find the unknown modal coefficients, the pressures and normal velocities across the regions are matched on interfaces. At interfaces $x = \pm L$, the continuity of pressures that give $\psi_1(-L, y) = \psi_2(-L, y)$ and $\psi_3(L, y) = \psi_2(L, y)$, leads to

$$\alpha_p \int_0^a \psi_1(-L, y)\Psi_1(\beta_m, y)dy = \alpha_p \int_0^a \psi_2(-L, y)\Psi_1(\beta_m, y)dy, \tag{5.25}$$

$$\alpha_p \int_0^a \psi_3(L, y)\Psi_1(\beta_m, y)dy = \alpha_p \int_0^a \psi_2(L, y)\Psi_1(\beta_m, y)dy. \tag{5.26}$$

On substituting the eigenfunction expansion (5.17)–(5.19) into (5.25)–(5.26), simplify with the aid of OR (2.5), after some rearrangements we get

$$A_m = -\frac{F_\ell \delta_{m\ell} E_\ell}{E_m} + \frac{\beta_m \sinh(\beta_m a)}{E_m}(J_1 + (\beta_m^2 + 2)J_2) + \frac{\alpha_p}{E_m}\sum_{n=0}^{\infty}(B_n e^{-is_n L} + C_n e^{is_n L})R_{mn}, \tag{5.27}$$

$$D_m = \frac{\beta_m \sinh(\beta_m a)}{E_m}(J_3 + (\beta_m^2 + 2)J_4) + \frac{\alpha_p}{E_m}\sum_{n=0}^{\infty}(B_n e^{is_n L} + C_n e^{-is_n L})R_{mn}, \tag{5.28}$$

where $J_1 = \psi_{1yyy}(-L, a)$, $J_2 = \psi_{1y}(-L, a)$, $J_3 = \psi_{3yyy}(L, a)$ and $J_4 = \psi_{3y}(L, a)$ are constants. These constants are determine from the physical condition being applied on the finite joints of horizontal plates at $(\pm L, a)$, and

$$R_{mn} = \int_0^a \Psi_1(\beta_m, y)\Psi_2(\gamma_n, y)dy. \tag{5.29}$$

On adding and subtracting (5.27) and(5.28), we get

$$\Psi_m^+ = -\frac{F_\ell \delta_{m\ell} E_\ell}{E_m} + \frac{\beta_m \sinh(\beta_m a)}{E_m}(J_{13}^+ + (\beta_m^2 + 2)J_{24}^+) + \frac{2\alpha_p}{E_m}\sum_{n=0}^{\infty} \chi_m^+ \cos(s_n L)R_{mn},$$
(5.30)

and

$$\Psi_m^- = -\frac{F_\ell \delta_{m\ell} E_\ell}{E_m} + \frac{\beta_m \sinh(\beta_m a)}{E_m}(J_{13}^- + (\beta_m^2 + 2)J_{24}^-) - \frac{2i\alpha_p}{E_m}\sum_{n=0}^{\infty} \chi_m^- \sin(s_n L)R_{mn},$$
(5.31)

where $\Psi_m^\pm = A_m \pm D_m$ and $\chi_m^\pm = B_m \pm C_m$ m=0,1,2,... represent the amplitudes of symmetric/anti-symmetric modes propagating in inlet/outlet and the expansion chamber, respectively. Whereas, the quantities $J_{13}^\pm = J_1 \pm J_3$ and $J_{24}^\pm = J_1 \pm J_4$ are obtained edge conditions that are discussed in next subsections.

5.4.1   Clamped Edge Conditions

The clamped connection of elastic plates at joints refers zero displacement and zero gradient at the edges $(x, y) = (\pm L, a)$, that gives

$$\psi_{1y}(-L, a) = 0 \qquad\qquad \psi_{1xy}(-L, a) = 0, \tag{5.32}$$

$$\psi_{3y}(L, a) = 0 \qquad\qquad \psi_{3xy}(L, a) = 0. \tag{5.33}$$

Here the subscript x and y represent the partial derivatives with respect to x and y, respectively. On substituting (5.32)–(5.33) into (5.30)–(5.31) it is found, after a little rearrangement, that $J_{24}^+ = 0$, $J_{24}^- = 0$ and

$$J_{13}^+ = \frac{2F_\ell \eta_\ell \beta_\ell \sinh(\beta_\ell a)}{S_1} - \frac{2\alpha_p}{S_1}\sum_{n=0}^{\infty}\sum_{m=0}^{\infty} \frac{\Psi_n^+ \beta_m \eta_m \cos(s_n L)\sinh(\beta_m a)R_{mn}}{E_m} \tag{5.34}$$

$$J_{13}^- = \frac{2F_\ell \eta_\ell \beta_\ell \sinh(\beta_\ell a)}{S_1} + \frac{2i\alpha_p}{S_1}\sum_{n=0}^{\infty}\sum_{m=0}^{\infty} \frac{\Psi_n^- \beta_m \eta_m \sin(s_n L)\sinh(\beta_m a)R_{mn}}{E_m}, \tag{5.35}$$

where

$$S_1 = \sum_{m=0}^{\infty} \frac{\eta_m \beta_m^2 \sinh^2(\beta_m a)}{E_m}. \tag{5.36}$$

5.4.2 Pin-jointed Edge Conditions

The pin-jointed or simply supported conditions of elastic plates at joints refer zero displacement and zero bending moment at the edges $(x, y) = (\pm L, a)$, that gives

$$\psi_{1y}(-L, a) = 0 \quad \text{and} \quad \psi_{1xxy}(-L, a) = 0. \tag{5.37}$$

$$\psi_{3y}(L, a) = 0 \quad \text{and} \quad \psi_{3xxy}(L, a) = 0. \tag{5.38}$$

On substituting (5.32)–(5.33) into (5.37)–(5.38) it is found, after some rearrangement, that $J_{24}^+ = 0$, $J_{24}^- = 0$ and

$$J_{13}^+ = -\frac{2\alpha_p}{S_2} \sum_{n=0}^{\infty} \sum_{m=0}^{\infty} \frac{\Psi_n^+ \beta_m \eta_m^2 \cos(s_n L) \sinh(\beta_m a) R_{mn}}{E_m} \tag{5.39}$$

$$J_{13}^- = \frac{2i\alpha_p}{S_2} \sum_{n=0}^{\infty} \sum_{m=0}^{\infty} \frac{\Psi_n^- \beta_m \eta_m^2 \sin(s_n L) \sinh(\beta_m a) R_{mn}}{E_m}, \tag{5.40}$$

where
$$S_2 = \sum_{m=0}^{\infty} \frac{\eta_m^2 \beta_m^2 \sinh^2(\beta_m a)}{E_m}. \tag{5.41}$$

Now we apply the continuity of normal velocities to match the velocity modes at $x = \pm L$. At aperture interfaces between $0 < y < a$ the normal velocities across the regions are same, but at the membrane interfaces between $a < y < b$ the normal velocities of cavity modes are equal to the displacements of membranes, that give

$$\psi_{2x}(x, y) = \begin{cases} \psi_{1x}(x, y), & x = -L, \quad 0 \leqslant y \leqslant a \\ w^+(y), & x = -L, \quad a \leqslant y \leqslant b \end{cases} \tag{5.42}$$

$$\psi_{2x}(x, y) = \begin{cases} \psi_{3x}(x, y), & x = L, \quad 0 \leqslant y \leqslant a \\ w^-(y), & x = L, \quad a \leqslant y \leqslant b, \end{cases} \tag{5.43}$$

As the formulation of $w^{\pm}(y)$ is given with Galerkin approach and tailored-Galerkin approach, therefore the matching conditions (5.42)-(5.43) lead to two sets of equations. For tailored-Galerkin approach, we substitute (5.17)–(5.19) into (5.42)–(5.43),

multiplying by $\alpha_M \Psi_2(\gamma_m, y)$, integrating over 0 to b, it is found that:

$$\sum_{n=0}^{\infty}(B_n e^{-is_n L} - C_n e^{is_n L})s_n \alpha_M \int_0^b \Psi_2(\gamma_m, y)\Psi_2(\gamma_n, y)dy =$$

$$\alpha_M F_\ell \eta_\ell \int_0^a Cosh(\beta_n y)\Psi_2(\gamma_m, y)dy - \alpha_M \sum_{n=0}^{\infty} A_n \eta_n \int_0^a \cosh(\beta_n y)\Psi_2(\gamma_m, y)dy$$

$$- i\alpha_M a_1 \int_a^b \cos(\mu_M y)\Psi_2(\gamma_m, y)dy - i\alpha_M a_2 \int_a^b \sin(\mu_M y)\Psi_2(\gamma_m, y)dy -$$

$$i\alpha_m \sum_{n=0}^{\infty} \frac{(B_n e^{-is_n L} + C_n e^{is_n L})}{\gamma_n^2 + \mu_M^2} \int_a^b \Psi_2(\gamma_m, y)\Psi_2(\gamma_n, y)dy \qquad (5.44)$$

and

$$\sum_{n=0}^{\infty}(B_n e^{is_n L} - C_n e^{-is_n L})s_n \alpha_M \int_0^b \Psi_2(\gamma_m, y)\Psi_2(\gamma_n, y)dy =$$

$$\alpha_M \sum_{n=0}^{\infty} D_n \eta_n \int_0^a \cosh(\beta_n y)\Psi_2(\gamma_m, y)dy - i\alpha_M a_1 \int_a^b \cos(\mu_M y)\Psi_2(\gamma_m, y)dy$$

$$- i\alpha_M a_2 \int_a^b \sin(\mu_M y)\Psi_2(\gamma_m, y)dy -$$

$$+ i\alpha_m \sum_{n=0}^{\infty} \frac{(B_n e^{-is_n L} + C_n e^{is_n L})}{\gamma_n^2 + \mu_M^2} \int_a^b \Psi_2(\gamma_m, y)\Psi_2(\gamma_n, y)dy. \qquad (5.45)$$

The addition and subtraction of these equations, after simplification with the aid of (5.8) lead to:

$$\chi_m^- = \frac{1}{2s_m H_m \cos(s_m L)}\{\gamma_m \sinh(\gamma_m b)E_{56}^+ + \alpha_M F_\ell \eta_\ell R_{\ell m} - \alpha_M \sum_{n=0}^{\infty} \Psi_n^- \eta_n R_{nm}\}$$

$$- \frac{i\alpha_M}{2s_m H_m \cos(s_m L)}\{a_{13}^+ P_{1m} + a_{24}^+ P_{2m} + 2\alpha_M \sum_{n=0}^{\infty} \frac{\chi_n^- \sin(s_n L)T_{nm}}{\gamma_n^2 + \mu_M^2}\} \quad (5.46)$$

and

$$\chi_m^+ = \frac{i}{2s_m H_m \sin(s_m L)}\{\gamma_m \sinh(\gamma_m b)E_{56}^- + \alpha_M F_\ell \eta_\ell R_{\ell m} - \alpha_M \sum_{n=0}^{\infty} \Psi_n^+ \eta_n R_{nm}\}$$

$$+ \frac{\alpha_M}{2s_m H_m \cos(s_m L)}\{a_{13}^- P_{1m} + a_{24}^- P_{2m} + 2\alpha_M \sum_{n=0}^{\infty} \frac{\chi_n^+ \cos(s_n L)T_{nm}}{\gamma_n^2 + \mu_M^2}\} \quad (5.47)$$

where

$$P_{1m} = \int_a^b \cos(\mu_M y)\Psi_2(\gamma_m, y)dy, \tag{5.48}$$

$$P_{2m} = \int_a^b \sin(\mu_M y)\Psi_2(\gamma_m, y)dy, \tag{5.49}$$

and

$$T_{mn} = \int_a^b \Psi_2(\gamma_n, y)\Psi_2(\gamma_m, y)dy. \tag{5.50}$$

Note that in (5.46) and (5.47) there appear unknown constants $E_{56}^{\pm}$ which describe the behavior of membranes bounding the central at edges. For fixed type of edge conditions ($\psi_{2y}(\pm L, b) = 0$), the following systems for $E_{56}^{\pm}$ are achieved:

$$
\begin{aligned}
E_{56}^+ S_3 =& \alpha_M \sum_{m=0}^{\infty} \frac{\gamma_m \sinh(\gamma_m b) \tan(s_m L)}{2s_m H_m}\{-F_\ell \eta_\ell R_{\ell m} + \sum_{n=0}^{\infty} \Psi_n^- \eta_n R_{nm}\} \\
&+ \alpha_M \sum_{m=0}^{\infty} \frac{\gamma_m \sinh(\gamma_m b) \tan(s_m L)}{2s_m H_m}\{ia_{13}^+ P_{1m} + ia_{24}^+ P_{2m}\} \\
&+ \alpha_M^2 \sum_{m=0}^{\infty} \frac{\gamma_m \sinh(\gamma_m b) \tan(s_m L)}{s_m H_m}\{\sum_{n=0}^{\infty} \frac{\chi_n^- \sin(s_n L) T_{mn}}{\gamma_n^2 + \mu_M^2}\},
\end{aligned} \tag{5.51}
$$

and

$$
\begin{aligned}
E_{56}^- S_4 =& \alpha_M \sum_{m=0}^{\infty} \frac{\gamma_m \sinh(\gamma_m b) \cot(s_m L)}{2s_m H_m}\{-F_\ell \eta_\ell R_{\ell m} + \sum_{n=0}^{\infty} \Psi_n^+ \eta_n R_{nm}\} \\
&+ \alpha_M \sum_{m=0}^{\infty} \frac{\gamma_m \sinh(\gamma_m b) \cot(s_m L)}{2s_m H_m}\{ia_{13}^- P_{1m} + ia_{24}^- P_{2m}\} \\
&+ i\alpha_M^2 \sum_{m=0}^{\infty} \frac{\gamma_m \sinh(\gamma_m b) \cot(s_m L)}{s_m H_m}\{\sum_{n=0}^{\infty} \frac{\chi_n^+ \cos(s_n L) T_{mn}}{\gamma_n^2 + \mu_M^2}\},
\end{aligned} \tag{5.52}
$$

where

$$S_3 = \sum_{m=0}^{\infty} \frac{[\gamma_m \sinh(\gamma_m b)]^2 \tan(s_m L)}{2s_m H_m}, \tag{5.53}$$

and

$$S_4 = \sum_{m=0}^{\infty} \frac{[\gamma_m \sinh(\gamma_m b)]^2 \cot(s_m L)}{2s_m H_m}. \tag{5.54}$$

In this wave we get two systems of equations defined by (5.30)-(5.31) and (5.46)-(5.47) along with (5.51)-(5.52). First these are truncated then are solved numerically. This procedure is termed as mode-matching tailored Galerkin (MMTG).

Accordingly, the displacements found through Galerkin procedure can be used in normal velocity conditions. Hence, we substitute (5.17)–(5.19) into (5.42)–(5.43), multiply with $\alpha_M \Psi_2(\gamma_m, y)$, integrate from 0 to b, then use OR (5.8), after some mathematical rearrangements, one can get:

$$
\chi_m^- = \frac{\gamma_m \sinh(\gamma_m b) J_{56}^+}{2 s_m H_m \cos(s_m L)} + \frac{\alpha_M}{2 s_m H_m \cos(s_m L)} \{ F_\ell R_{\ell m} - \sum_{n=0}^{\infty} \Psi_m^- \eta_n R_{nm} \}
$$
$$
- \frac{2\alpha_M^2}{s_m H_m \cos(s_m L)} \sum_{j=0}^{\infty} \sum_{q=0}^{\infty} \frac{\chi_q^- \cos(s_q L) I_{qm} I_{jm}}{(b-a)(\mu_M^2 - \lambda_j^2)}, \tag{5.55}
$$

and

$$
\chi_m^+ = \frac{\gamma_m \sinh(\gamma_m b) J_{56}^-}{2 i s_m H_m \sin(s_m L)} + \frac{\alpha_M}{2 i s_m H_m \sin(s_m L)} \{ F_\ell R_{\ell m} - \sum_{n=0}^{\infty} \Psi_n^+ \eta_n R_{nm} \}
$$
$$
- \frac{2\alpha_M^2}{s_m H_m \sin(s_m L)} \sum_{j=0}^{\infty} \sum_{q=0}^{\infty} \frac{\chi_q^+ \cos(s_q L) I_{qm} I_{jm}}{(b-a)(\mu_M^2 - \lambda_j^2)}. \tag{5.56}
$$

Before truncating and solving the system we use the edge conditions to determine values of $J_{56}^\pm$. Therefore we multiply (5.55) by $\gamma_m \sin(s_m L) \sinh(\gamma_m b)$ and (5.56) by $\gamma_m \cos(s_m L) \sinh(\gamma_m b)$, take summation over m, then by using edge conditions $\psi_{2y}(\pm L, b) = 0$, after some rearrangements it is found that:

$$
J_{56}^+ S_3 = \alpha_M \sum_{m=0}^{\infty} \frac{\gamma_m \sinh(\gamma_m b) \tan(s_m L)}{2 s_m H_m} \{ -F_\ell R_{\ell m} + \sum_{n=0}^{\infty} \Psi_n^- \eta_n R_{nm} \}
$$
$$
+ 4\alpha_M^2 \sum_{j=0}^{\infty} \sum_{m=0}^{\infty} \sum_{q=0}^{\infty} \frac{\gamma_m \sinh(\gamma_m b) \tan(s_m L) \chi_q^- \sin(s_q L) I_{qj} I_{jq}}{s_m H_m (\gamma_n^2 + \mu_M^2)(b-a)(\mu_M^2 - \lambda_j^2)^2}, \tag{5.57}
$$

and

$$
J_{56}^- S_4 = \alpha_M \sum_{m=0}^{\infty} \frac{\gamma_m \sinh(\gamma_m b) \cot(s_m L)}{2 s_m H_m} \{ -F_\ell R_{\ell m} + \sum_{n=0}^{\infty} \Psi_n^+ \eta_n R_{nm} \}
$$
$$
+ 4 i \alpha_M^2 \sum_{j=0}^{\infty} \sum_{m=0}^{\infty} \sum_{q=0}^{\infty} \frac{\gamma_m \sinh(\gamma_m b) \cot(s_m L) \chi_q^+ \sin(s_q L) I_{qj} I_{jq}}{s_m H_m (b-a)(\mu_M^2 - \lambda_j^2)^2 (\gamma_n^2 + \mu_M^2)}. \tag{5.58}
$$

Thus for membrane vertical strips the Mode-Matching procedure in conjunction with Galerkin approach (MMG) yields two systems of equations defined by (5.18)–(5.19) and (5.55)–(5.56) along with (5.57)-(5.58). First, we truncate the

systems of equations for different set of edge conditions imposed on vertical membrane strips and then solved numerically. The unknown amplitudes A_n, B_n, C_n and D_n are found easily after a little calculations.

5.5 Numerical Results and Discussion

The performance of a reactive device is generally measured by using transmission loss (TL). For unit incident power the expression for TL as given in [16] is

$$\text{TL} = -10 \log_{10}(\mathcal{E}_t), \tag{5.59}$$

where $\mathcal{E}_t$ represents the transmitted energy flux/power in the outlet region. The linear algebraic systems obtained in Sections 4 and 5 are truncated first upto N terms, and then are solved numerically. Here the results obtained from the truncated solutions are shown in terms of TL. To perform numerical experiments, density $\rho = 1.2043 \text{kgm}^{-3}$, sound speed $c = 344 \text{ms}^{-1}$, aluminum elastic plates with thickness $\bar{h} = 0.0006$m and plate mass density $\rho_p = 2700 \text{kgm}^{-3}$ remain fixed. The numerical values of Poisson's ratio $\nu = 0.34$ and Young's modulus $E = 7.2 \times 10^{10} \text{Nm}^{-2}$ are considered. The cavity chamber contains stainless steel having density $\rho_m = 0.1715 \text{kgm}^{-2}$ and tension $T = 350N$. The height and chamber half length in dimensional form are $\bar{b} = 0.085$m and $\bar{L} = 0.01$m, respectively, whilst, the inlet/outlet duct height $\bar{a} = 0.06$m is assumed. In Figs. 5.2–5.10, the curves are plotted by truncating and inverting the solution obtained with mode-matching tailored Galerkin (MMTG) approach and mode-matching Galerkin (MMG) approach by fixing $N = 20$ terms. The curves shown with symbols ● − for clamped and ■ − for pin-joint edges} have been achieved with MMTG solution whilst the curves shown with dashing depict the results found through MMG solution. Note that the parametric setting resembles with the setting considered by Lawrie and Afzal in [81].

The parts (a) of Figs. 5.2–5.10 show the transmission loss against frequency with structure-born mode ($\ell = 0$) excitation, whereas, the parts (b) of Figs. 5.2–5.10

(a) Structure-borne mode incident ($\ell = 0$).

(b) Fluid-borne mode incident ($\ell = 1$).

FIGURE 5.2: TL verses frequency having fixed edges of vertical membranes and comprising elastic plates with ($\blacksquare$ − pin-jointed and $\bullet$ − clamped edge conditions).

(a) Structure-borne mode incident ($\ell = 0$).

(b) Fluid-borne mode incident ($\ell = 1$).
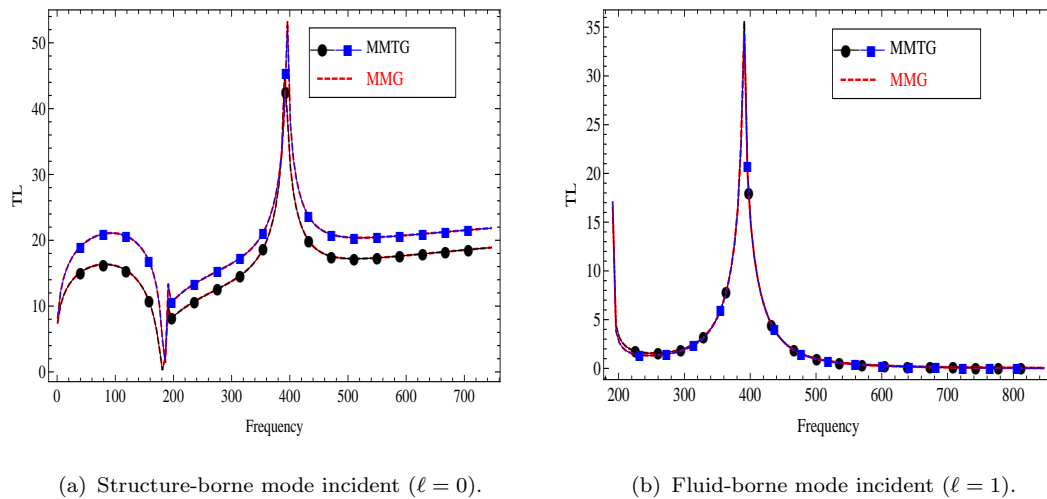
FIGURE 5.3: TL verses frequency with fixed and free edges of vertical membranes and comprising elastic plates with ($\blacksquare$ − pin-jointed and $\bullet$ − clamped edge conditions).

depict the transmission loss results against frequency with fluid-born mode ($\ell = 1$) excitation. The graphs of Fig. 5.2 are achieved by taking zero displacement at the edges of vertical membranes. It is seen that the majority of structure-borne mode excitation propagates along the structure and reveals a dome-like behavior in the frequency range 2 Hz $\leqslant f \leqslant$ 190 Hz. Moreover, a stopband before the cut-on frequency 191Hz of inlet and outlet is produced. However, after this cut-on limit, the TL escalates by increasing frequency. In other words, the addition of cut-on modes causes more attenuation. But when we interchange the clamped

edges with the pin-jointed edges, the TL is enhanced. It is because of the leakage of compressional waves with zero bending moment on the edges. The TL verses frequency with fluid-borne excitation which cuts-on at $f = 191$ Hz is shown in Fig. 5.2(b). It is interesting to see that, the variation of edge conditions from clamped to pin-jointed does not affect the acoustical performance. The reason behind is the propagation of majority of the energy via fluid with fluid-borne excitation. Accordingly, a stopband having band width ratio of 1.14 in frequency regime $730 - 840$ Hz is produced. Whereas, the maximum value of TL 30.2 dB at frequency 765 Hz is achieved.

(a) Structure-borne mode incident ($\ell = 0$).

(b) Fluid-borne mode incident ($\ell = 1$).

FIGURE 5.4: TL verses frequency with fixed and spring like edges of vertical membranes and comprising elastic plates with (■ − pin-jointed and ● − clamped edge conditions).

Fig. 5.3 show TL verses frequency with zero displacement conditions ($\xi_1 = \infty$) at edges $(x, y) = (\pm L, a)$ and having zero gradient ($\xi_2 = 0$), at edges $(x, y) = (\pm L, b)$. In case of structure-borne mode incident the dome-like behavior in frequency range $2 \leqslant f \leqslant 180$ Hz is seen. The transmission loss peak $52.1dB$ occurred at 443Hz before the second cut-on frequency of the expansion chamber at 453 Hz. Also a fixed TL of 20 or (23) dB for clamped or (pin-jointed) respectively, is seen after the second cut -on frequency of the expansion chamber in the increasing frequency regime, see Fig. 5.3(a). In Fig. 5.3(b), when system is radiated with fluid-borne mode, the maximum TL is 36 dB at 392 Hz before the second cut-on frequency of the expansion chamber and the stopband here is produced in frequency range of

(a) Structure-borne mode incident ($\ell = 0$).

(b) Fluid-borne mode incident ($\ell = 1$).

FIGURE 5.5: TL verses frequency with free and fixed edges of vertical membranes and comprising elastic plates with (■ − pin-jointed and ● − clamped edge conditions).

$350 - 430$ Hz with a band width of 1.02 cm. Fig. 5.4 contains TL verses frequency

(a) Structure-borne mode incident ($\ell = 0$).
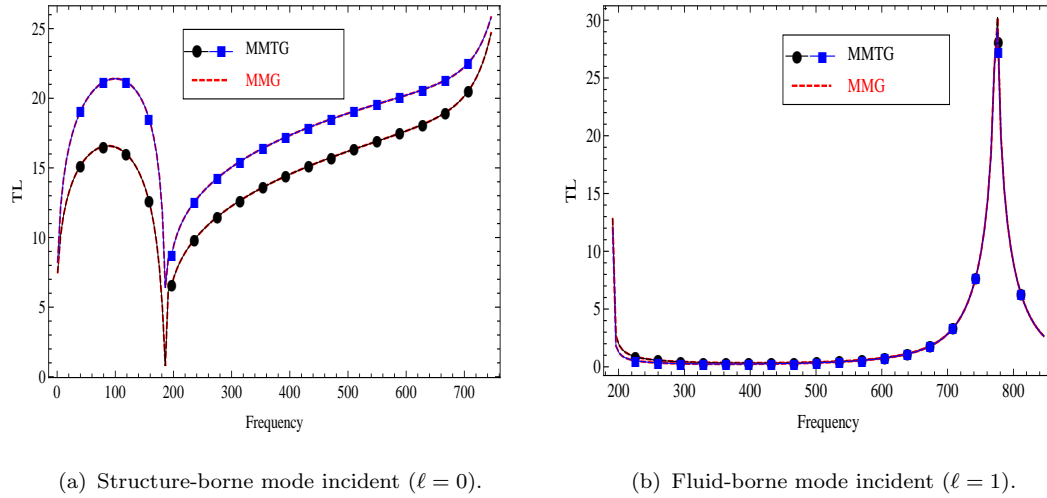
(b) Fluid-borne mode incident ($\ell = 1$).

FIGURE 5.6: TL verses frequency with free edges of vertical membranes and comprising elastic plates with (■ − pin-jointed and ● − clamped edge conditions).

comprising zero displacement condition ($\xi_1 = \infty$) at edges $(x, y) = (\pm L, a)$ and spring-like edge conditions ($\xi_2 = 1$) at $(x, y) = (\pm L, b)$. The peak value of TL, the stopbands and dome-like behavior are same as that produced in Fig. 5.3. The effect of clamped and pin-jointed edges of the expanded inlet/outlet on the TL is significant in case of fundamental mode incident ($\ell = 0$), however this effect is negligible when the structure is vibrated with higher order mode ($\ell = 1$) see each

Fig (a) and (b). It is due to the fact that for higher order mode ($\ell = 1$) the edges of expended inlet/outlet do not affect the transmission loss curves. Fig. 5.5 shows TL

(a) Structure-borne mode incident ($\ell = 0$).
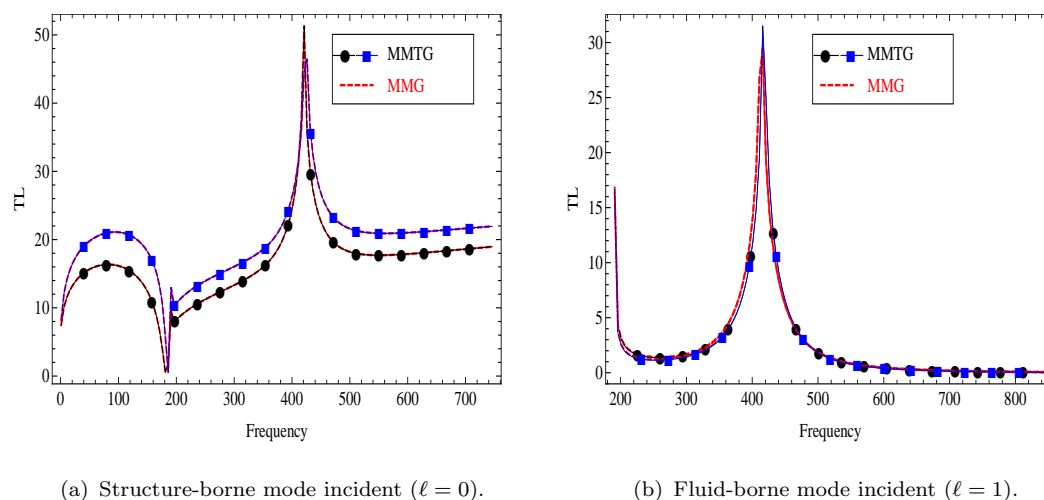
(b) Fluid-borne mode incident ($\ell = 1$).

FIGURE 5.7: TL verses frequency with free and spring like edges of vertical membranes and comprising elastic plates with (■ − pin-jointed and ● − clamped edge conditions).

verses frequency having zero gradient conditions ($\xi_1 = 0$) at edges $(x, y) = (\pm L, a)$ and zero displacement edge conditions ($\xi_2 = \infty$) at $(x, y) = (\pm L, b)$. The peak value of TL is 44.4dB at 425 Hz, the stopbands and dome-like behavior are same as that produced in Fig. 5.3. The effect of clamped and pin-joint edges of the expanded inlet/outlet on the TL is significant in case of fundamental mode incident ($\ell = 0$), however this effect is negligible when the structure is vibrated with higher order mode ($\ell = 1$) see each Fig (a) and (b). It is due to the fact that for higher order mode ($\ell = 1$) the edges of expended inlet/outlet do not affect the transmission loss curves. From Figs. 5.2–5.10, it is clear that when structure is radiated the TL curves obtained from both MMTG and MMG are exactly matched in all frequency regime for each set of edge conditions.

Fig. 5.6 portrays the TL verses frequency whereas both the vertical membrane are free to move on edges $(x, y) = (\pm L, a)$ and $(x, y) = (\pm L, b)$ that is ($\xi_1 = 0$) and ($\xi_2 = 0$). The behavior of curves obtained for fundamental mode incident ($\ell = 0$) is in resemblance with zero displacement curves of Fig. 5.2(a) but with increases transmission loss. However, in Fig. 5.6(b) the peak value of TL is 26.2dB at first cut-on of the expanded inlet/outlet and then decreasing to its
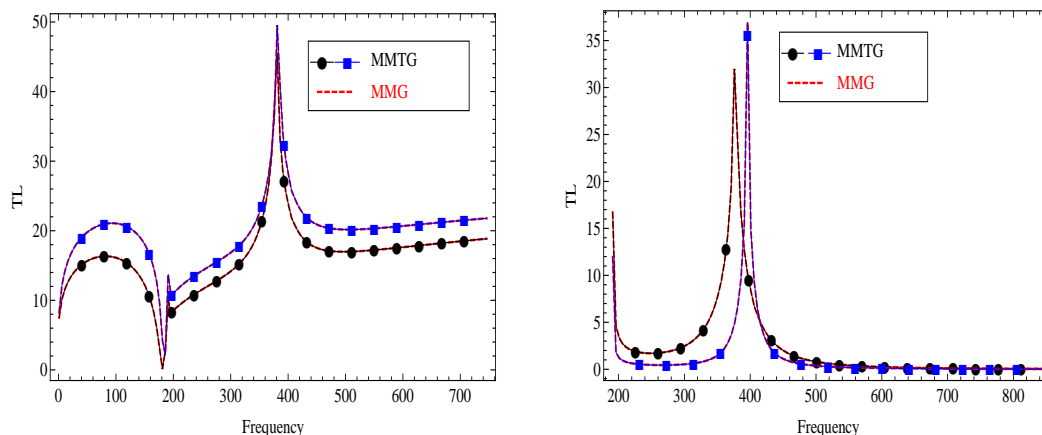
(a) Structure-borne mode incident ($\ell = 0$).

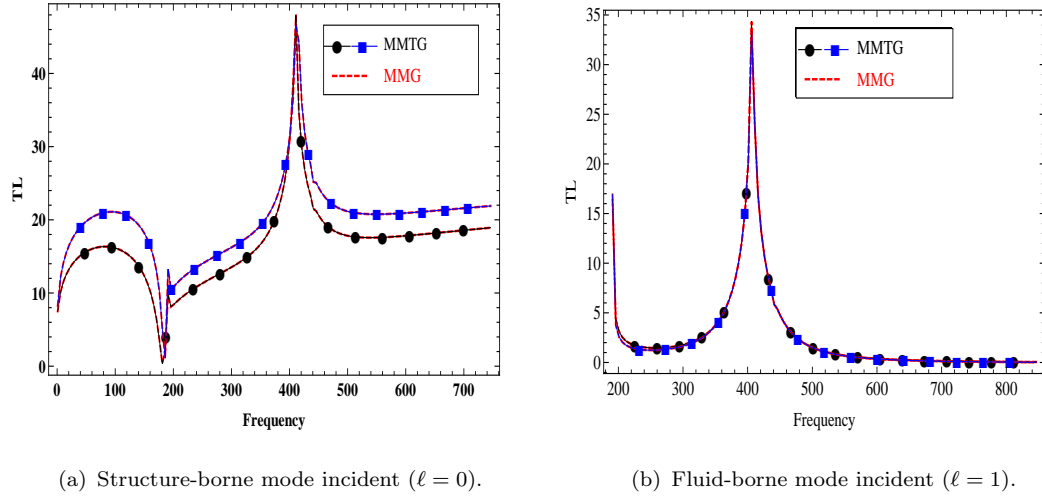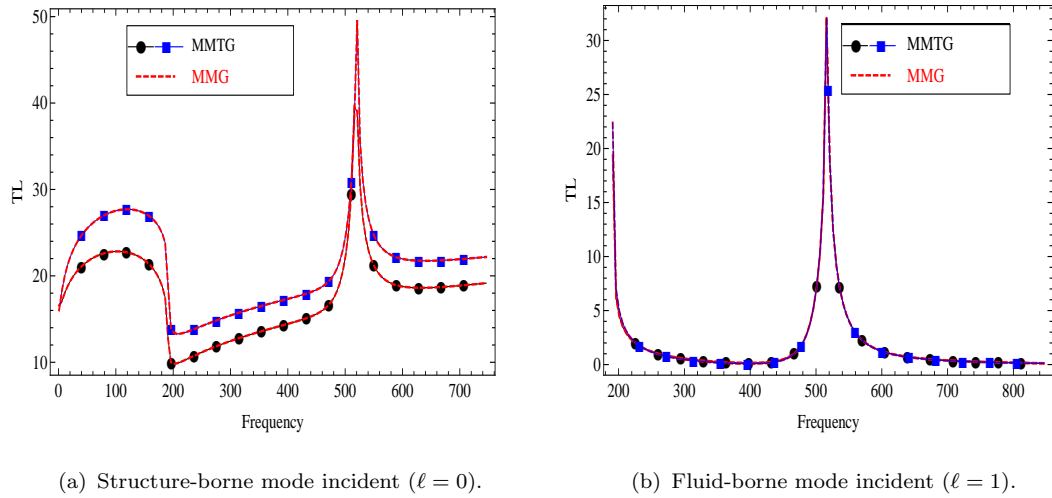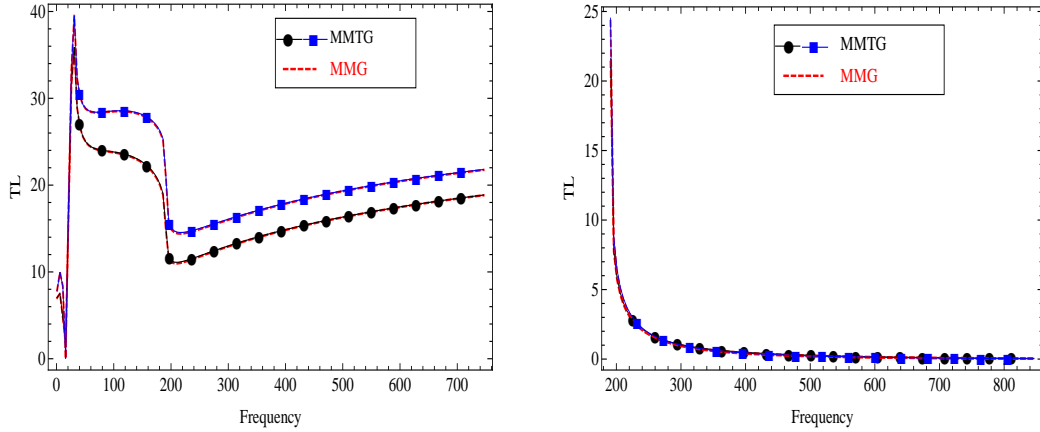(b) Fluid-borne mode incident ($\ell = 1$).

FIGURE 5.8: TL verses frequency with spring like and fixed edges of vertical membranes and comprising elastic plates with (■ − pin-jointed and ● − clamped edge conditions).

minimum for other cut-on frequencies. The effect of clamped and pin-joint edges of the expanded inlet/outlet on the TL is significant in case of fundamental mode incident ($\ell = 0$), however this effect is negligible when the structure is vibrated with higher order mode ($\ell = 1$) see each Fig (a) and (b). It is due to the fact that for higher order mode ($\ell = 1$) the edges of expended inlet/outlet do not affect the transmission loss curves. From Figs. 5.2–5.10, it is clear that when structure is radiated the TL curves obtained from both MMTG and MMG are exactly matched in all frequency regime for each set of edge conditions. Fig. 5.7 depicts the TL verses frequency with zero gradient ($\xi_1 = \infty$) at edges $(x, y) = (\pm L, a)$ and spring-like edge conditions ($\xi_2 = 1$) at $(x, y) = (\pm L, b)$. In Fig. 5.7(a) the maximum TL is 40 db at 20 Hz then TL curve is decreases to 9.5 dB when the frequency increases to first cut-on of the extended inlet and outlet. When frequency approaches the second cut-on and onward a fixed TL is obtained, for both the curves of pin-jointed and clamped edges. The maximum TL in Fig. 5.7(b) is 24 dB at the first cut-on of the extended inlet and outlet and then decreasing up to its minimum in the whole frequency regime. Fig. 5.8 indicate the TL against frequency with spring like and fixed edges of the vertical membrane. The maximum TL is 50 dB at frequency 402 Hz is obtained in Fig. 5.8(a) and two stopbands of bandwidth of 20 cm and 1.02 cm respectively, found in frequency ranges $10 \leq f \leq 190$ and $350 \leq f \leq 450$.

(a) Structure-borne mode incident ($\ell = 0$).

(b) Fluid-borne mode incident ($\ell = 1$).
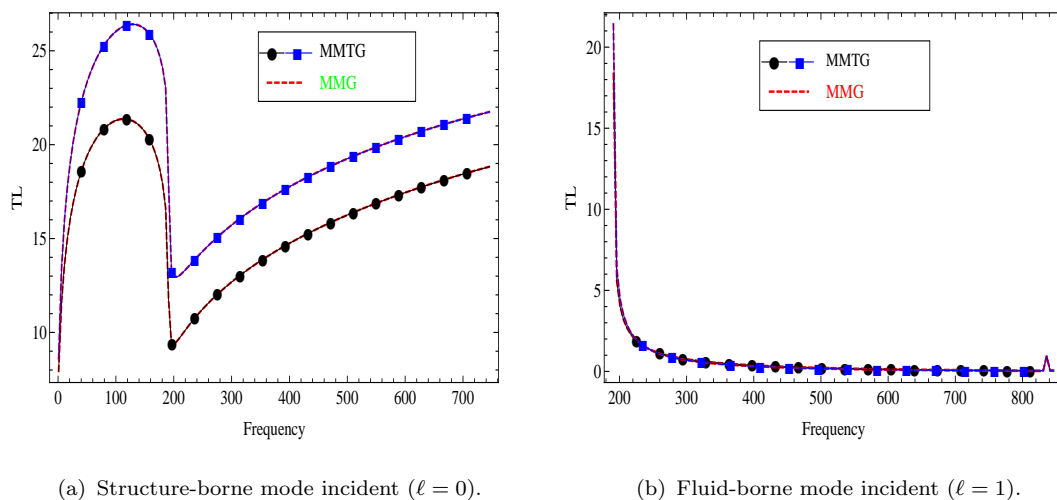
FIGURE 5.9: TL verses frequency with spring like and free edges of vertical membranes and comprising elastic plates with ($\blacksquare$ − pin-jointed and $\bullet$ − clamped edge conditions).

(a) Structure-borne mode incident ($\ell = 0$).

(b) Fluid-borne mode incident ($\ell = 1$).
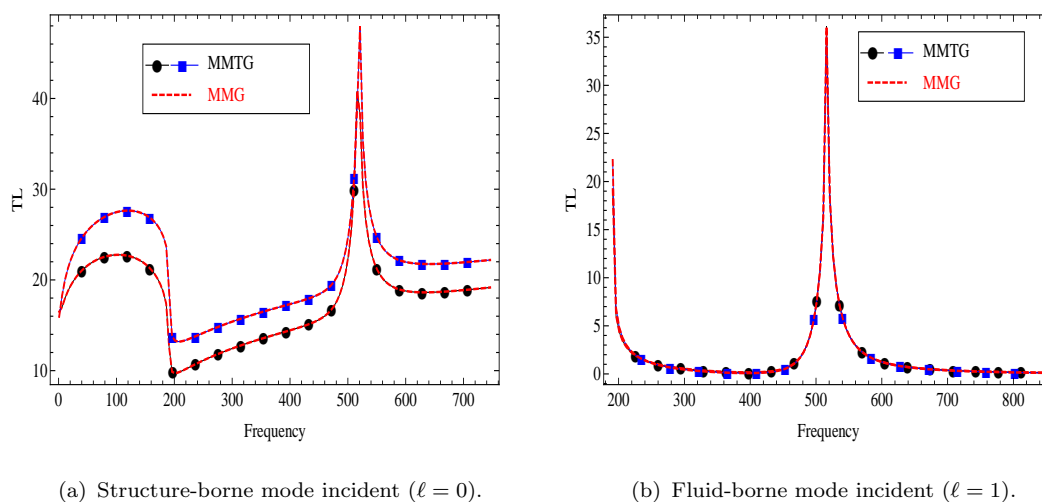
FIGURE 5.10: TL verses frequency with spring like edges of vertical membranes and comprising elastic plates with ($\blacksquare$ − pin-jointed and $\bullet$ − clamped) edge conditions.

Additionally, the MMTG and MMG solutions with truncation parameter $N = 40$ terms are used to plot the pressures and normal velocities at $x = \pm L$, where $f = 1000$Hz. Figs. 5.11–5.14 show pressures and normal velocities curves with zero displacement conditions on membranes edges and clamped conditions on plates edges.

Parts (a) of Figs. 5.11–5.14 depict the results with MMTG approach and parts (b) of these figures show the results with MMG approach. From the agreement of the real and imaginary parts of curves, it is found that the truncated MMTG

and MMG solutions are efficient enough to reconstruct the matching conditions as well as justify that the performed algebra is correct.

(a) Real parts of pressure

(b) Real parts of pressure
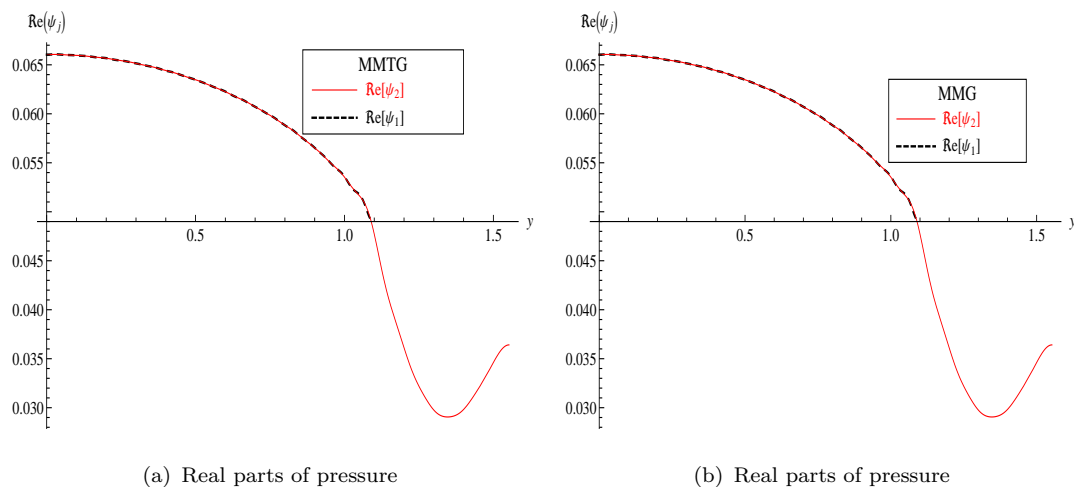
FIGURE 5.11: The real parts of pressures against duct height obtained via MMTG and MMG approaches with $N = 40$.

(a) Imaginary parts of pressure

(b) Imaginary parts of pressure
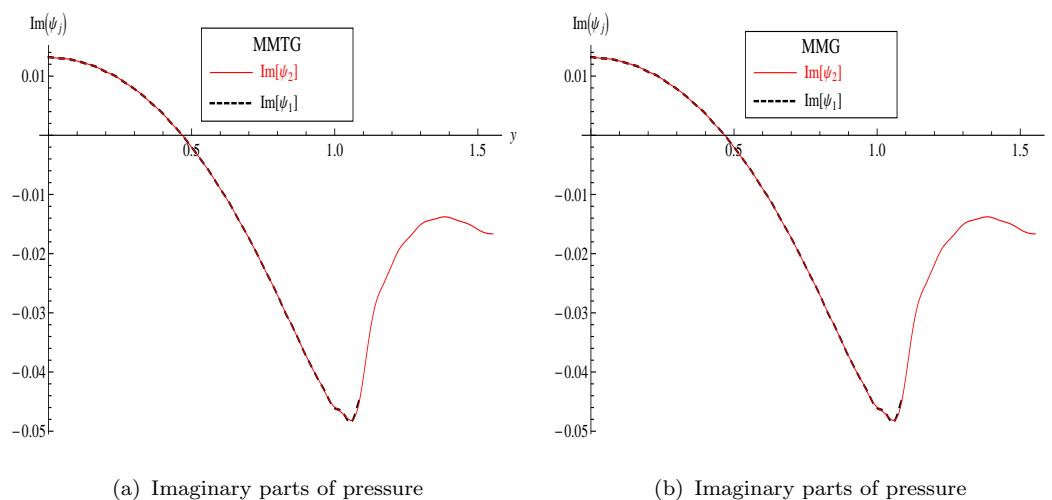
FIGURE 5.12: The imaginary parts of pressures against duct height obtained via MMTG and MMG approaches with $N = 40$.

Hence, the reconstruction of interface conditions by the truncated forms of MMTG and MMG solutions along with the satisfaction of laws of conservation of energies with a limited number of modes,

proves that the techniques adopted here, validate these solution altogether.

(a) Real parts of velocities obtained via MMTG

(b) Real parts of velocities obtained via MMG
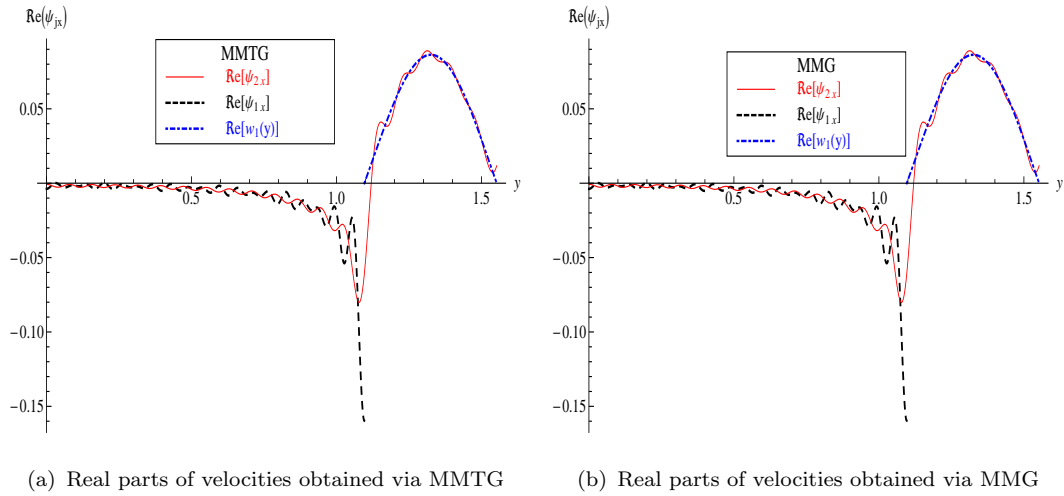
FIGURE 5.13: The real and imaginary parts of normal velocities against duct height with $N = 40$ terms.

(a) imaginary parts of velocities obtained via MMTG

(b) Imaginary parts of velocities obtained via MMG
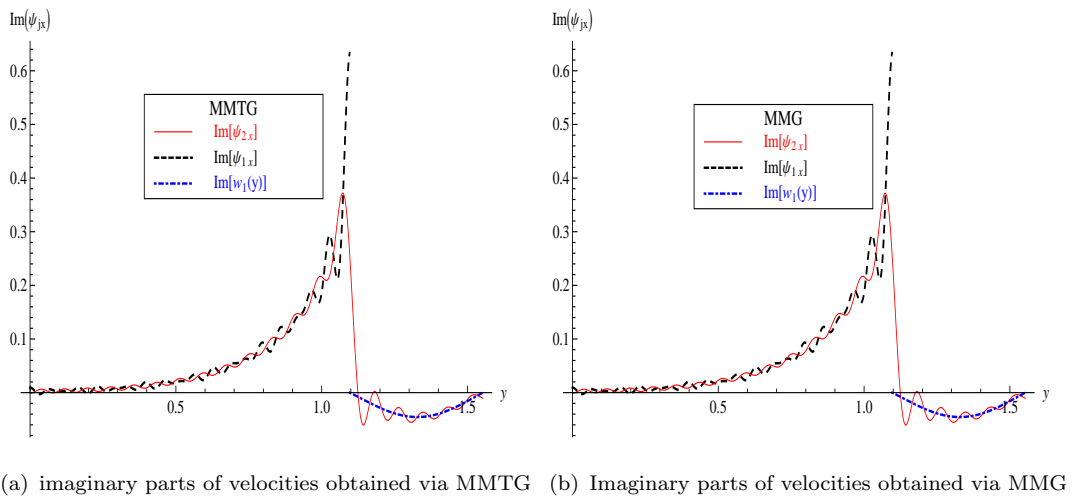
FIGURE 5.14: The real and imaginary parts of normal velocities against duct height with $N = 40$ terms.

Chapter 6

Silencing Performance Analysis of Plate Bounded Cavity with Different Edge Conditions

6.1   Introduction

This chapter is concerned with the scattering of acoustic waves in a flexible cavity bounded by elastic plates that is filled with a compressible fluid. This flexible cavity is connected with extended inlet and outlet which are bounded by elastic plates. The main interest of the authors in this chapter is to develop a new solution method that enables a wide range of conditions to be applied at the the edges of the vertical elastic plates without the need to change basis functions. The Greens function are used to obtain a closed-form expression for the vertical elastic plates displacement in terms of the the fluid modal amplitudes and this expression has sufficient degrees of freedom to enable a wide range of edge conditions to be applied. The comparison of the results achieved with model approach, the Mode-Matching Galerkin (MMTG) approach as suggested by Lawrie and Afzal [81] is developed.

The chapter is arranged as follows. The description of the physical problem and

governing boundary value problem is given in Section 2. The Mode-Matching tailored Galerkin solution of the problem is stated in Section 3. The Model approach are explained in Sections 4. The numerical results are explained in Section 5, whereas, the concluding remarks are portrayed in Section 6.

6.2   Problem Formulation

The boundary value problem is governed by considering an infinite, two dimensional rectangular waveguide stretched along $\bar{x}-$direction in dimensional coordinate plane $(\bar{x}, \bar{y})$, where over bars denote the dimensional setting of coordinates.

The interior of the cavity is filled with compressible fluid of density ρ and sound speed c, whereas the outside of it is set into *vacou*. The lower horizontal wall of the waveguide is assumed to be acoustically rigid, whilst, the upper horizontal walls of it are elastic plates.

Two vertical strips lying along $\bar{x} = \pm L$, $\bar{a} \leqslant \bar{y} \leqslant \bar{b}$ divide the waveguide into three duct regions i.e., the inlet, the expansion chamber and the outlet. The material properties of the vertical strips are assumed to be elastic plates. The waveguide configuration is depicted in Fig. 6.1.

The waveguide structure is exited by a duct mode from the region $(\infty, -\bar{L}) \times (0, \bar{a})$ that propagate from negative to positive $\bar{x}$-direction. The acoustic pressure, $\bar{\Psi}$ in term of dimensional acoustic pressure $\bar{p}$ and acoustic velocity $\bar{\mathbf{v}}$ are found as

$$\bar{p} = -\rho \frac{\partial \bar{\Psi}}{\partial \bar{t}} \quad \text{and} \quad \bar{\mathbf{v}} = \bar{\nabla} \bar{\Psi}. \tag{6.1}$$

Assuming a time harmonic dependence $e^{i\omega t}$ with angular frequency ω and wave number $k = \omega/c$ we define length scale k^{-1} and time scale ω^{-1} so that $x = k\bar{x}$, $y = k\bar{y}$ and $t = \omega\bar{t}$ become non-dimensional space and time coordinates. Thanks to relations in Eq.6.1, the time- harmonic non-dimensional fluid potential, $\psi(x, y, \omega)$,
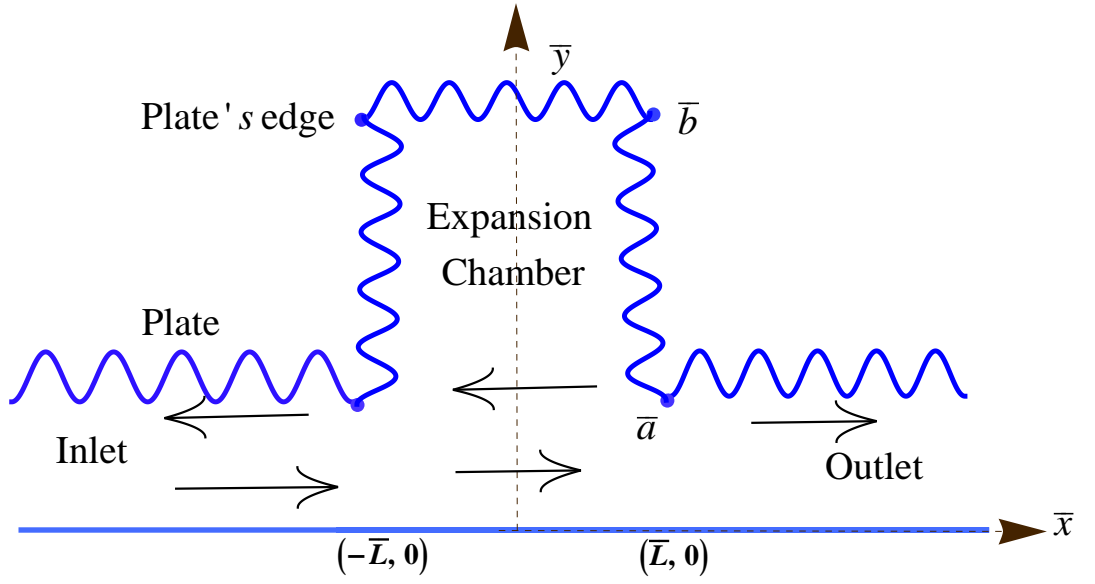
FIGURE 6.1: The waveguide configuration where elastic plates are represented by wavy boundaries.

satisfies the Helmholtz equation:

$$\nabla^2 \psi + \psi = 0. \tag{6.2}$$

The acoustically rigid and elastics plate boundaries [14] in non-dimensional form are

$$\frac{\partial \psi}{\partial y} = 0, \qquad\qquad y = 0, \qquad |x| < \infty, \tag{6.3}$$

and

$$\left(\frac{\partial^4}{\partial x^4} - \mu^4 \right) \frac{\partial \psi}{\partial y} - \alpha \psi = 0, \qquad y = a, b, \qquad |x| < \infty, \tag{6.4}$$

respectively. The quantities

$$\mu = \left(\frac{12(1-\nu^2)c^2\rho_p}{k^2 h^2 E} \right)^{1/4} \qquad \text{and} \qquad \alpha = \frac{12(1-\nu^2)c^2\rho}{k^3 h^3 E} \tag{6.5}$$

are respectively, the in *vacau* fluid loading parameter and plate wavenumber. Here,

E, ν and h respectively, are the Young's modulus, plate density, Poisson's ratio and thickness of the plate.

It is easy to verify from (6.2)-(6.4), the eigenvalues in regions $(x,y) \in \mathbb{R}^2 | L < |x|, 0 \leq y \leq a$ (inlet/outlet) and $(x,y) \in \mathbb{R}^2 | L < |x|, 0 \leq y \leq b$ (expansion chamber) are roots of characteristic equation,

$$\left((\varrho^2 + 1)^2 - \mu^4\right) \varrho \sinh(\varrho p) - \alpha \cosh(\varrho p) = 0, \tag{6.6}$$

where $\varrho = \tau$ (resp.$\varrho = \gamma$) when elastic plates lie along $p = a$ (resp.$p = b$). when elastic plate is situated at $p = b$. These roots are numerically obtained and the computation of all roots is essential for the successful implementation of MMT approach.

The reader are refer to [56] for the detail of such roots. The corresponding eigenfunctions $Y_j(\varrho_n, y) := \cos(\varrho_n y))$ in the inlet/outlet (with $j = 1$, $\varrho_n = \tau_n$) and in the expansion chamber (with $j = 2$, $\varrho_n = \gamma_n$) are linearly dependent and non-orthogonal [57].

Accordingly, the use of generalized orthogonality relations is indispensable to procure a convergent solution, the generalized orthogonality relations for different duct section are defined as:

$$\alpha \int_0^a Y_1(\tau_n, y) Y_1(\tau_m, y) dy = E_n \delta_{mn} - (\tau_m^2 + \tau_n^2 + 2) Y_1'(\tau_m, a) Y_1'(\tau_n, a), \tag{6.7}$$

and

$$\alpha \int_0^b Y_2(\gamma_n, y)(y) Y_2(\gamma_m, y) dy = G_n \delta_{mn} - (\gamma_m^2 + \gamma_n^2 + 2) Y_2'(\gamma_m, b) Y_2'(\gamma_n, b), \tag{6.8}$$

where
$$E_m = \frac{\alpha a}{2} + \frac{\alpha Y_1(\tau_m, a) Y_{1m}'(\tau_m, a)}{2\tau_m^2} + 2[(\tau_m^2 + 1) Y_1'(\tau_m, a)]^2 \tag{6.9}$$

and
$$H_m = \frac{\alpha b}{2} + \frac{\alpha Y_2(\gamma_m, b) Y_2'(\gamma_m, b)}{2\gamma_m^2} + 2[(\gamma_m^2 + 1) Y_2'(\gamma_m, b)]^2. \tag{6.10}$$

The eigenfunctions $Y_j(\varrho_q, y)$, $j = 1, 2$ are linearly dependent [81] and their properties are mentioned below:

$$\sum_{q=0}^{\infty} \Delta_{jq} Y_j(\varrho_q, y) = \sum_{q=0}^{\infty} \varrho_q^2 \Delta_j Y_j(\varrho_q, y) = 0, \qquad 0 \le y \le p \qquad (6.11)$$

and

$$\sum_{q=0}^{\infty} \Delta_{jq}^2 \kappa_q = 0, \quad \sum_{q=0}^{\infty} \varrho_q^2 \Delta_{jq}^2 \kappa_q = 1, \qquad 0 \le y \le p, \qquad (6.12)$$

where

$$\Delta_{jq} = \frac{Y_j'(\varrho_q, p)}{\kappa_q}, \qquad (6.13)$$

where $\kappa = E$ (resp. $\kappa = G$) for inlet/outlet duct region and expansion chamber respectively. The Green's function for the eigenfunctions [81] can be constructed as

$$\alpha \sum_{q=0}^{\infty} \frac{Y_{jq}(\varrho_q, \nu) Y_{jq}(\varrho_q, y)}{\kappa_q} = \delta(y - \nu) + \delta(y + \nu) + \delta(y + \nu - 2), \qquad -l \le \nu, \ y \le l,$$
$$(6.14)$$

this result show smooth function, that converge point-wise and $\delta(y)$ is the Dirac delta function. The MM models having strong singularities at the edges of vertical elastic boundaries, comprehensively addressed by Lawrie in [122].

6.3 Mode Matching Solution

We assume an ensemble time-independent fluid potential ansataz of the form

$$\psi(x, y) = \begin{cases} \psi_1(x, y), & x \le -L, \quad 0 \le y \le a \\ \psi_2(x, y), & |x| \le L, \quad 0 \le y \le b \\ \psi_3(x, y), & x \ge L, \quad 0 \le y \le a \end{cases} \qquad (6.15)$$

The eigenfunction expansion of fluid potential for inlet, outlet and expansion chamber takes the form:

$$\psi_1(x,y) = F_\ell Y_1(\tau_\ell, y)e^{i\eta_\ell(x+L)} + \sum_{n=0}^{\infty} A_n Y_1(\tau_n, y)e^{-i\eta_n(x+L)}, \tag{6.16}$$

$$\psi_2(x,y) = \sum_{n=0}^{\infty} \left(B_n e^{is_n x} + C_n e^{-is_n x} \right) Y_2(\gamma_n, y), \tag{6.17}$$

$$\psi_3(x,y) = \sum_{n=0}^{\infty} D_n Y_1(\tau_n, y)e^{i\eta_n(x-L)}, \tag{6.18}$$

where A_n, B_n, C_n and D_n, for $n \in \mathbb{Z}^+$ are the complex amplitudes of the reflected and transmitted modes to be determined. The first term on right hand side of the incident field with force F_ℓ. The index ℓ suggests weather the incident field consist of fundamental mode or higher mode. The quantities η_n and ν_n are the wave numbers and are defined in terms of eigenvalues as τ_n and γ_n, as

$$\eta_n = (\tau_n^2 + 1)^{1/2} \qquad \nu_n = (\gamma_n^2 + 1)^{1/2} \qquad n \in \mathbb{Z}, n \geq 0 \tag{6.19}$$

The goal of MM is to find the amplitudes A_n, B_n, C_n and D_n using continuity of pressure flux and normal velocities at the interfaces $x = \pm L$:

$$\int_0^a \psi_1(-L, y)Y_1(\tau_m, y)dy = \int_0^a \psi_2(-L, y)Y_1(\tau_m, y)dy \tag{6.20}$$

and

$$\int_0^a \psi_3(L, y)Y_1(\tau_m, y)dy = \int_0^a \psi_2(L, y)Y_1(\tau_m, y)dy. \tag{6.21}$$

On substituting (6.16)-(6.18) into (6.20) and (6.21) and then normalizing with the aid of the orthogonality relation (6.7), after simplification we may get

$$A_m = -F_\ell \delta_{m\ell} - \Delta_{1m}\{e_1 + (\tau_m^2 + 2)e_2\} + \frac{\alpha}{E_m} \sum_{n=0}^{\infty} R_{nm} \left(B_n e^{is_n L} - C_n e^{-is_n L} \right), \tag{6.22}$$

$$D_m = \Delta_{1m}\{e_3 + (\tau_m^2 + 2)e_4\} - \frac{\alpha}{E_m} \sum_{n=0}^{\infty} R_{nm} \left(B_n e^{-is_n L} - C_n e^{is_n L} \right), \tag{6.23}$$

where, $\Delta_{1m} = \tau_m \sinh(\tau_m a)/E_m$. Now by adding (6.22) and (6.23), it is found that

$$A_m + D_m = -F_\ell \delta_{m\ell} - \Delta_{1m}\{(e_1 - e_3) + (\tau_m^2 + 2)(e_2 - e_4)\}$$
$$+\frac{2\alpha}{E_m} \sum_{n=0}^{\infty} R_{nm} \cos(s_n L)(B_n + C_n). \qquad (6.24)$$

Likewise, the subtraction of (6.22) from (6.23), lead to

$$A_m - D_m = -F_\ell \delta_{m\ell} - \Delta_{1m}\{(e_1 + e_3) + (\tau_m^2 + 2)(e_2 + e_4)\}$$
$$-\frac{2i\alpha}{E_m} \sum_{n=0}^{\infty} R_{nm} \sin(s_n L)(B_n - C_n). \qquad (6.25)$$

Then by considering: $\Phi_m^\pm = (A_m \pm D_m)$, $\chi_n^\pm = (B_n \pm C_n)$, $U_1^\pm = e_1 \mp e_3$ and $U_2^\pm = e_2 \mp e_4$, the formulations of symmetric and anti-symmetric mode amplitudes (6.26) and (6.27) are achieved.

$$\Phi_m^+ = -F_\ell \delta_{m\ell} + \{U_1^+ + (\tau_m^2 + 2)U_2^+\}\Delta_{1m} + \frac{2\alpha}{E_m} \sum_{n=0}^{\infty} R_{mn} \cos(s_n L)\chi_n^+ \qquad (6.26)$$

and

$$\Phi_m^- = -F_\ell \delta_{m\ell} + \{U_1^- + (\tau_m^2 + 2)U_2^-\}\Delta_{1m} - \frac{2i\alpha}{E_m} \sum_{n=0}^{\infty} R_{mn} \sin(s_n L)\chi_n^-, \qquad (6.27)$$

respectively, where

$$R_{mn} = \int_0^a \cosh(\beta_m y) \cosh(\gamma_n y) dy. \qquad (6.28)$$

Here $\Phi_m^\pm = (A_m \pm D_m)$ and $\chi_n^\pm = (B_n \pm C_n)$ denote the amplitudes of symmetric/anti-symmetric modes propagating in side regions and central regions, respectively, and that yield the amplitudes of modes propagating towards the positive and negative directions of the waveguide through expressions:

• $A_m = \frac{1}{2}(\Phi_m^+ + \Phi_m^-)$ and $D_m = \frac{1}{2}(\Phi_m^+ - \Phi_m^-)$.

• $B_m = \frac{1}{2}(\chi_m^+ + \chi_m^-)$ and $C_m = \frac{1}{2}(\chi_m^+ - \chi_m^-)$.

Whereas, the quantities $U_1^\pm$ and $U_2^\pm$ involving in (6.26) and (6.27) are constants having values respectively: $U_1^\pm = e_1 \mp e_3$ and $U_2^\pm = e_2 \mp e_4$, in which $e_1 = -i\,\psi_{1xyyy}(-L, a)$, $e_2 = -i\,\psi_{1xy}(-L, a)$, $e_3 = -i\,\psi_{3xyyy}(L, a)$ and $e_4 = -i\,\psi_{3xy}(L, a)$

are governed during the normalization of (6.20) and (6.21) with generalized OR (6.7).

Now before using the continuity of normal velocities it is worthwhile to encounter the effect of vertical elastic plates, for this purpose we introduce two different approaches; first the tailored-Galerkin and second the Model approach.

6.3.1 Tailored-Galerkin Solution

The fundamentals of this approach are linked with the assortment of trial functions which determine the response along the vertical boundaries and their edges. The dimensionless elastic plate displacements $w_j(y)$ for $j = 1,\ 2$ satisfy

$$\frac{d^4 w_j}{dy^4} - \mu^4 w_1 = \alpha \psi_2, \quad x = \pm L, \quad a \le y \le b, \tag{6.29}$$

From (6.29), the plate displacements are obtained as

$$w_1(y) = a_1 \cos(\mu y) + a_2 \sin(\mu y) + a_3 \cosh(\mu y) + a_4 \sinh(\mu y) + \\ \alpha \sum_{n=0}^{\infty} \frac{\left(B_n e^{-i s_n L} + C_n e^{i s_n L}\right) \cosh(\gamma_n y)}{\gamma_n^4 - \mu^4}, \tag{6.30}$$

$$w_2(y) = a_5 \cos(\mu y) + a_6 \sin(\mu y) + a_7 \cosh(\mu y) + a_8 \sinh(\mu y) - \\ \alpha \sum_{n=0}^{\infty} \frac{\left(B_n e^{i s_n L} + C_n e^{-i s_n L}\right) \cosh(\gamma_n y)}{\gamma_n^4 - \mu^4}. \tag{6.31}$$

Here the quantities $a_i,\ i = 1 \ldots 8$ are unknown constants and that determine the physical behavior of vertical elastic plates at edges.

On adding and subtracting (6.30) and (6.31), the symmetric and anti-symmetric modes are found as

$$W^{\mp}(y) = a_{15}^{\mp} \cos(\mu y) + a_{26}^{\mp} \sin(\mu y) + a_{37}^{\mp} \cosh(\mu y) + a_{48}^{\mp} \sinh(\mu y) - \\ 2i\alpha \sum_{n=0}^{\infty} \frac{\chi_n^{\mp} \Pi_n^{\mp} L) \cosh(\gamma_n y)}{\gamma_n^4 - \mu^4}, \tag{6.32}$$

where, $\Pi_n^+ = \sin(s_n L)$, $\Pi_n^- = i\cos(s_n L)$, $a_{15}^\pm = a_1 \pm a_5$, $a_{26}^\pm = a_2 \pm a_6$, $a_{37}^\pm = a_3 \pm a_7$, $a_{48}^\pm = a_4 \pm a_8$ and $W^\pm(y) = w_1(y) \pm w_2(y)$ respectively.

Now we impose extra edge conditions which not only define the type of connection of vertical plates having at finite edges $y = a$ and $y = b$ but also ensure the uniqueness of the solution. In order to explain the versatility of approach two different types of such conditions are discussed in the subsequent subsections.

Clamped Edges of Vertical Elastic Plates

The edges are clamped if displacements as well as gradient are zero. The clamped edge conditions are expressed as:

$$W^\pm(a) = 0 = W^\pm(b), \tag{6.33}$$

$$W_y^\pm(a) = 0 = W_y^\pm(b). \tag{6.34}$$

On invoking (6.33)–(6.34) into (6.32), the matrix forms of unknown constants are obtained as:

$$a_{15}^\mp \cos(\mu p) + a_{26}^\mp \sin(\mu p) + a_{37}^\mp \cosh(\mu p) + a_{48}^\mp \sinh(\mu p) =$$
$$-2i\alpha \sum_{n=0}^{\infty} \frac{\chi^\mp \Pi_n^\mp \cosh(\gamma_q p)}{\gamma_n^4 - \mu^4} \text{ at } p = a, b \tag{6.35}$$

$$-a_{15}^\mp \sin(\mu p) + a_{26}^\mp \cos(\mu p) + a_{37}^\mp \sinh(\mu p) + a_{48}^\mp \cosh(\mu p) =$$
$$-\frac{2i\alpha}{\mu} \sum_{n=0}^{\infty} \frac{\chi^\mp \Pi_m^\mp \gamma_n \sinh(\gamma_q p)}{\gamma_n^4 - \mu^4} \text{ at } p = a, b. \tag{6.36}$$

The unknown constants $\{a_{15}^\pm, a_{26}^\pm, a_{37}^\pm, a_{48}^\pm\}$ can be obtained from (6.35)-(6.36) very easily.

Pin-jointed Connections of Vertical Plates

The connection at edges are pin-jointed if we assume a zero displacement as well as a zero bending moment over there, mathematically pin-jointed edge conditions

takes the form:

$$W^\pm(a) = 0 = W^\pm(b), \tag{6.37}$$

$$W_{yy}^\pm(a) = 0 = W_{yy}^\pm(b). \tag{6.38}$$

By substituting (6.37)–(6.38) into (6.32), the system in the form of unknown constants are found as

$$a_{15}^\mp \cos(\mu p) + a_{26}^\mp \sin(\mu p) + a_{37}^\mp \cosh(\mu p) + a_{48}^\mp \sinh(\mu p) =$$
$$-2i\alpha \sum_{n=0}^{\infty} \frac{\chi^\mp \Pi_n^\mp \cosh(\gamma_q p)}{\gamma_n^4 - \mu^4} \text{ at } p = a, b \tag{6.39}$$

$$-a_{15}^\mp \cos(\mu p) - a_{26}^\mp \sin(\mu p) + a_{37}^\mp \cosh(\mu p) + a_{48}^\mp \sinh(\mu p) =$$
$$-\frac{2i\alpha}{\mu^2} \sum_{n=0}^{\infty} \frac{\chi^\mp \Pi_n^\mp \gamma_n^2 \sinh(\gamma_q p)}{\gamma_n^4 - \mu^4} \text{ at } p = a, b \tag{6.40}$$

From (6.39)-(6.40) on solving simultaneously, the values of unknowns $\{a_{15}^\pm, a_{26}^\pm, a_{37}^\pm, a_{48}^\pm\}$ are found. Once these quantities become known, the constants a_j, $j = 1 \ldots 8$ are obtained in straightforward way from the expressions:

$$a_1 = \frac{1}{2}(a_{15}^+ + a_{15}^-), \quad a_3 = \frac{1}{2}(a_{37}^+ + a_{37}^-), \tag{6.41}$$

$$a_2 = \frac{1}{2}(a_{26}^+ + a_{26}^-), \quad a_4 = \frac{1}{2}(a_{28}^+ + a_{28}^-). \tag{6.42}$$

$$a_5 = \frac{1}{2}(a_{15}^+ - a_{15}^-), \quad a_6 = \frac{1}{2}(a_{37}^+ - a_{37}^-), \tag{6.43}$$

$$a_7 = \frac{1}{2}(a_{26}^+ - a_{26}^-), \quad a_8 = \frac{1}{2}(a_{28}^+ - a_{28}^-). \tag{6.44}$$

Likewise, the velocity flux conditions at interfaces take the form:

$$\int_0^b \psi_{2x}(-L, y) Y_2(\gamma_m, y) dy = \int_0^a \psi_{1x}(-L, y) Y_2(\gamma_m, y) dy$$
$$+ \int_a^b w_1(y) Y_2(\gamma_m, y) dy \tag{6.45}$$

and

$$\int_0^b \psi_{2x}(L,y)Y_2(\gamma_m,y)dy = \int_0^a \psi_3(L,y)Y_2(\gamma_m,y)dy$$
$$+ \int_a^b w_2(L,y)Y_2(\gamma_m,y)dy. \tag{6.46}$$

Accordingly, (6.45) and (6.46) link the acoustic velocity of central region to the acoustic velocities of inlet and outlet regions at $x = \pm L$, and that may lead to the values of amplitudes of symmetric and anti-symmetric modes propagating in the central region.

On invoking (6.16)-(6.18) into (6.45) and (6.46), and normalizing with the help of OR (6.8), after some rearrangement it is obtained that:

$$B_m e^{-is_m L} - C_m e^{is_n L} = \Omega_m\{e_5 + (\gamma_m^2 + 2)e_6\} + \frac{\alpha}{s_m H_m}\{F_\ell \eta_\ell R_{m\ell} - \sum_{n=0}^{\infty} R_{mn}\eta_n A_n\}$$
$$- \frac{i\alpha}{s_m H_m}\{a_1 A_{1m} + a_2 A_{2m} + a_3 A_{3m} + a_4 A_{4m}\} +$$
$$\frac{i\alpha^2}{s_m H_m}\sum_{n=0}^{\infty} \frac{T_{mn}(B_n e^{-is_n L} + C_n e^{is_n L})}{\gamma_n^4 - \mu^4} \tag{6.47}$$

$$B_m e^{is_m L} - C_m e^{-is_n L} = \Omega_m\{e_7 + (\gamma_m^2 + 2)e_8\} + \frac{\alpha}{s_m H_m}\sum_{n=0}^{\infty} R_{mn}\eta_n D_n$$
$$- \frac{i\alpha}{s_m H_m}\{a_5 A_{1m} + a_6 A_{2m} + a_7 A_{3m} + a_8 A_{4m}\} -$$
$$\frac{i\alpha^2}{s_m H_m}\sum_{n=0}^{\infty} \frac{T_{mn}(B_n e^{is_n L} + C_n e^{-is_n L})}{\gamma_n^4 - \mu^4} \tag{6.48}$$

where $\Omega_m = \Delta_{2m}/s_m$ and $\Delta_{2m} = \gamma_m \sinh(\gamma_m b)/H_m$. Now the addition and subtraction of (6.47) and (6.48) reveal

$$B_m + C_m = \frac{i\Omega_m}{2\sin(s_m L)}\left\{(e_5 - e_7) + (\gamma_m^2 + 2)(e_6 - e_8)\right\} -$$
$$\frac{i\alpha}{2s_m H_m \sin(s_m L)}\{F_\ell \eta_\ell R_{\ell m} - \sum_{n=0}^{\infty} R_{nm}\eta_\ell(A_n + D_n)\} -$$
$$\frac{i\alpha}{2s_m H_m \sin(s_n L)}\{(a_1 - a_5)A_{1m} + (a_2 - a_6)A_{2m} + (a_3 - a_7)A_{3m}\} +$$
$$\frac{i\alpha}{2s_m H_m \sin(s_n L)}\{(a_4 - a_8)A_{4m} - 2\alpha\sum_{n=0}^{\infty} \frac{T_{mn}\cos(s_m L)(B_n + C_n)}{\gamma_n^4 - \mu^4}\},$$

and

$$B_m - C_m = \frac{\Omega_m}{2\cos(s_mL)}\left\{(e_5+e_7)+(\gamma_m^2+2)(e_6+e_8)\right\}+$$

$$\frac{\alpha}{2s_mH_m\cos(s_mL)}\left\{F_\ell\eta_\ell R_{\ell m}-\sum_{n=0}^{\infty}R_{nm}\eta_\ell(A_n+D_n)\right\}-$$

$$\frac{i\alpha}{2s_mH_m\cos(s_nL)}\left\{(a_1+a_5)A_{1m}+(a_2+a_6)A_{2m}+(a_3+a_7)A_{3m}\right\}-$$

$$\frac{i\alpha}{2s_mH_m\cos(s_nL)}\left\{(a_4+a_8)A_{4m}+2\alpha\sum_{n=0}^{\infty}\frac{T_{mn}\sin(s_mL)(B_n-C_n)}{\gamma_n^4-\mu^4}\right\},$$

respectively. Then by considering $\chi_n^{\pm}=(B_n\pm C_n)$, $V_1^{\pm}=e_5\pm e_7$ and $V_2^{\pm}=e_6\pm e_8$, the amplitudes of symmetric and anti-symmetric modes propagating in the central region are found as

$$\chi_m^+ = \frac{i}{2\sin(s_mL)}\left\{(V_1^++(\gamma_m^2+2)V_2^+)\,\Omega_m-\frac{i\alpha}{2s_mH_m\sin(s_mL)}(\Theta_m^+(R)+\right.$$

$$\frac{\alpha}{2H_ms_m\sin(s_mL)}\left\{a_{15}^-A_{1m}+a_{26}^-A_{2m}+a_{37}^-A_{3m}+a_{48}^-A_{4m}\right\}$$

$$-\frac{\alpha^2}{H_ms_m\sin(s_mL)}\sum_{n=0}^{\infty}\frac{\chi_n^+\cos(s_nL)T_{nm}}{\gamma_n^4-\mu^4} \tag{6.51}$$

and

$$\chi_m^- = \frac{1}{2\cos(s_mL)}\left\{(V_1^++(\gamma_m^2+2)V_2^+)\,\Omega_m+\frac{\alpha}{2s_mH_m\cos(s_mL)}(\Theta_m^-(R)-\right.$$

$$\frac{i\alpha}{2H_ms_m\cos(s_mL)}\left\{a_{15}^+A_{1m}+a_{26}^+A_{2m}+a_{37}^+A_{3m}+a_{48}^+A_{4m}\right\}$$

$$-\frac{\alpha^2}{H_ms_m\cos(s_mL)}\sum_{n=0}^{\infty}\frac{\chi_n^-\sin(s_nL)T_{nm}}{\gamma_n^4-\mu^4} \tag{6.52}$$

where

$$\Theta_m^{\pm}(R)=F_\ell\eta_\ell R_{m\ell}-\sum_{n=0}^{\infty}R_{mn}\eta_n\Phi_n^{\pm}, \tag{6.53}$$

and

$$A_{1m}=\int_a^b\cos(\mu y)\cosh(\gamma_m y)dy,$$

$$A_{2m} = \int_a^b \sin(\mu y) \cosh(\gamma_m y) dy,$$

$$A_{3m} = \int_a^b \cosh(\mu y) \cosh(\gamma_m y) dy,$$

$$A_{4m} = \int_a^b \sinh(\mu y) \cosh(\gamma_m y) dy,$$

and

$$T_{mn} = \int_d^b \cosh(\gamma_m y) \cosh(\gamma_n y) dy. \tag{6.54}$$

Here quantities $V_1^\pm = e_5 \pm e_7$ and $V_2^\pm = e_6 \pm e_8$ which include additional constants $e_5 = \psi_{2yyy}(-L, b)$, $e_6 = \psi_{2y}(-L, b)$, $e_7 = \psi_{2yyy}(L, b)$ and $e_8 = \psi_{2y}(L, b)$, have appeared during the normalizing of (6.45) and (6.46) with generalized OR (6.8). We still need to cater for additional unknowns $U_j^\pm$ and $V_j^\pm$ for $j = 1, 2$ they can be found by taking into account the physical behavior of horizontal elastic plates at the joints. For this we need to impose additional physical conditions on horizontal connection of elastic plates that may be clamped, pin jointed or pivoted. The are evaluated in the following subsections.

6.3.2 Clamped Edges of Horizontal Elastic Plates

The edges are clamped if displacements as well as gradient are zero, that are:

$$\psi_{1y}(-L, a) = 0 = \psi_{3y}(L, a), \tag{6.55}$$

$$\psi_{1xy}(-L, a) = 0 = \psi_{3xy}(L, a), \tag{6.56}$$

$$\psi_{2y}(\pm L, b) = 0, \tag{6.57}$$

$$\psi_{2xy}(\pm L, b) = 0. \tag{6.58}$$

The above equations are helpful, to evaluate the values of physical constants $\{U_j, V_j\}$ and that yield $U_2^\pm = V_2^\pm = 0$, whereas, for $U_1^\pm$ and $V_1^\pm$, the edge conditions

(6.55) and (6.58) lead to

To achieve $U_1^{\pm}$, the multiplication of (6.26)-(6.27) with $\gamma_m \sinh(\gamma_m a)$ results:

$$\Delta_{1m} E_m \Phi_m^+ = -\Delta_{1m} F_\ell \delta_{m\ell} E_\ell + \Delta_{1m}^2 E_m \{ U_1^+ + (\gamma_m^2 + 2) U_2^+ \}$$
$$+ 2\alpha \Delta_{1m} \sum_{n=0}^{\infty} R_{mn} \cos(s_n L) \chi_n^+, \tag{6.59}$$

$$\Delta_{1m} E_m \Phi_m^- = \Delta_{1m} E_m F_\ell \delta_{m\ell} E_\ell - \Delta_{1m}^2 E_m \{ U_1^- + (\gamma_m^2 + 2) U_2^- \}$$
$$- 2i\alpha \Delta_{1m} \sum_{n=0}^{\infty} R_{mn} \sin(s_n L) \chi_n^-. \tag{6.60}$$

However, by using (6.16)-(6.18) into edge conditions (6.55) one finds

$$F_\ell \Delta_{1\ell} E_\ell + \sum_{n=0}^{\infty} \Delta_{1n} E_n A_n = 0, \tag{6.61}$$

$$\sum_{n=0}^{\infty} \Delta_{1n} E_n D_n = 0. \tag{6.62}$$

Then by performing the operation of addition and subtraction on (6.61) and (6.62) simultaneously results:

$$\sum_{n=0}^{\infty} \Delta_{1n} E_n \Phi_n^{\pm} = -F_\ell \Delta_{1\ell} E_\ell. \tag{6.63}$$

Now the summation from zero to infinity over m of (6.59) and (6.60), then putting into (6.63), we accomplish (6.64) and (6.65).

Similarly, to obtained $V_1^{\pm}$ multiply (6.51)-(6.52) by $\Delta_{2m} H_m s_m \sin(s_m L)$ and then taking summation from zero to infinity over m and using edge conditions (6.58), finally conclude to (6.66) and (6.68).

$$U_1^- = -\frac{2}{S_1} \{ F_\ell \eta_\ell \Delta_{1\ell} E_\ell + i\alpha \sum_{m=0}^{\infty} \sum_{n=0}^{\infty} \Delta_{1m} \eta_m R_{mn} \sin(s_n L) \Phi_n^- \}, \tag{6.64}$$

$$U_1^+ = -\frac{2}{S_1} \{ F_\ell \eta_\ell \Delta_{1\ell} E_\ell - \alpha \sum_{m=0}^{\infty} \sum_{n=0}^{\infty} \Delta_{1m} \eta_n R_{mn} \cos(s_n L) \Phi_n^+ \}, \tag{6.65}$$

$$V_1^+ = -\frac{\alpha}{2S_2} \sum_{m=0}^{\infty} \Omega_m \tan(s_m L)\Theta_m^+(R) -$$

$$\frac{i\alpha}{2S_2} \sum_{m=0}^{\infty} \Omega_m \tan(s_m L)\{a_{15}^- A_{1m} + a_{26}^- A_{2m} + a_{37}^- A_{3m} + a_{48}^- A_{4m}\}$$

$$-\frac{i\alpha^2}{S_2} \sum_{m=0}^{\infty} \Omega_m \tan(s_m L) \sum_{n=0}^{\infty} \frac{\sin(s_n L)T_{mn}\chi_n^+}{\gamma_n^4 - \mu^4} \tag{6.66}$$

$$V_1^- = -\frac{\alpha}{2S_3} \sum_{m=0}^{\infty} \Omega_m \cot(s_m L)\Theta_m^-(R) - \tag{6.67}$$

$$\frac{i\alpha}{2S_3} \sum_{m=0}^{\infty} \Omega_m \cot(s_m L)\{a_{15}^+ A_{1m} + a_{26}^+ A_{2m} + a_{37}^+ A_{3m} + a_{48}^+ A_{4m}\}$$

$$+\frac{i\alpha^2}{S_3} \sum_{m=0}^{\infty} \Omega_m \cot(s_m L) \sum_{n=0}^{\infty} \frac{\cos(s_n L)T_{mn}\chi_n^-}{\gamma_n^4 - \mu^4} \quad , \tag{6.68}$$

where

$$S_1 = \sum_{m=0}^{\infty} \Delta_{1m}^2 E_m \eta_m, \quad S_2 = \frac{1}{2} \sum_{m=0}^{\infty} \frac{\Omega_m^2 s_m H_m \tan(s_m L)}{\gamma_m^4 - \mu^4}$$

and

$$S_3 = \frac{1}{2} \sum_{m=0}^{\infty} \frac{\Omega_m^2 s_m H_m \cot(s_m L)}{\gamma_m^4 - \mu^4}.$$

6.3.3 Pin-jointed Edges of Horizontal Elastic Plates

For horizontal elastic plate pin-jointed edge conditions take the form

$$\psi_{1y}(-L, a) = 0 = \psi_{3y}(L, a), \tag{6.69}$$

$$\psi_{1xxy}(-L, a) = 0 = \psi_{3yxx}(L, a), \tag{6.70}$$

$$\psi_{2y}(\pm L, b) = 0, \tag{6.71}$$

$$\psi_{2xxy}(-L, b) = 0 = \psi_{2yxx}(L, b). \tag{6.72}$$

From (6.71) it is found that $U_2^\pm = 0$, whereas, to determine $U_1^\pm$, the equations (6.69) and (6.70) apply, By multiplying (6.51) with $\sum_{m=0}^{\infty} \Delta_{2m} H_m s_m^2 \cos(s_m L)$ and then using (6.72), it is found that

$$S_{11}V_1^+ + S_{12}V_2^+ = -\alpha \sum_{m=0}^{\infty} \Omega_m s_m^2 \tan(s_m L)\Theta_m^-(R) -$$
$$i\alpha \sum_{m=0}^{\infty} \Omega_m s_m^2 \tan(s_m L)\{a_{15}^+ A_{1m} + a_{26}^+ A_{2m} + a_{37}^+ A_{3m} + a_{48}^+ A_{4m}\}$$
$$-2i\alpha^2 \sum_{m=0}^{\infty} \Omega_m s_m^2 \tan(s_m L) \sum_{n=0}^{\infty} \frac{\chi_n^- \sin(s_n L) T_{mn}}{\gamma_n^4 - \mu^4}, \tag{6.73}$$

substituting $\Theta_m^-(R)$ from (6.53), it is straightforward to obtain

$$S_{11}V_1^+ + S_{12}V_2^+ = -\alpha \sum_{m=0}^{\infty} \Omega_m s_m^2 \tan(s_m L)\{F_\ell \eta_\ell R_{\ell m} - \sum_{n=0}^{\infty} \Phi_m^- \eta_n R_{nm}\} -$$
$$i\alpha \sum_{m=0}^{\infty} \Omega_m s_m^2 \tan(s_m L)\{a_{15}^+ A_{1m} + a_{26}^+ A_{2m} + a_{37}^+ A_{3m} + a_{48}^+ A_{4m}\}$$
$$-2i\alpha^2 \sum_{m=0}^{\infty} \Omega_m s_m^2 \tan(s_m L) \sum_{n=0}^{\infty} \frac{\chi_n^- \sin(s_n L) T_{mn}}{\gamma_n^4 - \mu^4}, \tag{6.74}$$

Now the smooth convergence of summations in (6.73), is achieved with the help of Green's identity (6.11) and the integrals of R_{mn} and T_{mn} can be splitted as:

$$R_{nm} = \int_0^b \cosh(\gamma_m y)\cosh(\tau_n y)dy - \int_a^b \cosh(\gamma_m y)\cosh(\tau_n y)dy \tag{6.75}$$

and

$$T_{mn} = \int_0^b \cosh(\gamma_m y)\cosh(\tau_n y)dy - \int_0^a \cosh(\gamma_m y)\cosh(\tau_n y)dy. \tag{6.76}$$

By using these values, (6.73) can be expressed as:

$$S_{11}V_1^+ + S_{12}V_2^+ = -\alpha \sum_{m=0}^{\infty} \Omega_m s_m^2 \tan(s_m L)\{\int_0^b \cosh(\gamma_m y)\cosh(\tau_\ell y)dy - P_{\ell m}\}$$

$$+\alpha \sum_{n=0}^{\infty}\sum_{m=0}^{\infty} \Omega_m s_m^2 \tan(s_m L)\Phi_n^+\{\int_0^b \cosh(\gamma_m y)\cosh(\tau_n y)dy - P_{mn}\}$$

$$i\alpha \sum_{m=0}^{\infty} \Omega_m s_m^2 \tan(s_m L)\{a_{15}^+ A_{1m} + a_{26}^+ A_{2m} + a_{37}^+ A_{3m} + a_{48}^+ A_{4m}\}$$

$$-2i\alpha^2 \sum_{m=0}^{\infty} \Omega_m s_m^2 \tan(s_m L)\sum_{n=0}^{\infty} \frac{\chi_n^- \sin(s_n L)}{\gamma_n^4 - \mu^4}\{\int_0^b \cosh(\gamma_n y)\cosh(\gamma_n y)dy - Q_{mn}\} \tag{6.77}$$

where

$$P_{mn} = \int_a^b \cosh(\gamma_m y)\cosh(\tau_n y)dy \tag{6.78}$$

and

$$Q_{mn} = \int_a^b \cosh(\gamma_m y)\cosh(\gamma_n y)dy. \tag{6.79}$$

However, form the Green's identity (6.11) when $y \in [0, b]$, it is observed that:

$$\sum_{m=0}^{\infty} \Omega_m s_m^2 \tan(s_m L)\int_0^b \cosh(\gamma_m y)\cosh(\tau_\ell y)dy = 0 \tag{6.80}$$

$$\sum_{n=0}^{\infty} \Phi_n^- \sum_{m=0}^{\infty} \Omega_m s_m^2 \int_0^b \cosh(\gamma_m y)\cosh(\tau_n y)dy = 0 \tag{6.81}$$

$$\sum_{m=0}^{\infty} \Omega_m s_m^2 \tan(s_m L)\sum_{n=0}^{\infty} \frac{\chi_n^- \sin(s_n L)}{\gamma_n^4 - \mu^4}\int_0^b \cosh(\gamma_n y)\cosh(\gamma_n y)dy = 0. \tag{6.82}$$

Hence, on making use of (6.80)-(6.82), (6.77) is simplified to (6.85).

$$S_4 U_1^+ = -2\alpha \sum_{m=0}^{\infty}\sum_{n=0}^{\infty} \Delta_{1m}\eta_m^2 R_{mn}\Phi_n^+ \cos(s_n L), \tag{6.83}$$

$$S_4 U_1^- = 2i\alpha \sum_{m=0}^{\infty}\sum_{n=0}^{\infty} \Delta_{1m}\eta_m^2 R_{mn}\Phi_n^- \sin(\nu_n L), \tag{6.84}$$

where

$$S_4 = \sum_{m=0}^{\infty} \Delta_{1m}^2 \eta_m^2 E_m. $$

Now by solving (6.83) and (6.84) simultaneously give $\{U_1^+, U_1^1\}$ However, to get $\{V_1^\pm, V_2^\pm\}$ we use (6.72) with (6.11)-(6.14), which finally lead to:

$$S_5 V_1^- + S_6 V_2^- = -\alpha \sum_{m=0}^{\infty} \Omega_m \cot(s_m L)\Theta_m^+(R) -$$

$$i\alpha \sum_{m=0}^{\infty} \Omega_m \cot(s_m L)\{a_{15}^- A_{1m} + a_{26}^- A_{2m} + a_{37}^- A_{3m} + a_{48}^- A_{4m}\}$$

$$+2i\alpha^2 \sum_{m=0}^{\infty} \Omega_m \cot(s_m L) \sum_{n=0}^{\infty} \frac{\chi_n^+ \cos(s_n L)T_{mn}}{\gamma_n^4 - \mu^4}, \tag{6.85}$$

$$S_7 V_1^+ + S_8 V_2^+ = -\alpha \sum_{m=0}^{\infty} \Omega_m \tan(s_m L)\Theta_m^-(R) -$$

$$i\alpha \sum_{m=0}^{\infty} \Omega_m \tan(s_m L)\{a_{15}^+ A_{1m} + a_{26}^+ A_{2m} + a_{37}^+ A_{3m} + a_{48}^+ A_{4m}\}$$

$$-2i\alpha^2 \sum_{m=0}^{\infty} \Omega_m \tan(s_m L) \sum_{n=0}^{\infty} \frac{\chi_n^- \sin(s_n L)T_{mn}}{\gamma_n^4 - \mu^4}, \tag{6.86}$$

$$S_9 V_1^- + S_{10} V_2^- = -\alpha \sum_{m=0}^{\infty} \Omega_m s_m^2 \cot(s_m L)\Theta_m^+(R) -$$

$$i\alpha \sum_{m=0}^{\infty} \Omega_m s_m^2 \cot(s_m L)\{a_{15}^- A_{1m} + a_{26}^- A_{2m} + a_{37}^- A_{3m} + a_{48}^- A_{4m}\}$$

$$+2i\alpha^2 \sum_{m=0}^{\infty} \Omega_m s_m^2 \cot(s_m L) \sum_{n=0}^{\infty} \frac{\chi_n^+ \cos(s_n L)T_{mn}}{\gamma_n^4 - \mu^4}, \tag{6.87}$$

$$S_{11} V_1^+ + S_{12} V_2^+ = -\alpha \sum_{m=0}^{\infty} \Omega_m s_m^2 \tan(s_m L)\Theta_m^-(R) -$$

$$i\alpha \sum_{m=0}^{\infty} \Omega_m s_m^2 \tan(s_m L)\{a_{15}^+ A_{1m} + a_{26}^+ A_{2m} + a_{37}^+ A_{3m} + a_{48}^+ A_{4m}\}$$

$$-2i\alpha^2 \sum_{m=0}^{\infty} \Omega_m s_m^2 \tan(s_m L) \sum_{n=0}^{\infty} \frac{\chi_n^- \sin(s_n L)T_{mn}}{\gamma_n^4 - \mu^4}, \tag{6.88}$$

where

$$S_5 = \sum_{m=0}^{\infty} \Omega_m^2 H_m s_m \cot(s_m L) \quad \text{and} \quad S_6 = \sum_{m=0}^{\infty} \Omega_m^2 H_m s_m \cot(s_m L)(\gamma_m^2 + 2)$$

$$S_7 = \sum_{m=0}^{\infty} \Omega_m^2 H_m s_m \tan(s_m L) \ \text{ and } \ S_8 = \sum_{m=0}^{\infty} \Omega_m^2 H_m s_m \tan(s_m L)(\gamma_m^2 + 2)$$

$$S_9 = \sum_{m=0}^{\infty} \Delta_{2m}^2 H_m s_m \cot(s_m L) \ \text{ and } \ S_{10} = \sum_{m=0}^{\infty} \Delta_{2m}^2 H_m s_m \cot(s_m L)(\gamma_m^2 + 2)$$

$$S_{11} = \sum_{m=0}^{\infty} \Delta_{2m}^2 H_m s_m \tan(s_m L) \ \text{ and } \ S_{12} = \sum_{m=0}^{\infty} \Delta_{2m}^2 H_m s_m \tan(s_m L)(\gamma_m^2 + 2) \tag{6.89}$$

whereas, to get (6.86)-(6.88) similar procedure may be adopted.

6.4 Modal Approach

To check the validity of MMTG approach it is useful to compare the obtained results with outcome of some other technique, for this purpose, an appropriate solution method Modal approach is developed. This approach broaden the range of edge conditions that can be addressed and avoid the need for additional root-finding.

For this purpose the vertical plates displacement is expressed in terms of a set of basis functions that are already known, and are non-zero and have non-zero derivatives at $y = a, b$. Thus, it is convenient to express the displacement as a modal expansion using the eigenfunctions for the duct height b. As previously mentioned, key to the success of this approach are the properties of these eigenfunctions, namely, their linearly dependence and the Greens function representation [123]]. The fundamentals of this approach can be seen in Afzal and Lawrie [81]. The vertical elastic plates displacements at $a \leqslant y \leqslant b$ and $x = \pm L$ can be found as The vertical elastic plates displacements at $a \leqslant y \leqslant b$ and $x = \pm L$ can be expressed in the form of model coefficients as

$$w_1(y) = \sum_{n=0}^{\infty} G_{1n} \cosh(\gamma_n y), \tag{6.90}$$

$$w_2(y) = \sum_{n=0}^{\infty} G_{2n} \cosh(\gamma_n y). \tag{6.91}$$

where the G_{1n} and G_{2n} are unknown Modal coefficients. Substituting (6.90) into (6.29), multiplying by $\cosh(\gamma_q y)$ and integrating from $a < y < b$ it is found that :

$$\sum_{n=0}^{\infty} G_{1n}\{\gamma_n^4 - \mu^4\}\cosh(\gamma_n y) = \alpha \sum_{n=0}^{\infty}(B_n e^{-is_n L} + C_n e^{is_n L})\cosh(\gamma_n y). \quad (6.92)$$

Multiplying (6.92) by $\cosh(\gamma_q y)$ and integrating over $a < y < b$ reveal as:

$$\sum_{n=0}^{\infty} G_{1n}\{\gamma_n^4 - \mu^4\}T_{nq} = \alpha \sum_{n=0}^{\infty}(B_n e^{-is_n L} + C_n e^{is_n L})T_{nq}, \quad (6.93)$$

where

$$T_{nq} = \int_a^b \cosh(\gamma_q y)\cosh(\gamma_n y)dy, \quad (6.94)$$

twice integrating by parts (6.94) lead to

$$\gamma_n^2 T_{nq} = \gamma_q^2 T_{nq} + \gamma_n \cosh(\gamma_q b)\sinh(\gamma_n b) - \gamma_n \cosh(\gamma_q a)\sinh(\gamma_n a)$$

$$+\gamma_q \cosh(\gamma_n a)\sinh(\gamma_q a) - \gamma_q \cosh(\gamma_n b)\sinh(\gamma_q b) \quad (6.95)$$

Multiplying (6.95) by γ_n^2 and using again (6.94) in the obtained equation, after a little rearrangement it is found that

$$\gamma_n^4 T_{nq} = \gamma_q^4 T_{nq} + \gamma_q^2 \gamma_n \cosh(\gamma_q b)\sinh(\gamma_n b) - \gamma_q^2 \gamma_n \cosh(\gamma_q a)\sinh(\gamma_n a)$$

$$+\gamma_q^3 \cosh(\gamma_n a)\sinh(\gamma_q a) - \gamma_q^3 \cosh(\gamma_n b)\sinh(\gamma_q b)$$

$$+\gamma_n^3 \cosh(\gamma_q b)\sinh(\gamma_n b) - \gamma_n^3 \cosh(\gamma_q a)\sinh(\gamma_n a)$$

$$+\gamma_q \gamma_n^2 \cosh(\gamma_n a)\sinh(\gamma_q a) - \gamma_q \gamma_n^2 \cosh(\gamma_n b)\sinh(\gamma_q b). \quad (6.96)$$

Invoking (6.96) into (6.93) and after some rearrangements it is found that

$$\sum_{n=0}^{\infty} G_{1n} T_{nq} = -\frac{L_1 \cosh(\gamma_q a)}{\gamma_q^4 - \mu^4} - \frac{L_2 \cosh(\gamma_q b)}{\gamma_q^4 - \mu^4} - \frac{L_3 \gamma_q \sinh(\gamma_q a)}{\gamma_q^4 - \mu^4} - \frac{L_4 \gamma_q \sinh(\gamma_q b)}{\gamma_q^4 - \mu^4}$$

$$-\frac{E_5 \gamma_q^2 \cosh(\gamma_q a)}{\gamma_q^4 - \mu^4} - \frac{L_6 \gamma_q^2 \cosh(\gamma_q b)}{\gamma_q^4 - \mu^4} - \frac{L_7 \gamma_q^3 \sinh(\gamma_q a)}{\gamma_q^4 - \mu^4} - $$

$$\frac{L_8 \gamma_q^3 \sinh(\gamma_q b)}{\gamma_q^4 - \mu^4} + \frac{\alpha}{\gamma_q^4 - \mu^4} \sum_{n=0}^{\infty} (B_n e^{-is_n L} + C_n e^{is_n L}) T_{nq} \quad (6.97)$$

where $L_1 = -w_{1yyy}(a)$, $L_2 = w_{1yyy}(b)$, $L_3 = w_{1yy}(a)$, $L_4 = -w_{1yy}(b)$, $L_5 = -w_{1y}(a)$, $L_6 = w_{1y}(b)$, $L_7 = w_1(a)$, $and L_8 = -w_1(b)$ and $w_1(y)$ is defined by (6.90)). On multiplying (6.97) by $\alpha \cosh(\gamma_q y)/D_q$ and summing over q that leads to

$$\alpha \sum_{n=0}^{\infty} \sum_{q=0}^{\infty} \frac{G_{1n} \cosh(\gamma_q y) T_{nq}}{D_q} = -L_1 \psi^1(y) - L_2 \psi^2(y) - L_3 \psi^3(y) - L_4 \psi^4(y)$$

$$-L_5 \psi^5(y) - L_6 \psi^6(y) - L_7 \psi^7(y) - L_8 \psi^8(y)$$

$$+\alpha_2 \sum_{n=0}^{\infty} \sum_{q=0}^{\infty} \frac{(B_n e^{-is_n L} + C_n e^{is_n L}) \cosh(\gamma_q y) T_{nq}}{D_q (\gamma_q^4 - \mu^4)}, \quad (6.98)$$

where the function $\psi^j(y)$, $j = 1 \ldots 8$ are defined by a function as,

$$z(p) = \alpha \sum_{q=0}^{\infty} \frac{\cosh(\gamma_q y) \cosh(\gamma_q p)}{D_q (\gamma_q^4 - \mu^4)},$$

here, $\{\psi^1(y) = z(a)$, $\psi^2(y) = z(b)$, $\psi^3(y) = z'(a)$, $\psi^4(y) = z'(b)$, $\psi^5(y) = z''(a)$, $\psi^6(y) = z''(b)$, $\psi^7(y) = z'''(a)$, $\psi^8(y) = z'''(b)\}$ and the prime represents derivative with respect to p.

The reader is reminded that the aim is to construct $w(y)$ from (6.98), and also that no explicit OR exists for the functions $\cosh(\gamma_n y)$ on the range $a \leqslant y \leqslant b$. The quantity T_{nq} is, however, defined in (6.94) as an integral and this enables the Greens function (6.14) to be used in lieu.

Thus, on interchanging the orders of summation and integration on the left hand side of (6.94) and using (6.14), it is obtained as

$$w_1(y) = -L_1\psi^1(y) - L_2\psi^2(y) - L_3\psi^3(y) - L_4\psi^4(y) - L_5\psi^5(y) - L_6\psi^6(y)$$

$$-L_7\psi^7(y) - L_8\psi^8(y) + \alpha^2 \sum_{n=0}^{\infty}\sum_{q=0}^{\infty} \frac{(B_n e^{-is_n L} + C_n e^{is_n L})\cosh(\gamma_q y)T_{nq}}{D_q(\gamma_q^4 - \mu^4)}. \quad (6.99)$$

Similarly adopting the same procedure one can found the elastic plate displacement at $x = L$, $a \leqslant y \leqslant b$ as:

$$w_2(y) = -M_1\psi^1(y) - M_2\psi^2(y) - M_3\psi^3(y) - M_4\psi^4(y) - M_5\psi^5(y) - M_6\psi^6(y)$$

$$-M_7\psi^7(y) - M_8\psi^8(y) - \alpha^2 \sum_{n=0}^{\infty}\sum_{q=0}^{\infty} \frac{(B_n e^{is_n L} + C_n e^{-is_n L})\cosh(\gamma_q y)T_{nq}}{D_q(\gamma_q^4 - \mu^4)} \quad (6.100)$$

Here, L_i, M_i for $i = 1,\ldots 8$ are constants respectively and can obtained from edge conditions. Adding and subtracting (6.99) and (6.100) respectively, it is found as

$$W_1^+(y) = -N_1^+\psi^1(y) - N_2^+\psi^2(y) - N_3^+\psi^3(y) - N_4^+\psi^4(y) - N_5^+\psi^5(y) - N_6^+\psi^6(y)$$

$$-N_7^+\psi^7(y) - N_8^+\psi^8(y) - 2i\alpha^2 \sum_{n=0}^{\infty}\sum_{q=0}^{\infty} \frac{\chi^- \sin(s_n L)\cosh(\gamma_q y)T_{nq}}{D_q(\gamma_q^4 - \mu^4)} \quad (6.101)$$

$$W_1^-(y) = -N_1^-\psi^1(y) - N_2^-\psi^2(y) - N_3^-\psi^3(y) - N_4^-\psi^4(y) - N_5^-\psi^5(y) - N_6^-\psi^6(y)$$

$$-N_7^-\psi^7(y) - N_8^-\psi^8(y) + 2\alpha^2 \sum_{n=0}^{\infty}\sum_{q=0}^{\infty} \frac{\chi^+ \cos(s_n L)\cosh(\gamma_q y)T_{nq}}{D_q(\gamma_q^4 - \mu^4)} \quad (6.102)$$

Here, $N_i^{\pm} = L_i \pm M_i$ for $i = 1,\ldots,8$. Furthermore, the effects of edge conditions are assimilated in subsequent subsections.

6.4.1   Clamped Edges of Vertical Elastic Plates.

For clamped edges at $x = \pm L$, $a \leqslant y \leqslant b$ the equations (6.33)-(6.34) in association with the (6.101)-(6.102) give

$$N_5^{\pm} = 0 = N_6^{\pm}, \ N_7^{\pm} = 0 = N_8^{\pm} \quad (6.103)$$

and

$$N_1^\pm \psi^1(p) + N_2^\pm \psi^2(p) + N_3^\pm \psi^3(p) + N_4^\pm \psi^4(p) =$$
$$-2i\alpha^2 \sum_{n=0}^\infty \sum_{n=0}^\infty \frac{\chi^\mp \Pi_n^\mp \cosh(\gamma_q p) T_{nq}}{D_q(\gamma_q^4 - \mu^4)} \text{ at } p = a, b \tag{6.104}$$

$$N_1^\pm \psi_y^1(p) + N_2^\pm \psi_y^2(p) + N_3^\pm \psi_y^3(p) + N_4^\pm \psi_y^4(p) =$$
$$-2i\alpha^2 \sum_{n=0}^\infty \sum_{n=0}^\infty \frac{\chi^\mp \Pi_m^\mp \gamma_q \sinh(\gamma_q p) T_{nq}}{D_q(\gamma_q^4 - \mu^4)} \text{ at } p = a, b \tag{6.105}$$

where, Π_n is defined earlier and at $p = a, b$ thus for this set of edge conditions $\{N_i^\pm, i = 1, \ldots, 4\}$ can be obtained from $(6.104) - (6.105)$ respectively.

6.4.2 Pin-jointed Edges of Vertical Elastic Plates

For this set of edge conditions, (6.37) and (6.38) together with $((6.101))$-$((6.102))$ lead to

$$N_3^\pm = N_4^\pm = 0 = N_7^\pm = N_8^\pm, \tag{6.106}$$

and the pin-jointed edge conditions of vertical elastic plate at $x = -L$ and $a \leqslant y \leqslant b$ leads to

$$N_1^\pm \psi^1(p) + N_2^\pm \psi^2(p) + N_5^\pm \psi^5(p) + N_6^\pm \psi^6(p) =$$
$$-2i\alpha^2 \sum_{n=0}^\infty \sum_{n=0}^\infty \frac{\chi^\mp \Pi_n^\pm \cosh(\gamma_q y) T_{nq}}{D_q(\gamma_q^4 - \mu^4)} \text{ at } p = a, b \tag{6.107}$$

$$N_1^\pm \psi_{yy}^1(p) + N_2^\pm \psi_{yy}^2(p) + N_5^\pm \psi_{yy}^5(p) + N_6^\pm \psi_{yy}^6(y) =$$
$$-2i\alpha^2 \sum_{n=0}^\infty \sum_{n=0}^\infty \frac{\chi^\mp \Pi_n^\pm \gamma_q \sinh(\gamma_q y) T_{nq}}{D_q(\gamma_q^4 - \mu^4)} \text{ at } p = a, b. \tag{6.108}$$

For this set of edge conditions $\{N_i^\pm, i = 1, \ldots, 4\}$ can be obtained from $(6.107) - (6.108)$ and $p = a, b$ respectively.

Once these quantities become known, the constants $\{L_j,\ M_j\}$, $j = 1\ldots8$ are obtained in straightforward way from the expressions:

$$L_1 = \frac{1}{2}(N_1^+ + N_1^-), \quad L_3 = \frac{1}{2}(N_3^+ + N_3^-), \tag{6.109}$$

$$L_2 = \frac{1}{2}(N_2^+ + N_2^-), \quad L_4 = \frac{1}{2}(N_4^+ + N_4^-). \tag{6.110}$$

$$M_1 = \frac{1}{2}(N_1^+ - N_1^-), \quad M_3 = \frac{1}{2}(N_3^+ - N_3^-), \tag{6.111}$$

$$M_2 = \frac{1}{2}(N_2^+ - N_2^-), \quad M_4 = \frac{1}{2}(N_4^+ - N_4^-). \tag{6.112}$$

Likewise to evaluate the velocity flux conditions at interfaces $x = \pm L$, $a < y < b$, substituting (6.16)-(6.18) along with (6.99)-(6.100) into (6.45)-(6.46) and normalizing with the aid of OR (6.8), after some arrangement it is found that

$$B_m e^{-is_m L} - C_m e^{is_n L} = \Omega_m\{e_5 + (\gamma_m^2 + 2)e_6\} + \frac{\alpha}{s_m H_m}\{F_\ell \eta_\ell R_{m\ell} - \sum_{n=0}^\infty R_{mn}\eta_n A_n\}$$
$$-\frac{i\alpha}{s_m H_m}\{L_1\Psi_m^1 + L_2\Psi_m^2 + L_3\Psi_m^3 + L_4\Psi_m^4\} -$$
$$\frac{i\alpha^3}{s_m H_m}\sum_{n=0}^\infty\sum_{q=0}^\infty \frac{(B_n e^{-is_n L} + C_n e^{is_n L})T_{mq}T_{nq}}{D_q(\gamma_q^4 - \mu^4)}, \tag{6.113}$$

$$B_m e^{is_m L} - C_m e^{-is_n L} = \Omega_m\{e_7 + (\gamma_m^2 + 2)e_8\} + \frac{\alpha}{s_m H_m}\sum_{n=0}^\infty R_{mn}\eta_n D_n$$
$$+\frac{i\alpha}{s_m H_m}\{M_1\Psi_m^1 + M_2\Psi_m^2 + M_3\Psi_m^3 + M_4\Psi_m^4\}$$
$$-\frac{i\alpha^3}{s_m H_m}\sum_{n=0}^\infty\sum_{q=0}^\infty \frac{(B_n e^{is_n L} + C_n e^{-is_n L})T_{mq}T_{nq}}{D_q(\gamma_q^4 - \mu^4)}, \tag{6.114}$$

addition and subtraction of (6.113),(6.114) yields system of equations in the form of amplitudes of symmetric and anti-symmetric modes propagating in the central

region as

$$B_m + C_m = \frac{i\Omega_m}{2\sin(s_mL)} \left\{ (e_5 + e_7) + (\gamma_m^2 + 2)(e_6 + e_8) \right\} +$$

$$\frac{i\alpha}{2s_mH_m\sin(s_mL)} \left\{ F_\ell\eta_\ell R_{\ell m} - \sum_{n=0}^{\infty} R_{nm}\eta_\ell(A_n + D_n) \right\} -$$

$$\frac{\alpha}{2s_mH_m\sin(s_nL)} \left\{ (L_1 - M_1)\Psi_m^1 + (L_2 - M_2)\Psi_m^2 + (L_3 - M_3)\Psi_m^3 \right\} -$$

$$\frac{\alpha}{2s_mH_m\sin(s_nL)} \left\{ (L_4 - M_4)\Psi_m^4 - 2\alpha^2 \sum_{n=0}^{\infty}\sum_{q=0}^{\infty} \frac{T_{mq}T_{nq}\cos(s_nL)(B_n + C_n)}{D_q(\gamma_q^4 - \mu^4)} \right\}, \qquad (\,$$

and

$$B_m - C_m = \frac{\Omega_m}{2\cos(s_mL)} \left\{ (e_5 - e_7) + (\gamma_m^2 + 2)(e_6 - e_8) \right\} +$$

$$\frac{\alpha}{2s_mH_m\cos(s_mL)} \left\{ F_\ell\eta_\ell R_{\ell m} - \sum_{n=0}^{\infty} R_{nm}\eta_\ell(A_n - D_n) \right\} +$$

$$\frac{i\alpha}{2s_mH_m\cos(s_nL)} \left\{ (L_1 + M_1)\Psi_m^1 + (L_2 + M_2)\Psi_m^2 + (L_3 + M_3)\Psi_m^3 \right\} +$$

$$\frac{i\alpha}{2s_mH_m\cos(s_nL)} \left\{ (L_4 + M_4)\Psi_m^4 - 2\alpha^2 \sum_{n=0}^{\infty}\sum_{q=0}^{\infty} \frac{T_{mq}T_{nq}\sin(s_nL)(B_n - C_n)}{D_q(\gamma_q^4 - \mu^4)} \right\}, \qquad (\,$$

$$\chi_m^+ = \frac{i}{2\sin(s_mL)} \left\{ (V_1^- + (\gamma_m^2 + 2)V_2^-) \right\} \Omega_m - \frac{i\alpha}{2s_mH_m\sin(s_mL)}(\Theta_m^+(R) -$$

$$\frac{\alpha}{2H_ms_m\sin(s_mL)} \left\{ N_1^-\Psi_m^1 + N_2^-\Psi_m^2 + N_3^-\Psi_m^3 + N_4^-\Psi_m^4 \right\}$$

$$+ \frac{\alpha^3}{H_ms_m\sin(s_mL)} \sum_{n=0}^{\infty}\sum_{q=0}^{\infty} \frac{\chi_n^+\cos(s_nL)T_{mq}T_{nq}}{D_q(\gamma_n^4 - \mu^4)} \qquad (6.117)$$

and

$$\chi_m^- = \frac{1}{2\cos(s_mL)} \left\{ (V_1^+ + (\gamma_m^2 + 2)V_2^+) \right\} \Omega_m + \frac{\alpha}{2s_mH_m\cos(s_mL)}(\Theta_m^-(R) +$$

$$\frac{i\alpha}{2H_ms_m\cos(s_mL)} \left\{ N_1^+\Psi_m^1 + N_2^+\Psi_m^2 + N_3^+\Psi_m^3 + N+-_4\Psi_m^4 \right\}$$

$$- \frac{\alpha^3}{H_ms_m\cos(s_mL)} \sum_{n=0}^{\infty}\sum_{q=0}^{\infty} \frac{\chi_n^-\sin(s_nL)T_{mq}T_{nq}}{D_q(\gamma_n^4 - \mu^4)} \qquad (6.118)$$

where

$$\Psi_m^j = \int_a^b \psi^j(y) Y_2(\gamma_m, y) dy \quad m = 1, \ldots, 4. \tag{6.119}$$

6.4.3 Clamped Edges of Horizontal Elastic Plates

In case of clamped edges, the conditions (6.57)-(6.58) and (6.117)-(6.118) in association with the field potentials (6.17) yield

$$V_2^{\pm} = e_2 \pm e_4 = 0, \tag{6.120}$$

and $V_1^{\pm}$ can be obtained by multiplying (6.117), (6.118) by $\gamma_m \sinh(\gamma_m) \cos(s_m L)$, $\gamma_m \sinh(\gamma_m) \sin(s_m L)$ respectively, summing over m obtained

$$V_1^+ S_1 = -\frac{\alpha}{2} \sum_{m=0}^{\infty} \Omega_m \tan s_m L) \Theta_m^-(R) - \tag{6.121}$$

$$\frac{i\alpha}{2} \sum_{m=0}^{\infty} \Omega_m \tan(s_m L) \{ N_1^+ \Psi_m^1 + N_2^+ \Psi_m^2 + N_3^+ \Psi_m^3 + N_4^+ \Psi_m^4 \}$$

$$+ \alpha^3 \sum_{m=0}^{\infty} \Omega_m \tan(s_m L) \sum_{n=0}^{\infty} \sum_{q=0}^{\infty} \frac{\chi_n^- \sin(s_n L) T_{mq} T_{nq}}{D_q(\gamma_q^4 - \mu^4)},$$

and

$$V_1^- S_2 = -\frac{\alpha}{2} \sum_{m=0}^{\infty} \Omega_m \cot s_m L) \Theta_m^+(R) - \tag{6.122}$$

$$\frac{i\alpha}{2} \sum_{m=0}^{\infty} \Omega_m \cot(s_m L) \{ N_1^- \Psi_m^1 + N_2^- \Psi_m^2 + N_3^- \Psi_m^3 + N_4^- \Psi_m^4 \}$$

$$+ \alpha^3 \sum_{m=0}^{\infty} \Omega_m \cot(s_m L) \sum_{n=0}^{\infty} \sum_{q=0}^{\infty} \frac{\chi_n^+ \sin(s_n L) T_{mq} T_{nq}}{D_q(\gamma_q^4 - \mu^4)},$$

respectively, where S_1 and S_2 are defined in the previous section.

6.4.4 Pin-jointed Edges of Horizontal Elastic Plates

The pin-jointed edge conditions for Modal approach are obtained by invoking (6.17) into (6.71)-(6.72) Now by solving (6.83) and (6.84) simultaneously give

$\{U_1^+, U_2^+\}$ and likewise by solving (6.69) and (6.70) yield $\{U_1^-, U_2^-\}$. However, to get $V_1^{\pm}$ we use (6.72) together with the characteristics of linearly dependent eigenfunctions (6.11)-(6.14), which finally lead to:

$$
\begin{aligned}
S_5 V_1^- + S_6 V_2^- = {} & \frac{\alpha}{2} \sum_{m=0}^{\infty} \Omega_m \cot(s_m L) \Theta_m^+(R) - \\
& \frac{i\alpha}{2} \sum_{m=0}^{\infty} \Omega_m \cot(s_m L) \{ N_1^- \Psi_m^1 + N_2^- \Psi_m^2 + N_3^- \Psi_m^3 + N_4^- \Psi_m^4 \} \\
& + i\alpha^3 \sum_{m=0}^{\infty} \Omega_m \cot(s_m L) \sum_{n=0}^{\infty} \sum_{q=0}^{\infty} \frac{\chi_n^+ \cos(s_n L) T_{mq} T_{nq}}{D_q(\gamma_n^4 - \mu^4)},
\end{aligned} \tag{6.123}
$$

$$
\begin{aligned}
S_7 V_1^+ + S_8 V_2^+ = {} & -\frac{\alpha}{2} \sum_{m=0}^{\infty} \Omega_m \tan(s_m L) \Theta_m^-(R) - \\
& i\alpha \sum_{m=0}^{\infty} \Omega_m \tan(s_m L) \{ N_1^+ \Psi_m^1 + N_2^+ \Psi_m^2 + N_3^+ \Psi_m^3 + N_4^+ \Psi_m^4 \} \\
& - i\alpha^3 \sum_{m=0}^{\infty} \Omega_m \tan(s_m L) \sum_{n=0}^{\infty} \sum_{q=0}^{\infty} \frac{\chi_n^- \sin(s_n L) T_{mq} T_{nq}}{D_q(\gamma_n^4 - \mu^4)},
\end{aligned} \tag{6.124}
$$

$$
\begin{aligned}
S_9 V_1^- + S_{10} V_2^- = {} & -\frac{\alpha}{2} \sum_{m=0}^{\infty} \Omega_m s_m^2 \cot(s_m L) \Theta_m^+(R) - \\
& i\alpha \sum_{m=0}^{\infty} \Omega_m s_m^2 \cot(s_m L) \{ N_1^- \Psi_m^1 + N_2^- \Psi_m^2 + N_3^- \Psi_m^3 + N_4^- \Psi_m^4 \} \\
& + i\alpha^3 \sum_{m=0}^{\infty} \Omega_m s_m^2 \cot(s_m L) \sum_{n=0}^{\infty} \sum_{q=0}^{\infty} \frac{\chi_n^+ \cos(s_n L) T_{mq} T_{nq}}{D_q(\gamma_n^4 - \mu^4)},
\end{aligned} \tag{6.125}
$$

$$
\begin{aligned}
S_{11} V_1^+ + S_{12} V_2^+ = {} & -\frac{\alpha}{2} \sum_{m=0}^{\infty} \Omega_m s_m^2 \tan(s_m L) \Theta_m^-(R) - \\
& i\alpha \sum_{m=0}^{\infty} \Omega_m s_m^2 \tan(s_m L) \{ N_1^+ \Psi_m^1 + N_2^+ \Psi_m^2 + N_3^+ \Psi_m^3 + N_4^+ \Psi_m^4 \} \\
& - 2\alpha^3 \sum_{m=0}^{\infty} \Omega_m s_m^2 \tan(s_m L) \sum_{n=0}^{\infty} \sum_{q=0}^{\infty} \frac{\chi_n^- \sin(s_n L) T_{mq} T_{nq}}{D_q(\gamma_n^4 - \mu^4)},
\end{aligned} \tag{6.126}
$$

6.5   Numerical Results and Discussion

In this section the validity is analyzed for mode-matching tailored-Galerkin (MMTG) as well as Modal approach (MA) methods numerically. The linear algebraic systems retained against these methods are truncated up to N terms, the truncated solutions are used to investigate the effects of edge conditions on the scattering energies, and transmission loss versus frequency. According to the definition stated in [112], the reflected energy flux or power in inlet and transmitted energy flux or power in outlet can be formulated as

$$\mathcal{E}_{\mathrm{r}} = \frac{1}{\alpha} \sum_{m=0}^{\mathcal{K}-1} |A_m|^2 \eta_m E_m \tag{6.127}$$

and

$$\mathcal{E}_{\mathrm{t}} = \frac{1}{\alpha} \sum_{m=0}^{\mathcal{K}-1} |D_m|^2 \eta_m E m, \tag{6.128}$$

where the incident energy flux or power is scaled at unity and $\mathcal{K}$ denotes the number of cut-on modes in extended inlet/outlet region. The conservation of energy flux of confined system can be expressed through the conserve power identity, that is

$$\mathcal{E}_r + \mathcal{E}_t = 1. \tag{6.129}$$

Note sum of the reflected energy flux and transmitted energy flux that is equal to unit number (6.129) represents the incident energy flux or power fed into the system .

The numerical results are obtained by taking the values of parameters discussed in [114] as: density $\rho_p = 2700$ kgm^{-3}, the thickness of the elastic plates of aluminum as $\bar{h} = 0.0006$ m, the values of Young's modulus and Poisson's ratio are $E = 7.2 \times 10^{10}$ Nm^{-2} and $\upsilon = 0.34$,, sound speed $c = 344$ ms^{-1} and density of air $\rho_a = 1.2$ kgm^{-3}. The dimensional parameters are fixed as $\bar{a} = 0.06$m, $\bar{b} = 0.085$m, and $\bar{L} = 0.02$m. The structural-borne fundamental mode ($\ell = 0$) and the fluid-borne second mode ($\ell = 1$) are considered as; two different incident fields.
In Figs. 2-5 the curves are plotted by truncating and inverting the MMTG and

MA systems with $N = 25$ terms and the results are displayed in the form of transmitted and reflected powers against frequency. The curves with symbols (▲■) are obtained by using MMTG solution whilst the dashed curves represent the results achieved via Modal approach solution. In each Figs. 2-3 two different curves one with symbol (▲) and the other with symbol (■) are obtained when the connections of elastic plates at both ends are clamped and pin-jointed respectively. While in each Figs. 4-5 the curves with symbol (●) are obtained when the elastic plates edges at $y = a$ are clamped and at $y = b$ are pin-jointed where as the curves with symbol (■) are found when the elastic plates edges at $y = a$ are pin-jointed and at $y = b$ are clamped. Also a close agreement between MMTG and Model approach curves is seen in all in all frequency regimes see Figs. 2-5. The results presented in Fig. 6.2 relate to horizontal and vertical elastic plates having clamped and pin-jointed edges at $x = \pm L$, $a < y < b$ and include a comparison of scattering energies versus frequency, for fundamental or structure-borne mode incident ($\ell = 0$) Fig. 6.2(a) and of the fluid-borne mode incident ($\ell = 1$) Fig. 6.2(b). The reflected powers against frequency, the results with clamped and pin-jointed edges of the vertical as will as vertical elastic plates at $y = a$ and $y = b$ respectively are displayed in Fig. 6.2. Clearly, the systems converge more rapidly for the structure born mode incident (see Fig. 6.2(a)) than the fluid-borne mode incident (see Fig. 6.2(b)). The effects of clamped and pin-jointed edge conditions on the vertical and horizontal elastic plates are significant and becomes more apparent when the second cut-on mode of inlet/outlet starts propagating. From Fig. 2 (a) it is observed that at $f = 1$Hz maximum of the radiated energy goes on reflection which decreases by increasing frequency and reaches to its decremented value before the point whereby the second mode of the chamber cavity starts propagating. Nevertheless, by changing the edge conditions of the vertical flexible walls at $x = \pm L$, $a < y < b$, a variation in reflection energies is evident. This behavior is more significant about the points where the cuts-on of the chamber cavity occurred (see Fig. 2(a) and 2(b)). Note that the fundamental mode ($n = 0$) of extended inlet/outlet is always cut-on (whole frequency regime) due to the presence of zero eigenvalue and that results a plane acoustic wave, a

(a) fundamental mode incident ($\ell = 0$).

(b) fluid-borne mode incident ($\ell = 1$).
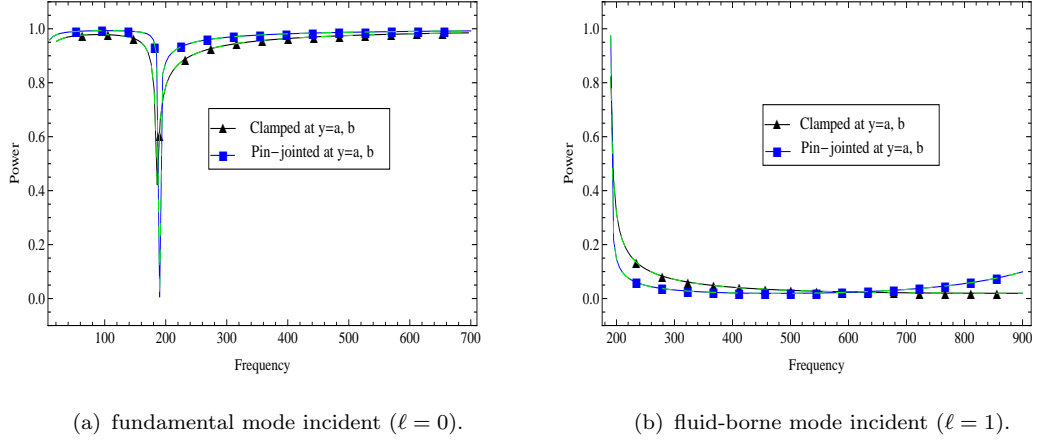
FIGURE 6.2: The reflected power against frequency obtained via MMTG technique ($\blacksquare\blacktriangle$) and Modal approach ($- - -$) with $N = 40$ terms.

TABLE 6.1: Propagating Modes

Cut-on f(Hz)	Inlet-Outlet Region	Expansion Chamber Region
191	1	1
1161	1	2
2301	1	3
2881	2	3
3446	2	4
3996	2	5
4015	3	5

mode which exist all the time in a duct having rigid boundary conditions. The next energy propagating modes appear on higher frequencies; such as the second cut-on mode of extended inlet/outlet arise at $f = 2881$Hz, however, lies out of the frequency regime considered herein for analysis. Likewise in cavity containing duct which bounded below with rigid wall and upper with elastic plates includes fundamental duct mode throughout the frequency regime due to the presence of one real root of dispersion relation (3.12), which always exists. However, the cut-on frequencies of second and third modes of the duct including flexible cavity are 1161Hz and 2301Hz, respectively, and thus affect the scattering energies. The list of cut-on frequencies is depicted in Table:1. Fig. 6.3 shows the transmitted powers

against frequency, with all clamped (first curve) and all pin-jointed edges (second curve) of horizontal as will as vertical elastic plates at $y = a$ and $y = b$. Fig. 6.3(a) and Fig. 6.3(b). It is clear from figures that the convergence in case of fluid-borne mode incident (see Fig. 6.3(b)) is rapid than that of structure born mode incident (see Fig. 6.3(a)). A close agreement between MMTG and Model approach for the above mentioned edge conditions are seen in all frequency regimes. More over the effects of these edges conditions is significant and becomes more apparent when the first cut-on of inlet/outlet start propagating. In Fig. 6.4 the effects of clamped

(a) fundamental mode incident ($\ell = 0$).

(b) fluid-borne mode incident ($\ell = 1$).
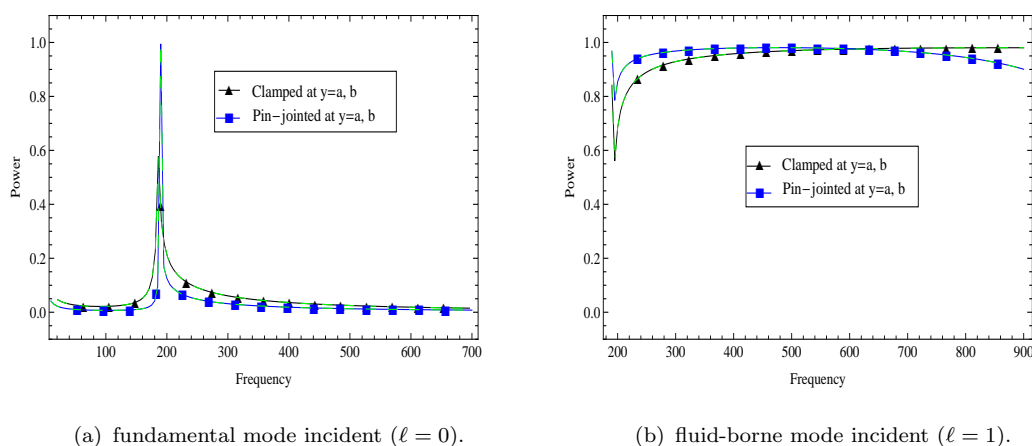
FIGURE 6.3: Transmitted power against frequency obtained via MMTG technique (■▲) and Modal approach ($- - -$) with $N = 40$ terms.

connections of horizontal elastic plates and pin-jointed connections of vertical elastic plates to the pin-jointed of horizontal and clamped of vertical elastic plates are investigated in the form of reflected powers against frequency. Clearly, their effect on reflected power is significant and becomes more prominent when the second mode of inlet/outlet at $f = 191$ Hz starts propagating. The curves in Fig. 6.4(a) and Fig. 6.4(b) are obtained respectively for the fundamental or structure-borne mode incident ($\ell = 0$) and of the fluid-borne mode incident ($\ell = 1$). In case of fundamental mode incident the maximum energy goes to reflection while for fluid born mode incident a minimum amount of energy goes to reflection. Clearly, the convergence is rapid for the case of structure born mode incident than fluid-borne mode incident (see see Fig. 6.4(a) and Fig. 6.4(b)).

(a) fundamental mode incident ($\ell = 0$).

(b) fluid-borne mode incident ($\ell = 1$).
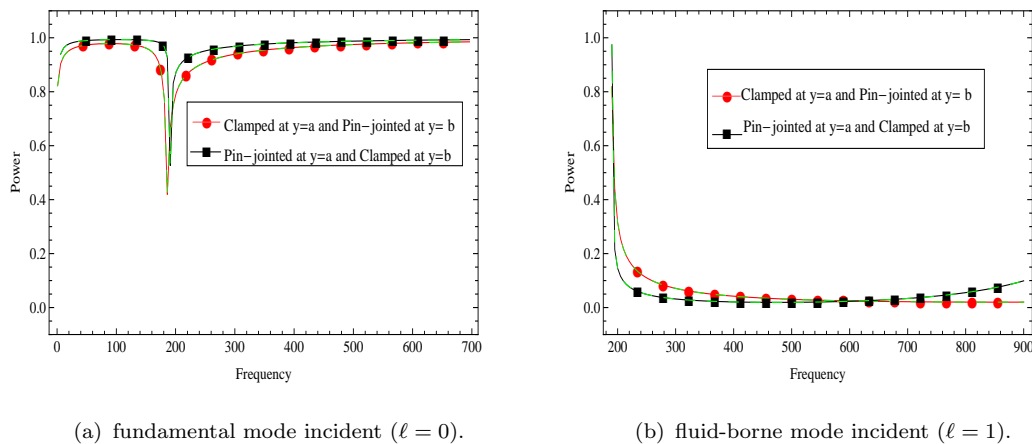
FIGURE 6.4: Reflected power against frequency obtained via MMTG technique ($\blacksquare\bullet$) and Model approach ($---$) with N=25 terms.

Fig. 6.5 shows the transmitted energies against frequency for structure born mode incident ($\ell = 0$) see Fig. 6.5(a) and fluid born mode incident ($\ell = 1$) see Fig. 6.5(b). The maximum energy goes on transmission for fluid born mode incident and a negligible amount of scattering energies for structure born mode incident goes on transmission. Clearly, the converge is more rapid for the structure born mode incident than the fluid-borne mode incident (see Fig. 6.5(a) and Fig. 6.5(b)). The results in Fig. 6.5 are the outcomes of MMTG and Model approaches when the connections of horizontal and vertical elastic plates at the edges are clamped at $y = a$, pin-jointed at $y = b$ and pin-jointed at $y = a$ and clamped at $y = b$ respectively. The effects of these edge conditions for both structure born mode and fluid born mode on transmitted energies are significant and becomes more prominent when higher order mode of chamber cavity starts propagating.

The performance of a HVAC silencer is measured usually with the help of transmission loss (TL) and for unit incident power it is found in [123] as:

$$\text{TL} = -10\log_{10}(\mathcal{E}_t). \tag{6.130}$$

where, $\mathcal{E}_t$ represents the transmitted power.

The results in in Fig. 6.6 shows TL verses frequency whereas at the edges $y = a$, b there are clamped as well as pin-jointed connections. The graphs in Fig. 6.6(a)

(a) fundamental mode incident ($\ell = 0$).

(b) fluid-borne mode incident ($\ell = 1$).
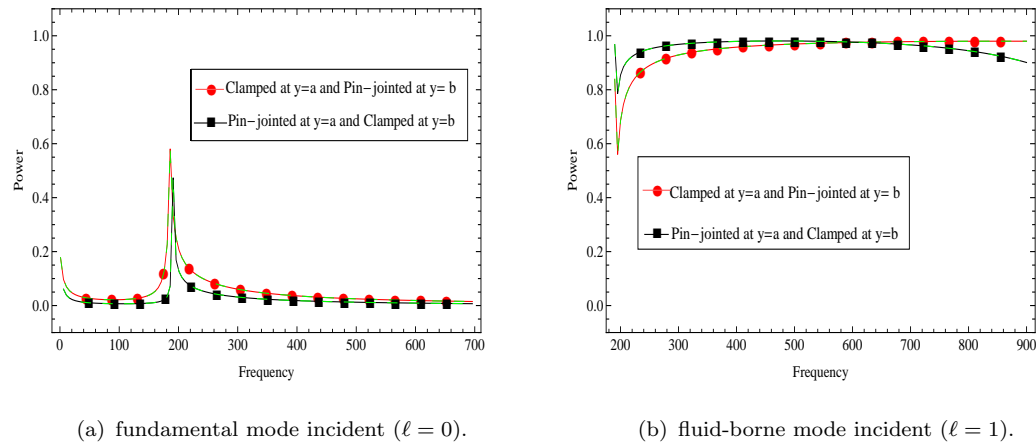
FIGURE 6.5: Transmitted power against frequency via MMTG technique (■●) and Model approach ($- - -$) with N=25 terms.

(a) fundamental mode incident ($\ell = 0$).

(b) fluid-borne mode incident ($\ell = 1$).
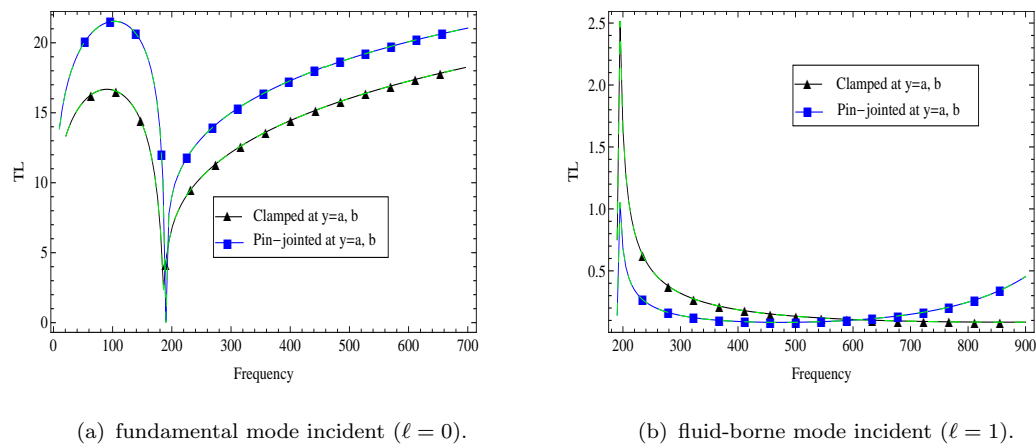
FIGURE 6.6: Transmission loss (TL) against frequency obtained via MMTG technique (■▲) and Modal approach ($- - -$) with $N = 40$ terms.

reveal the case when the system being radiated through fundamental mode incident ($\ell = 0$) while in Fig. 6.6(b) the fluid-born mode ($\ell = 1$) . The dimensions of waveguide are fixed with $\bar{a} = 0.06$m, $\bar{b} = 0.085$m and $\bar{L} = 0.02$m and are assumed along the surface of horizontal as will as vertical elastic plates. Accordingly, a stop-band that suppresses until the next mode of inlet duct becomes cut-on at $f = 191$ Hz which is basically the fluid-borne mode and maximum energy propagates along the structure is produced in regime $1\text{Hz} \leq f \leq 190\text{Hz}$. The TL starts increasing when both modes start propagating, with the increasing frequencies. Thus with the participation of additional modes more reflection and absorption are seen. Moreover, an increase in the magnitude of TL curves occurs due to zero bending moment at the edges when changing the edge conditions from all

clamped to all pin-jointed i.e., more leakage in compressional waves, see second curve in (Fig. 6.5(a)). Also a close agreement between the curves obtained from

(a) fundamental mode incident ($\ell = 0$).

(b) fluid-borne mode incident ($\ell = 1$).
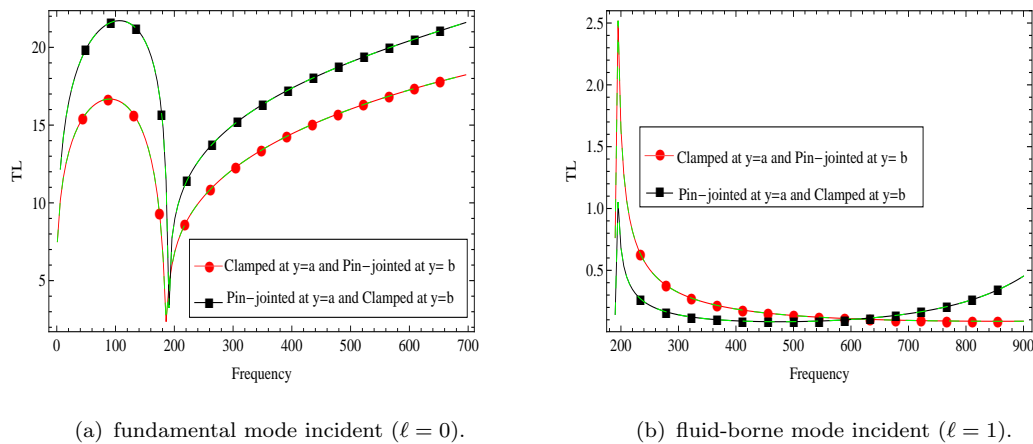
FIGURE 6.7: Transmission loss against frequency with N=20 terms, obtained via MMTG technique (■●) and Model approach ($---$).

MMTG technique and Modal approach are found in all frequency regimes. Fig. 6.7 shows two different responses of the edges on TL against frequency. The first curve is obtained when the responses at the edges $y = a$ and $y = b$ are clamped and pin-jointed respectively, while the second curve found graphical results when the responses at the edges $y = a$ and $y = b$ are pin-jointed and clamped respectively (see Fig. 6.7(a) and Fig. 6.7(b)). The graphs in Fig. 6.7(a) reveal the case when the system being radiated through fundamental mode incident ($\ell = 0$) while in Fig. 6.7(b) the fluid-born mode ($\ell = 1$). The dimensions of waveguide are fixed with $\bar{a} = 0.06$m, $\bar{b} = 0.085$m and $\bar{L} = 0.02$m and are assumed along the surface of horizontal as well as vertical elastic plates. Accordingly, a stop-band that suppresses until the next mode of inlet duct becomes cut-on at $f = 191$ Hz which is basically the fluid-borne mode and maximum energy propagates along the structure is produced in regime $1\text{Hz} \leq f \leq 190\text{Hz}$. Thus with the participation of additional modes more reflection and absorption are seen. Moreover, an increase in the magnitude of TL curves is observed due to zero bending moment at the edges when changing the edge conditions from clamped and pin-jointed at $y = a$, b to pin-jointed and clamped at $y = a$, b respectively, more leakage in compressional waves, see second curve in (Fig. 6.7(a)). Moreover a close agreement in MMTG technique and Model approach results is found in all frequency regimes. Also extra

leakage of compressional waves with pin-jointed at $y = a$ and clamped at $y = b$ conditions is clearly evident. The validity of the applied techniques (MMTG and

(a) Real parts of velocities.

(b) Real parts of pressures.
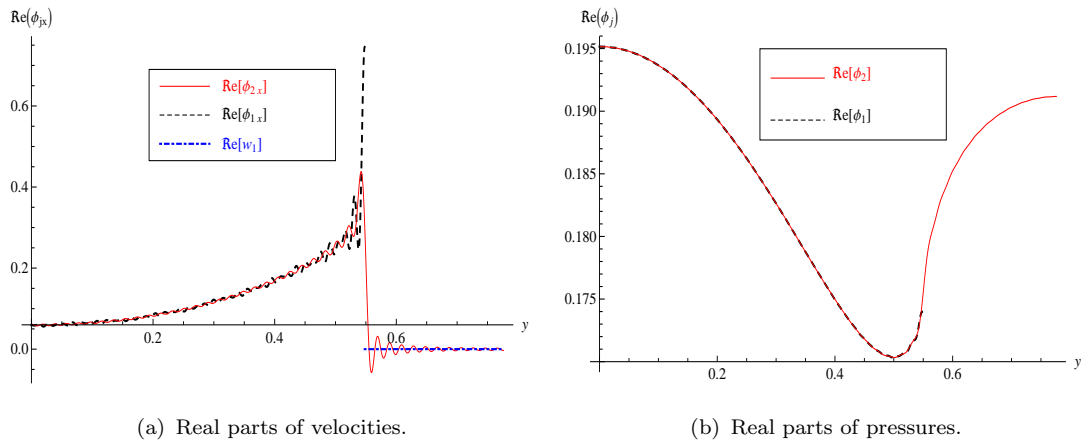
FIGURE 6.8: The real part of normal velocities and acoustic pressures against duct height at $(-L, y)$ for clamped edge condition in the presence of vertical elastic plates at $\bar{a} = 0.06$m, $\bar{b} = 0.085$m, $\bar{\ell} = 0.045$m, $f = 700$ Hz, and $N = 80$.

(a) Imaginary parts of velocities.

(b) Imaginary parts of pressures.
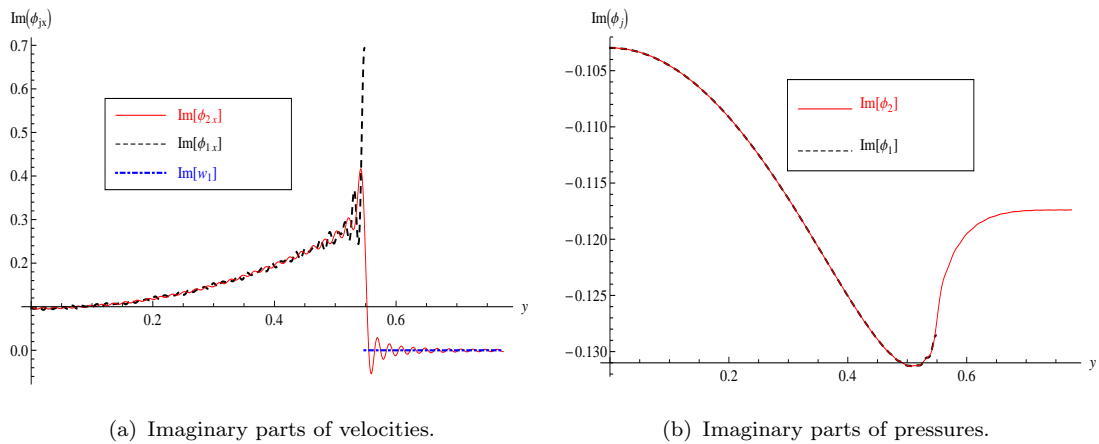
FIGURE 6.9: The imaginary part of normal velocities and acoustic pressures against duct height at $(-L, y)$ for clamped edge condition in the presence of vertical elastic plates at $\bar{a} = 0.06$m, $\bar{b} = 0.085$m, $\bar{\ell} = 0.045$m, $f = 700$ Hz, and $N = 80$.

Model approach) is measured with the reconstruction of matching conditions, it not only validate the truncated solutions but also confirm the performed algebra. The real and imaginary parts of non-dimensional pressures and normal velocities at interface $x = -L$ against cavity height y are presented in Fig. 6.9, likewise can be shown for $x = L$. It is clear from Fig. 6.9 that the curves for real as well as imaginary parts of pressures and normal velocities overlie when $0 \leq y \leq b$. Thus,

the matching conditions (6.20) and (6.45) are fully satisfied. It is observed that the amplitude of oscillation reduces along y direction, close to the corners $y = a$ and b and both the curves oscillate around their mean position. The singular behavior at the corners is comprehensively addressed in [56].

Chapter 7

Summary and Conclusions

In this thesis the scattering analysis of problems involving different boundary conditions and structural discontinuities is presented. The model problems contain boundary conditions of Dirichlet, Neumann, Robin and/or higher order boundary category and are governed by Helmholtz equation. The MM technique in conjunction with Galerkin tailored-Galerkin and Model approach are applied to solve the governing boundary value problems. The results obtained from different techniques are compared and found close agreement between the curves of scattering energies and transmission loss. In some cases the LFA is developed and compared with MM technique through numerical results.

The chapter wise summary of the present study are enclosed in this chapter. Chapter 1 depicts the general introduction relevant to the current study along with the literature overview. The objective of this dissertation toward physical problem are also addressed. The fundamental concepts that are necessary to understand the scattering analysis of acoustic wave in different waveguide structure, the derivation of linear acoustic wave equation along with different types of boundary conditions for different waveguide models have been discussed in Chapter 2. Also, the standard and generalized orthogonality relations have been explored on the basis of physical models in the category of either SL or non SL systems in this chapter.

In Chapter 3, the mode-matching technique is extended to analyze scattering through rectangular wave-bearing cavity in a rigid waveguide. The wave-bearing cavity comprises an elastic component stretched along horizontal direction and two elastic components lying along the vertical direction. The inside of the waveguide is filled with the compressible fluid. The fluid-structure coupled response of the horizontal flexible component and the inside fluid is incorporated by means of eigenfunctions. However, to incorporate the vibrational response of the vertical elastic components two approaches are discussed. In the first approach (referred as the mode-matching tailored-Galerkin (MMTG)), the displacements of flexible components along vertical direction are defined such that their homogeneous parts involve the material properties of elastic components, whilst their integral parts link the cavity vibrations. A unique general description that represents the displacement of vertical elastic component can deal a variety of edge conditions [45]. Whereas, the later method (mode-matching Galerkin (MMG)) relies on the a priori solutions of vertical elastic components, and that are chosen to be the orthogonal basis eigenfunctions [14-19]. For different set of edge conditions, the displacements along the vertical components is represented via a different set of basis functions. Accordingly, for some sets of edge conditions the eigenvalues cannot be expressed explicitly and must be found numerically. The eigenfunction expansions generated by MMTG and MMG converge to required physical solution. The eigen modes of cavity region satisfy a generalized orthogonal conditions. Such conditions are useful in proving the convergence of the system, and has already been established for the problems involving higher order boundary conditions [18]. The particular form of such important properties for the considered problem is stated in Section 2. These properties are sufficient to ensure the point-wise convergence of the systems. Moreover, the truncated MMTG and MMG solutions have reconstructed the matching conditions as well as satisfy the conserved power identity. It confirms the accuracy of performed algebra and retained solutions. Furthermore, the transmission loss against number of terms is plotted which ensures that the truncated solutions converge adequately when number of terms $N > 40$.

Physically, the work presented in Chapter 3 investigates the effects of flexible cavity

on scattering in a rigid duct or channel. Attention is restricted to the attenuation analysis with variation of edge conditions of bridging elastic components. The study is important for the reactive silencer containing low aspect ratio [124], and that tends to produce narrow, high stopbands by changing the physical conditions on elastic components [39]. The scattering powers and transmission loss against frequency have been analyzed through the numerical experiments. It is observed that by changing the physical conditions at the edges of bridging elastic components, a significant variation in scattering energies as well as transmission loss is achieved [127]. Also it is seen that the variation of edge conditions helps to enhance and shift the stop-band regimes as well as broaden the narrow frequency regimes. Furthermore, the results achieved via MMTG and MMG show an excellent agreement which indicates similar numerical convergence of these methods within the studied class of dynamic problems.

In Chapter 4, the acoustic scattering through a wave-bearing cavity in a flexible waveguide is discussed. The vertical boundaries of the cavity are assumed to be rigid plates or elastic membranes. The problem with the rigid vertical walls of the cavity is solved by following the traditional MM procedure whilst the solution of later problem is found though MMTG approach. The new approach is conceptually simpler and can be applied directly without using the extra root finding algorithms, that are required to determine the displacements along the vertical boundaries containing different edge conditions. The matching process along with generalized characteristics enables to recast the differential system to linear algebraic system. The system is truncated and then inverted for unknown coefficients. The accuracy of truncated solution is checked through the reconstruction of matching conditions and the satisfaction of conserved power identity. To extract the information from Gibb's oscillation in normal velocity curves, the practice of Lanczos filter is efficacious. Moreover, both the problems have been solved with the LFA, whose results show agreement with MM and MMTG in low frequency regime only. There many practical applications in HVAC wherein the choice of conditions (displacement, gradient and/or bending moment) between the junction

of horizontal and vertical surfaces play a pivoted role. The graphical results presented in numerical section demonstrate that the choice of vertical surfaces of the cavity as well as the variation of edge conditions applied on the edges of vertical membranes significantly affect the scattering power and the transmission loss. Furthermore, the variation of scattering behavior by changing the edge conditions is evident for both type of forcing either it is structure-born mode or fluid-born mode.

In Chapter 5, The study applies the Galerkin and tailored-Galerkin procedure to model the response of membrane cavity connected with the elastic plates of inlet and outlet regions. The plates of inlet and outlet regions are connected to finite edges in clamped or pin-jointed types of edge conditions, whereas, the horizontal membrane of central region is fixed at the edges and the vertical membranes may contain fixed, free or spring-like edge conditions. In duct regions, the energy propagation is carried out along the walls as well as through the fluid. The fluid-structure coupled waves response is incorporated in terms of eigenfunctions, whilst the surface vibrations of the membranes lying at interfaces are modeled by using Galerkin and tailored-Galerkin approaches. In the first approach, the vibrational response of vertical membranes is expressed by using the Fourier series. The eigenvalues and eigenfunctions depend upon the edge conditions and vary with the variation of edge conditions. For each set of edge conditions there is a different set of basis functions. Moreover, for spring-like edge conditions the eigenvalues are roots of dispersion relation that are found numerically. It requires an additional root finding algorithm which increases the computational cost. Whereas, in later approach, vibrational response of vertical membranes is taken such that its homogeneous part includes the material properties and the integral part contain the cavity vibrations. A single general description represents the displacement of a vertical elastic component and can deal a verity of edge conditions without solving any dispersion relation. The accuracy of both solution procedures is confirmed through the satisfaction of conserved power identity and through the reconstruction of matching conditions.

In Chapter 6, the performance of reactive device in a two-dimensional duct bounded by elastic plates has been studied. The model problem that contain structure-borne mode or fluid-borne mode as incident radiations is solved by using an established MMTG and Model approach. Model approach is developed here to overcome the difficulty of additional root finding in the expansion chamber. Although, it has slow convergence rate, for this purpose Green function are established to overcome the convergence issues. An appropriate solution of the problem involving flexible boundaries is found by MMTG and Model approach along with the generalized orthogonal characteristics. Also these techniques helps to impose extra conditions for accommodating the physical behavior at edges. Numerical results in the form of scattering energies and transmission loss have been presented for various types of conditions imposed on horizontal and vertical elastic plate edges. Note that the edges for both horizontal and vertical elastic plates are clamped or pin-jointed types. The results of scattering energies and TL versus frequency are analyzed for two different set of edge conditions. It is observed that imposing different conditions on the edges of elastic plates significantly affects the attenuation of structure and fluid-borne mode vibrations. Moreover, the specific impedance and different choices of edge conditions significantly effects the transmission loss. Furthermore, the results obtained by both techniques (MMTG and Model approach) are found in close agreement for all frequency regimes.

Future Work

- The physical problems discussed in this thesis can be extended by considering the insertion of double flexible expansion chambers bounded by elastic membranes and plates. The impact of acoustically rigid double expansion chamber on scattering is analyzed by Kirby in [68]. The analysis of double elastic chambers with different set of edge conditions would be interesting.

- This work can also be extended if the porosity is included in any of the flexible cavity considered in this dissertation.

- The presence of compressible fluid flow through ducts is commonly observed in HVAC. It would be interesting to model and investigate the configurations in presence of mean flow.

- The MM solutions of the boundary value problems mainly depend on the roots of dispersion relations. It would be a remarkable contribution if the problems involving flexible boundaries are solved by MM methods without root finding technique, see for instance [84].

- The fluid-structure coupled wave scattering is analyzed in this dissertation by bounding the fluid apace through elastic materials such as elastic membranes and elastic plates. The variation of physical properties of an elastic material have impact on the occurrence of resonance phenomenon, and that usually helps to build up metamaterials having exceptional attenuation characteristics, for more detail see [127]. This is a hybrid physical process that couples the acoustic and elastic responses in a single domain. It would be remarkable to investigate the structures in this direction.

Bibliography

[1] H. Levine and J. Schwinger, "On the radiation of sound from an unflanged circular pipe", *Journal of Sound and Vibration*, vol. 73, no. 4, pp. 383, 1948.

[2] J. B. Keller, "Geometric theory of diffraction", *Journal of the Optical Society of America*, vol. 52, no. 2, pp. 116-130, 1962.

[3] P. A. Cannell, "Edge scattering of aerodynamic sound by a lightly loaded elastic half-plane", *Proceeding of the Royal Society of London A*, vol. 347, no. 1649, pp. 213-238, 1975.

[4] P. H. Masterman and P. J. B. Clarricoats, "Computer field-matching solution of waveguide transverse discontinuities", *Proceedings of the Institution of Electrical Engineers*, vol. 118, no. 1, pp. 51-63, 1971.

[5] R. Munt, "Acoustic radiation properties of a jet pipe with subsonic jet flow: I. The cold jet reflection coefficient", *Journal of Sound and Vibration*, vol. 142, no. 3, pp. 413-436, 1990.

[6] E. Brambley, "Fundamental problems with the model of uniform flow over acoustic linings", *Journal of Sound and Vibration*, vol. 322, no. 4-5, pp. 1026-1037, 2009.

[7] N. S. Dickey, A. Selamet, J. M. Novak, "Multi-pass perforated tube silencers: A computational approach", *Journal of Sound and Vibration*, vol. 211, no. 3, pp. 435-447, 2001.

[8] A. McAlpine and M. Wright, "Acoustic scattering by a spliced turbofan inlet duct liner at supersonic fan speeds", *Journal of Sound and Vibration*, vol. 292, no. 3-5, pp. 911-934, 2006.

[9] R. Munt, "Acoustic transmission properties of a jet pipe with subsonic jet flow: I. The cold jet reflection coefficient", *Journal of Sound and Vibration*, vol. 142, no. 3, pp. 413-436, 1990.

[10] A. H. Nayfeh, J. E. Kaiser, and D. P. Telionis, "Acoustics of aircraft engine duct systems", *AIAA Journal*, vol. 13, no. 2, pp. 130-153, 1975.

[11] J. Wall, "Dynamics study of an automobile exhaust system", Ph.D. dissertation, *Blekinge Institute of Technology*, 2003.

[12] B. Veitch and N. Peake, "Models for acoustic propagation through turbofan exhaust flows", *13th AIAA/CEAS Aeroacoustics Conference (28th AIAA Aeroacoustics Conference)*, pp. 35-43, 2007.

[13] M. A. Swinbanks, "The active control of sound propagation in long ducts", *Journal of Sound and Vibration*, vol. 27, no. 3, pp. 411-436, 1973.

[14] S. Laugesen, "Active control of multi-modal propagation of tonal noise in ducts", *Journal of Sound and Vibration*, vol. 195, no. 1, pp. 33-56, 1996.

[15] V. Martin, A. Cummings, and C. Gronier, "Discrimination of coupled structural/acoustical duct modes by active control: principles and experimental results", *Journal of Sound and Vibration*, vol. 274, pp. 583–603, 2004.

[16] A. Preumont, "Vibration control of active structures: an introduction", *Springer*, vol. 246, 2018.

[17] K. Natarajan, and L. Venkatakrishnan, "Influence of launch platform cutouts on flow and acoustic behavior of rocket exhaust", *The Journal of the Acoustical Society of America*, vol. 140, no. 4, pp. 3042-3042, 2016.

[18] I. Klotz, "Recycling rockets", *Aerospace America*, vol. 55, no. 8, pp. 32–37, 2017.

[19] B. R. Wyerman, "A theoretical and experimental study of acoustic propagation in multisectioned circular ducts", Ph.D. dissertation, *Pennsylvania State University*, 1976.

[20] N. S. Dickey, A. Selamet and J. M. Novak, "Multi-pass perforated tube silencers: A computational approach", *Journal of Sound and Vibration*, vol. 211, no. 3, pp. 435-447, 1998.

[21] T. Bravo and C. Maury, "Sound attenuation and absorption by microperforated panels backed by anisotropic fibrous materials: Theoretical and experimental study", *Journal of Sound and Vibration*, vol. 425, no. 3, pp. 189-207, 2018.

[22] R. J. Astley and A. Cummings, "A finite element scheme for attenuation in ducts lined with porous material: comparison with experiment", *Journal of Sound and Vibration*, vol. 116, no. 2, pp. 239-263, 1987.

[23] S. W. Rienstra, "Fundamentals of duct acoustics", *Von Karman Institute Lecture Notes*, 2015.

[24] Y. Auregan, "On the use of a stress-impedance model to describe sound propagation in a lined duct with grazing flow", *The Journal of the Acoustical Society of America*, vol. 143, no. 5, pp. 2975-2979, 2018.

[25] P. Morse and K. Ingard, "Encyclopedia of Physics", *Acoustics I. SpringerVerlag, Berlin*, 1961.

[26] J. B. Lawrie and I. D. Abrahams, "A brief historical perspective of the Wiener-Hopf technique", *Journal of Engineering Mathematics*, vol. 59, no. 4, pp. 351-358, 2007.

[27] A. D. Rawlins, "Wave propagation in a bifurcated impedance-lined cylindrical waveguide", *Journal of Engineering Mathematics*, vol. 59, no. 4, pp. 419-435, 2007.

[28] A. D. Rawlins, "Two waveguide trifurcation problems", *Mathematical Proceedings of the Cambridge Philosophical Society*, vol. 121, no. 3, pp. 555-573, 1997.

[29] T. Nawaz, M. Afzal and R. Nawaz, "The scattering analysis of trifurcated waveguide involving structural discontinuities", *Advances in Mechanical Engineering*, vol. 11, no. 7, pp. 1-10, 2019.

[30] A. D. Rawlins, "A trifurcated waveguide problem", *Brunel University Mathematics Technical Papers collection*, pp.1-22, 1994.

[31] M. Ayub, M. H. Tiwana, and A. B. Mann, "Influence of acoustic dominant mode propagation in a trifurcated lined duct with different impedances", *Physica Scripta*, vol. 81, no. 3, pp. 035402, 2010.

[32] M. Hassan, M. H. Michael, A. Bashir, and M. Sumbul, "Mode matching analysis for wave scattering in triple and pentafurcated spaced ducts", *Brunel University Mathematics Technical Papers collection*, vol. 39, no. 11, pp. 3043-3057, 2016.

[33] M. Hassan and M. Naz, "Reflection coefficient of a dominant mode in a penta-furcated duct", *Boundary Value Problems*, vol. 2017, no. 1, pp. 1-17, 2017.

[34] J. B. Lawrie and I. D. Abrahams, "An orthogonality relation for a class of problems with high-order boundary conditions; applications in sound/structure interaction", *The Quarterly Journal of Mechanics and Applied Mathematics*, vol. 52, no. 2, pp. 161-181, 1999.

[35] J. Satti, M. Afzal, and R. Nawaz, "Scattering analysis of a partitioned wave-bearing cavity containing different material properties", *Physica Scripta*, vol. 94, no. 11, pp. 1-22, 2019.

[36] R. Nawaz and J. B. Lawrie, "Scattering of a fluid-structure coupled wave at a flanged junction between two flexible waveguides", *The Journal of the Acoustical Society of America*, vol. 134, no. 3, pp. 1939-1949, 2013.

[37] R. Nawaz, M. Afzal, and M. Ayub, "Acoustic propagation in two-dimensional waveguide for membrane bounded ducts", *Communications in Nonlinear Science and Numerical Simulation*, vol. 20, no. 2, pp. 421-433, 2015.

[38] D. Warren, J. Lawrie, and I. Mohamed, "Acoustic scattering in waveguides that are discontinuous in geometry and material property", *Wave Motion*, vol. 36, no. 2, pp. 119-142, 2002.

[39] B. Veitch and N. Peake, "Acoustic propagation and scattering in the exhaust flow from coaxial cylinders", *Journal of Fluid Mechanics*, vol. 613, pp. 275-307, 2008.

[40] I. Abrahams, "Radiation and scattering of waves on an elastic half-space; a non-commutative matrix Wiener-Hopf problem", *Journal of the Mechanics and Physics of Solids*, vol. 44, no. 12, pp. 2125-2154, 1996.

[41] A. Büyükaksoy and B. Polat, "A bifurcated waveguide problem", *ARI-An International Journal for Physical and Engineering Sciences*, vol. 51, no. 3, pp. 196-202, 1999.

[42] S. Shafique, M. Afzal, and R. Nawaz, "On mode-matching analysis of fluid-structure coupled wave scattering between two flexible waveguides", *Wave Motion*, vol. 95, no. 6, pp. 581-589, 2017.

[43] S. Shafique, M. Afzal, and R. Nawaz, "On the attenuation of fluid-structure coupled modes in a non-planar waveguide", *Mathematics and Mechanics of Solids*, vol. 25, no. 10, pp. 1831–1850, 2020.

[44] M. Afzal, J. U. Satti, and R. Nawaz, "Scattering characteristics of non-planar trifurcated waveguides", *Meccanica*, vol. 55, pp. 1-12, 2020.

[45] J. B. Lawrie, "Comments on a class of orthogonality relations relevant to fluid-structure interaction," *Meccanica*, vol. 47, no. 3, pp. 783-788, 2012.

[46] J. B. Lawrie and J. Kaplunov "Edge waves and resonance on elastic structures: an overview", *Mathematics and Mechanics of Solids*, vol. 17, no. 1, pp. 4-16, 2012.

[47] P. E. Doak, Excitation, transmission and radiation of sound from source distributions in hard-walled ducts of finite length (I): the effects of duct cross-section geometry and source distribution space-time pattern, Journal of Sound and Vibration, 31: 1-72 (1973).

[48] E. H. Dowell, G. F. Gorman and D. A. Smith, Acoustoelasticity: general theory, Acoustic natural modes and forced response to sinusoidal excitation, including comparisons with experiment, Journal of Sound and Vibration, 52: 519-542 (1977).

[49] M. L. Munjal, Acoustics of ducts and mufflers with application to exhaust and ventilation system design, John Wiley and Sons, New York: (1987).

[50] L. Huang, A theoretical study of duct noise control by flexible panels, The Journal of the Acoustical Society of America, 106: 1801-1809 (1999).

[51] S. K. Lau and S. K. Tang, Active control on sound transmission into an enclosure through a flexible boundary with edges elastically restrained against translation and rotation, Journal of Sound and Vibration, 259(3): 701-710 (2003).

[52] T. Kaizuka and N. Tanaka, Radiation clusters and the active control of sound transmission into a symmetric enclosure, The Journal of the Acoustical Society of America, 121(2): 922-937 (2007).

[53] C. Hazard and E. Luneville, An improved multimodal approach for non-uniform acoustic waveguides, IMA Journal of Applied Mathematics, 73: 668-690 (2008).

[54] J. Pan and D. A. Bies, The effect of fluidstructural coupling on sound waves in an enclosure-Theoretical part, The Journal of the Acoustical Society of America, 87: 691 (1990).

[55] S. M. Kim and M. J. Brennan, Active control of harmonic sound transmission into an acoustic enclosure using both structural and acoustic actuators, The Journal of the Acoustical Society of America, 107: 2523 (2000).

[56] R. Ming, and J. Pan, Insertion loss of an acoustic enclosure, The Journal of the Acoustical Society of America, 116: 3453 (2004).

[57] J. T. Du, W. L. Li, H. A. Xu and Z. G. Liu, Vibro-acoustic analysis of a rectangular cavity bounded by a flexible panel with elastically restrained edges, The Journal of the Acoustical Society of America, 131: 2799 (2012).

[58] F. J. Fahy, Sound and Structural Vibration: Radiation, Transmission and Response, Academic, New York: 241-269 (1985).

[59] J. Pan, C. H. Hansen, and D. A. Bies, Active control of noise transmission through a panel into a cavity: I. Analytical study, The Journal of the Acoustical Society of America, 87: 2098-2108 (1990).

[60] S. K. Lau and S. K. Tang, Modeling sound propagation in acoustic waveguides using a hybrid numerical method, The Journal of the Acoustical Society of America, 124(4): 1930-1940, (2009).

[61] I. V. Andronov and B. P. Belinsky, On acoustic boundary-contact problems for a vertically stratifed medium bounded from above by a plate with concentrated inhomogeneities, Prikl. Matem. Mekhan, 54: 366-371 (1990).

[62] J. B. Lawrie and I. D. Abrahams, An orthogonality condition for the class of problems with higher order boundary conditions; application in sound/ structure interaction, The Quarterly Journal of Mechanics and Applied Mathematics, 52: 161-181 (1999).

[63] Y. D. Kaplunov, I. V. Kirillova and Y. A. Postnova, Dispersion of waves in a plane acoustic layer with flexible elastic walls, Acoustical Physics, 50: pp. 694-698 (2004).

[64] J. B. Lawrie, On eigenfunction expansion associated with wave propagation along ducts with wave bearing boundaries, IMA Journal of Applied Mathematics, 72: 376-394 (2007).

[65] B. Venkatesham, M. Tiwari and M. L. Munjal, Analytical prediction of the breakout noise from a rectangular cavity with one compliant wall, The Journal of the Acoustical Society of America, 124: 2952-2962 (2008).

[66] M. U. Hassan, M. H. Meylan and M. A. Peter, Water-wave scattering by submerged elastic plates, The Quarterly Journal of Mechanics and Applied Mathematics, 62(3): 321-344 (2009).

[67] A. Selamet and Z.L. Ji, Acoustic attenuation performance of circular expansion chambers with extended inlet/outlet, Journal of Sound and Vibration, 223: 197-212 (1999).

[68] R. Kirby and J. B. Lawrie A point collocation approach to modeling large dissipative silencers, Journal of Sound and Vibration, 286: 313-39 (2005).

[69] J. B. Lawrie and and I. M. M. Guled, On tuning a reactive silencer by varying the position of an internal membrane, The Journal of the Acoustical Society of America, 120(2): 780-790 (2006).

[70] J. B. Lawrie and J. Kaplunov, Edge waves and resonance on elastic structures: an overview, Mathematics and Mechanic of Solids, 17(1): 4-16 (2012).

[71] A. Mural, J. F. Mercier and V. Pagneux, Improved multimodel admittance method in varies cross section waveguides, Proceedings of the Royal Society A, 470: 30130448 (2014).

[72] K. J. Satzinger, Quantum control of surface acoustic-wave phonons. Nature 563: 661665 (2018).

[73] H. He, Topological negative refraction of surface acoustic waves in a Weyl phononic crystal. Nature 560, 6164 (2018).

[74] A. N. Norris. Acoustic cloaking theory. Proceedings of the Royal Society America (464): 24112434 (2008).

[75] R. Nawaz and J. B. Lawrie, Scattering of a fluid-structure coupled wave at flange junction between two flexible waveguides, The Journal of the Acoustical Society of America, 134(3): 1939-1949 (2013).

[76] M. Kanoria, D. P. Dolai, and B. N. Mandal, Water-wave scattering by thick vertical barriers, Journal of Engineering Mathematics, 35, 361-384 (1999).

[77] D. Homentcovschi and R. N. Miles, A re-expansion method for determining the acoustical impedance and the scattering matrix for the waveguide discontinuity problem, The Journal of the Acoustical Society of America, 128(2): 628-638 (2010).

[78] R. W. Ogden. Non-Linear Elastic Deformations. Dover Publications, (1997)

[79] J. B. Lawrie, Orthogonality relations for fluid-structural waves in a 3-D rectangular duct with flexible walls, Proceedings of the Royal Society A, 465: 2347-2367 (2009).

[80] J. B. Lawrie, On acoustic propagation in three dimensional rectangular ducts with flexible walls and porous linings, The Journal of the Acoustical Society of America, 131(3): 1890-1901 (2012).

[81] J. B. Lawrie and M. Afzal, Acoustic scattering in a waveguide with the height discontinuity bridged by membrane: a tailored Galerkin approach, Journal of Engineering Mathematics, 105(1): 99-115 (2016).

[82] D. V. Evans and M. Fernyhough, Edge waves along periodic coastlines. Part 2, Journal of Fluid Mechanics, 297: 307-325 (1995).

[83] S. H. Ko, Theoretical analysis of sound attenuation in acoustically lined flow ducts separated by porous splitters (rectangular, annular and circular ducts), Journal of Sound and Vibration 39 471-487 (1975).

[84] B. Nilsson and O. Brander, The propagation of sound in cylindrical ducts with mean flow and bulk-reacting lining I-Modes in an infinite duct, Journal of the Institute of Mathematics and its Applications 26: 269-298 (1980).

[85] I. D. Abrahams, Scattering of sound by two parallel semi-infinite screens, Wave Motion 9: 289-300 (1987).

[86] M. Hassan and A. D. Rawlins, Radiation from a two dimensional duct, Canadian Journal Physics 1: 375-384 (1997).

[87] A. Demir and A. Buyukaksoy, Transmission of sound waves in a cylindrical duct with an acoustically lined muffler, International Journal of Engineering Science 41: 2411-2427 (2003).

[88] A. Demir and A. Buyukaksoy, Wiener-Hopf approach for predicting the transmission loss of a circular silencer with a locally reacting lining, International Journal of Engineering Science, 43 398-416 (2005).

[89] D. Karmakar, J. Bhattacharjee and T. Sahoo, Oblique flexural gravity-wave scattering due to changes in bottom topography, Journal of Engineering Mathematics 66 325-341 (2010).

[90] S. C. Mohapatra, D. Karmakar and T. Sahoo On capillary gravity-wave motion in two-layer fluids, Journal of Engineering Mathematics 71: 253-277 (2011).

[91] S. C. Mohapatra, T. Sahoo, Wave interaction with a floating and submerged elastic plate system, Journal of Engineering Mathematics 87: 47-71 (2014).

[92] J. B. Lawrie and I. D. Abrahams , An orthogonality condition for the class of problems with higher order boundary conditions; application in sound/ structure interaction. The Quarterly Journal of Mechanics and Applied Mathematics, 52(2): 161-181 (1999).

[93] D. P. Warren , J. B. Lawrie and I. M. Mohammad, Acoustic scattering in wave-guides with discontinuities in height and material property. Journal of wave motion, 36: 119-142 (2002).

[94] M. J. P. Musgrave. Crystal Acoustics. Acoustical Society of America, New York, (2003).

[95] A. N. Norris, Euler-Rodrigues and Cayley, Formulas for rotation of elasticity tensors. Mathematics and Mechanics of Solids, 3:243 260, (2008).

[96] A. Nakamura,R. Takeuchi and S. Oie, Nonlinear attenuation of an N wave propagation in tube, including dissipation due to wall effects, The Journal of Acoustical Society of America72(3): 376-394 (1978).

[97] O. K. Mawardi, On acoustic boundary layer heating.The Journal of Acoustical Society of America 63(1): 346-352 (1954).

[98] D. V. Evans and M. Fernyhough, Edge waves along periodic coastlines. Part 2. Journal of Fluid Mechanics 297: 307-325 (1995).

[99] D. Gorman, Free vibration analysis of completely free rectangular plates by the superposition-galerkin method, Journal of Sound Vibration 237(5):901-914 (2000).

[100] L. Huang, Modal analysis of a drumlike silencer. The Journal of Acoustical Society of America 112(5): 2014-2025 (2002).

[101] J. Backus, Acoustic impedance of annular capillary, Journal of Acoustical Society of America, 58: 1078-1081 (1975).

[102] L.Reyleigh, "The Theory of Sound (2nd edition)" , *Dover*, *New York*, Vol(2): pp 317-328 1945.

[103] D. Gottlieb and C. W. Shu, On the Gibb's phenomenon and its resolution, SIAM Review 39(4): 644-668 (1997).

[104] R. Panneton and N. Atalla, Numerical prediction of transmission through finite multilayer system with poroelastic materials, The Journal of the Acoustical Society of America, 100: 346-354 (1996).

[105] S. K. Lau and S. K. Tang, Active control on sound transmission into an enclosure through a flexible boundary with edges elastically restrained against translation and rotation, Journal of Sound and Vibration, 259(3): 701-710 (2003).

[106] T. Kaizuka and N. Tanaka, Radiation clusters and the active control of sound transmission into a symmetric enclosure, The Journal of the Acoustical Society of America, 121(2): 922-937 (2007).

[107] A. W. Leissa, Vibration of plates, Acoustical Society of America, Chapter 4: New york (1993).

[108] Z. Ni, H. Hua, Axial-bending coupled vibration analysis of an axially-loaded stepped multi-layered beam with arbitrary boundary conditions, International Journal Mechanical Sciences, 138-139, 187-198 (2018).

[109] R. A. Scott, The propagation of sound between walls of porous materials, Proceedings of the Physical Society, New York: (1987).

[110] R. H. Lyon, Noise reduction of rectangular enclosures with one flexible wall, The Journal of the Acoustical Society of America, 58: 358-368 (1946).

[111] A. J. Pretlove, Free vibrations of a rectangular panels backed by a close rectangular cavity , Journal of Sound and Vibration, 2: 197-209 (1965).

[112] L. Cheng, Fluid-structural coupling of a plate-ended cylindrical shell: vibration and internal sound field, Journal of Sound and Vibration, 174: 641-654 (1994).

[113] A. Selemet, I. J. Lee and N. T. Huff,Acoustic attenuation of hybrid silencers, Journal of Sound and Vibration, 202: 109-123 (1997).

[114] I. M. M. Gulled, Acoustic transmission: waveguide with scattering or dissipative components, Thesis Brunal University, United Kingdom (2003).

[115] M. E. Delany and E. N. Bazley , Acoustic properties of fibrous materials, Applied Acoustic **3**, pp:105-116 (1970).

[116] F. P. Mechel, Theory of baffle-type silencers, Acustica, 70: 93-111 (1990).

[117] M. Hassan, M. H. Meylan, A. Bashir, and M. Sumbul, Mode-matching analysis for wave scattering in triple and pentafurcated spaced ducts, Mathematical Methods in Applied Sciences, 9(5), 1687814017692697 (2017).

[118] M. Hassan, M. Naz and R. Nawaz, Reflected field analysis of soft-hard pentafurcated waveguide, Advances in Mechanical Engineering, 9(5) 1-11 (2017).

[119] J. k. Kruger, The calculation of actively absorbing silencers in rectangular ducts, Journal of Sound and Vibration, 257(5): 887-902 (2002).

[120] A. McAlpine and M. J. Fisher, On the prediction of 'buzz-saw' noise in acoustically lined aero-engine inlet ducts, Journal of Sound and Vibration, 265(1): 175-200 (2003).

[121] D. Gorman, Free vibration analysis of completely free rectangular plates by the superposition-Galerkin method, Journal of Sound and Vibration, 237(5): 901-914 (2000).

[122] C. Wang, L. Cheng and L.Huang, Realization of a broadband low-frequency plate silencer using sandwich plates, Journal of Sound and Vibration, 318: 792808 (2008).

[123] G. Liu, X. Zhao, W. Zhang and S. Li, Study on plate silencer with general boundary conditions, Journal of Sound and Vibration, 333(20): 4881-4896 (2014).

[124] A. Grant and J. Lawrie, "Propagation of fluid-loaded structural waves along a duct with smoothly varying bending characteristics", *Quarterly Journal of Mechanics and Applied Mathematics*, vol. 53, no. 2, pp. 299-321, 2000.

[125] R. V. Churchill, "Fourier series and boundary value problems", 1941.

[126] N. N. Lebedev, I. P. Skalskaya and Y. S. Uflyand. Worked problems in applied mathematics, *Dover, New York*, 1979.

[127] L. E. Kinsler, A. R. Frey, A. B. Coppens and J. V. Sanders, "Fundamentals of acoustics (4th edition)", 1999.